Non-linear dynamical analysis of operant behavior

Inaugural - Dissertation

zur

Erlangung des Doktorgrades der

Mathematisch-Naturwissenschaftlichen Fakultät

der Heinrich-Heine-Universität Düsseldorf

vorgelegt von

Jay-Shake Li

aus Tainan, Taiwan

Düsseldorf 2003

Aus dem Institut für Physiologische Psychologie I

der Heinrich-Heine-Universität Düsseldorf

Gedruckt mit der Genehmigung der Mathematisch-Naturwissenschaftlichen Fakultät der Heinrich-Heine-Universität Düsseldorf

Referent: Prof. Dr. J. P. Huston

Korreferent: Prof. Dr. J. Krauth

Tag(e) der mündlichen Prüfung: 16 Juli 2003

Acknowledgements

I am very grateful for Prof. Huston's effort in supporting my experiments and providing such an excellent environment for my research.

I also wish to say thanks to Prof. Krauth for the intensive and helpful discussions during the past four years.

Additionally, I would like to thank all my colleagues for their kind help and suggestions. Especially I would like to thank Mr. Manfred Mittelstaedt for his assistance in the installation of the equipment, and Mr. Patrick Schmitz for his assistance in my experiments.

Finally, I want to thank my family for their support during the whole period of my study in Germany.

Contents

Abstract

The present work investigated operant behavior of rats under the control of fixed-interval reinforcement schedules from a dynamical perspective. The central point is a newly invented analyzing tool, the "extended return map (ERM)". It is a modification of the original return map (also known as recurrent plot). The ERM is a multi-dimensional diagram reconstructed out of an one-dimensional data set of the inter-response times (IRT) acquired, for example, from an operant lever-pressing experiment. Our results indicated that there are certain patterns in the ERM, which cannot be seen using the original return map. Further studies suggested that these patterns indeed reflect long term dynamics of the IRT data. Analytical considerations as well as simulation studies indicated that a model based on a "two-state" conception can describe the dynamics of FI-responding quite well. However, the "two-state" conception in the original form as proposed by its inventors is not sufficient to describe FI-responding. Additional properties, such as acceleration of rate of responses, or multiple switches during the inter-reinforcement period must be taken into consideration.

A study, using amphetamine as an example, demonstrated that the ERM-patterns can serve as dependent variables in pharmacological studies. Furthermore, the ERM-patterns change in different way as the rate of responses and the averaged scallop curve do. These findings evoked concern about the use of rate of responses and the averaged scallop curve alone to measure the effects of pharmacological treatments. The findings also evoked concern about the way to build groups, since animals might react qualitatively differently to the same treatment. The simulation studies indicated that, in addition to the scalloped curve, the switching rate between behavioral states also plays an important role in accounting for behaviors under amphetamine treatment. This new information can only be acquired using the ERM.

1. Introduction

1.1 Basic concepts

1.1.1 Predicting behavior

From a certain perspective, natural science can be regarded as an art of prediction. The starting point of science is the experience that certain observations have always related to some conditions, which underlie the so-called principle of causality, namely, that the same experimental conditions always lead to the same outcomes. Of course, modern science is more than merely creating a table of conditions and their corresponding outcomes. Efforts were made to find logical and, when possible, mathematical relationships between the subjects of observation, leading to the building of models, which enable the prediction of results under a novel set of experimental conditions.

In the study of operant behavior employing the Skinner-box, reinforcement schedules are one of the most important parameters for setting up experimental conditions. Models such as Herrnstein's "matching law" (1970; 1974), or Killeen's "mathematical principles of reinforcement" (1994) address the relationship between schedules of reinforcement and the rate of operant behavior. Such models can help us to calculate rate of responding, by employing a particular reinforcement schedule, without having previously observed behaviors under that condition.

1.1.2 Learning as a kind of behavioral dynamics

Conceptually the term "prediction" strongly suggests the involvement of "time". Given that a rat in a Skinner-box has learned to respond under a certain reinforcement schedule, say, continuous reinforcement, to "predict" the rate of responding under a new schedule implies that the animal now faces a new situation and must adapt its behavior accordingly. A static model such as the "matching law" (Herrnstein, 1974) or the "mathematical principles of reinforcement" (Killeen 1994), allows us to make predictions

about the final rate of responding, the so-called steady-state-behavior. How the animal arrives at this steady-state-behavior is a problem of behavioral dynamics, which we might understand under the framework of learning theory. The study of this dynamical process is obviously different from the static models mentioned above.

Machado and his coworkers were one of the few groups to investigate this dynamical process (Machado, 1997; Machado & Cevik, 1998). Unlike other researchers, Machado et al. did not shape the animal's behavior through a stepwise increase of the inter-reinforcement-period, but changed the reinforcement schedule abruptly from continuous reinforcement (CRF) to fixed-interval (FI). They analyzed the average rate of responding versus time after reinforcements, and found that in the beginning of this learning process animals exhibited a higher response rate after they received a reinforcement, and a gradual decline in rate of responding until the onset of the next reinforcement. After several sessions of training the pattern of responding was inversed. The rate of responding became lower after a reinforcement and increased steadily until the onset of the next reinforcement. Machado and

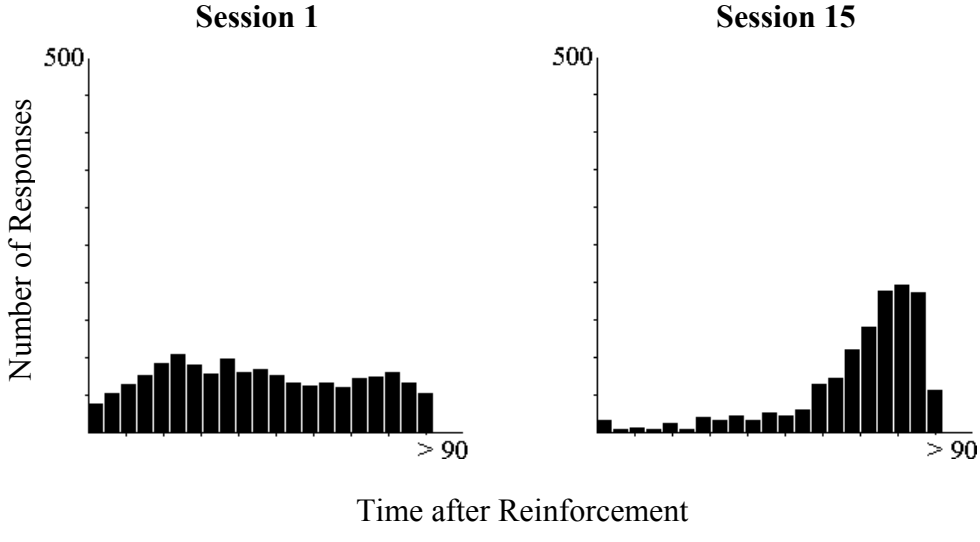

Figure 1: Typical FI-responding seen in the averaged scallop curve. In the first session of the FI-schedule control animals tend to respond more frequently after the delivery of foods, or more homogeneously during the inter-reinforcement period. After intensive learning (15 sessions), the rate of responses decreases after the delivery of foods, and increases gradually to a maximal value shortly before the next food delivery.

Cevik also presented a model that could describe this transition (1998). Similar results were also found in the present study. An example is shown in figure 1.

1.1.3 Behavior as a real-time dynamical system

The use of "rate of responding" is a convenient way to describe operant behavior. However, behavior also changes with "real-time". Consequently, the concept of "behavioral dynamics" should also be understood in terms of real-time dynamical systems, similar to those known in classical mechanics. Although Machado and Cevik's model can describe the transition of behavior from one set of environmental conditions to another; it is still very remote from Newton's "equation of motions" of classical mechanics.

Our efforts to understand animal behavior in terms of real-time dynamical systems have been hampered by the irregularity of data acquired in our observations. Several general styles of explanation for this chronic variability have been advanced. For examples: in terms of overcompensating homeostatic processes, such as response strength mechanisms (Herrnstein & Morse, 1958) or stimulus control mechanisms (Ferster & Skinner, 1957), external perturbation or noise (Sidman, 1960), and intrinsic variability. In conclusion, the irregularity of data has generally been regarded as a problem of the system's complexity. Either there are too many intrinsic variables that influence the animal's behavior, or there are difficulties with experimental control, that is, too many external variables interact and "disturb" the animal's behavior.

However, precisely why homeostatic mechanisms fail eventually to dampen is left unexplained, and how small amounts of noise can overpower the generally very strong schedule effects also remains unclear. Finally, the postulation of intrinsic causes for variability has also failed to provide fruitful solutions. Facing these problems, we try to find an alternative approach. Our efforts begin by posing the following question: does a complex appearance necessarily result from a complex system?

1.2 Emergence of "Chaos Theory"

1.2.1 Classical dynamics and determinism

Ever since Galileo, one of the central problems of physics has been the description of acceleration: "How can a continuously varying speed be defined?". The answer to this question made use of developments in both physics and mathematics. Progress in the research of planetary motion formed the physics-basement of Newton's law of motion, and the invention of calculus provided the necessary mathematical tools. Calculus introduced the concept of "infinitesimal quantities", the result of a limiting process. It is typically the variation in a quantity occurring between two successive instants when the time elapsed between these instants tends toward zero. In this way the "acceleration", that is, the change of the state of motion, becomes an "infinite" series of "infinitely" small changes.

In Newtonian language, to study acceleration means to determine the various "forces" acting on the points in the system under examination. Newton's second law, F = ma, states that the force applied at any point is proportional to the acceleration it produces. In the case of a system consisting of multiple points, the problem is more complicated, since the forces acting on a given point are determined at each instant by the relative distances between points of the system. Such a problem in dynamics is expressed in the form of a set of differential equations: the instantaneous state of each point of the system is defined by means of its position as well as by its velocity and acceleration, that is, first and second derivatives of the position.

While the differential equations constitute the problem of dynamics, their "integration" represents the solution of this problem. It leads to the calculation of a trajectory in the phase space. A trajectory contains all the information relevant for dynamics, and provides a complete description of the dynamical system. The description includes two parts: the initial states and the equations of motion. The initial state is the position and velocity of

each of the system's points at one arbitrary instant. The equations of motion relate the dynamic forces to the accelerations. The integration of the dynamic equations starting from the initial state unfolds the succession of states, that is, the trajectory of its constitutive points (for an introduction to classical dynamics, see for example: Marion & Thornton 1995).

The basic characteristic of trajectories are lawfulness, determinism, and reversibility. In order to calculate a trajectory we need an empirical definition of a single initial state of the system in addition to our knowledge of the law of motions. The general law then deduces from the initial state the series of states the system passes through as time progresses. Once the forces are known, any single state is sufficient to define the system completely, not only its future but also its past. The reversibility of a dynamic trajectory implies that if the velocities of all the points of a system are reversed, the system will go "backward in time". This orthodox was the central topic of a series of books by Prigogine (1980; Prigogine & Stengers 1984, 1997).

Extrapolative interpretation of the deterministic nature of classical dynamics has a symbol- the "demon" imagined by Laplace, capable at any given instant of observing the position and velocity of each mass that forms part of the universe. Of course, no one has ever dreamed that physicists might one day have this God-like power of knowledge. The "demon" simply illuminates the fact that a deterministic prediction of the course of events is possible *in principle*. Laplace himself only used this fiction to emphasize the extent of our ignorance of the initial state. In the context of classical dynamics, a deterministic description may be unreachable *in practice*, nevertheless, this does not preclude the objective truth of determinism as it would be seen by Laplace's demon.

1.2.2 The breakdown of determinism

Today classical dynamics can be formulated in a compact and elegant way. All the properties of a dynamic system can be summarized in terms of a single function, the

Hamiltonian $\boldsymbol{H}$. This function is simply the total energy, the sum of the system's potential and kinetic energy. This energy is no longer expressed in terms of positions and velocities, but in terms of so-called canonical variables, coordinates $\boldsymbol{q}$ and momenta $\boldsymbol{p}$. The time variation of the coordinate and of the momenta is given by the derivatives of $\boldsymbol{H}(\boldsymbol{p}, \boldsymbol{q})$ in respect to momenta $\boldsymbol{p}$ and coordinates $\boldsymbol{q}$ respectively (Marion & Thornton 1995).

In dynamics the same system can have different representations. In classical dynamics all these representations are equivalent, and they correspond to different sets of variables $\boldsymbol{p}$ and $\boldsymbol{q}$. We can go from one representation to another by a transformation of variables, without effecting the system itself. One of the basic problems of classical dynamics is to select a set of variables $\boldsymbol{p}$ and $\boldsymbol{q}$, so that the Hamiltonian $\boldsymbol{H}(\boldsymbol{p}, \boldsymbol{q})$ has the simplest form. For example, it is advantageous to look for canonical variables by which the Hamiltonian is reduced to kinetic energy and depends only on the momenta. In this case, interactions between compartments of the same system are eliminated, and the momenta become constants of motion. Such systems can be regarded as consisting of multiple "free particles", that is, consisting of particles that are isolated and free of interactions. The behavior of a free-particle-system is simple, and its solution is trivial. Systems that can be reduced to free-particle-systems by change of variables are called "integrable systems".

It was believed that integrable systems were the prototype of dynamic systems. Generations of physicists and mathematicians tried to find for every kind of system the right variables that could eliminate interactions. One widely studied example was the three-body problem. For example, the motion of the moon, influenced by both earth and sun, is a three-body system. At the end of the nineteenth century Bruns and Poincaré showed that it is impossible to find a set of canonical variables to transform the Hamiltonians of three-body systems to a free-particle representation (for a review of this history, see Prigogine 1980, pp. 57-77). If dynamics as simple as the three-body problem are not integrable systems, there is

little hope to expect dynamics in general to have simple behaviors like the free-particle-system.

1.2.3 The beginning of "Chaos Theory"

The work of Bruns and Poincaré was not completely understood at that time. It was more than half a century later, when Edward Lorenz found another system that possesses such complicated behavior. He simplified a theoretical model of an experiment on the convection of fluid induced by temperature differences in a bounded space (Rayleigh 1916), and arrived at three differential equations with three independent variables (Lorenz 1962, 1963). Although the Lorenz system appeared to be very simple, it has been impossible to solve it analytically, due to its non-linear terms. Under certain conditions, the system is neither stable nor periodical. Furthermore, small deviations in the initial conditions will grow exponentially during the time evolution of the system. As a consequence, long term prediction becomes impossible, unless infinite accuracy of the initial condition can be acquired. Lorenz called this property: "sensitivity to the initial conditions".

As with Bruns and Poincaré, Lorenz's work was not adequately appreciated in the beginning. Decades later, some mathematicians also began to study nonlinear dynamical systems, and Lorenz' work was rediscovered (Li & Yorke 1975). This marked the beginning of "Chaos Theory". Almost twenty years after Lorenz's discovery, Libchaber and Maurer (1982) accomplished the convection experiment. They observed the convection of liquidized helium in a very small cell, and found indeed the non-periodical behaviors foreseen by Lorenz (for the history of Chaos Theory, see: Gleick, 1987).

Lorenz's finding changed the deterministic nature of classical dynamics. In the view of Laplace, the problem of uncertainty is due to our ignorance about the initial conditions, that is, it is only a problem *in practice*. Now, due to the property "sensitivity to the initial conditions" of non-linear dynamical systems, we need infinite accuracy about their initial

conditions in order to make a long-term prediction. Since, principally, every measurement has limited resolution, our efforts to make a long term prediction about such a non-linear, non-periodical system will certainly fail. So, this "sensitivity to the initial conditions" is a problem *in principle*. This property forces us to give up deterministic trajectories and to use statistical descriptions instead.

From another point of view, Lorenz's finding suggested an alternative way to approach phenomena with complex appearance. A traditional linear dynamical system's approach would regard complex appearance as a problem of experimental control. The causes of complexity are either external disturbances, or it is due to the system's intrinsic complexity in terms of the large number of independent variables. Lorenz' finding suggested that simple, non-linear dynamical systems can have non-periodical, complex behavior. Here the term "simple" means that the number of independent variables is low. For example, Lorenz's system has only three independent variables, and can be outlined with three differential equations. However, the time series of the three variables have very complex appearance.

1.2.4 Application of chaos theory in neuroscience and psychology

In recent years, the application of chaos theory has been extended beyond the fields of mathematics and physics. It is also widely applied in the study of complicated phenomena in neuroscience and psychology.

The beat-to-beat variation in the heart rate of man and other animals is generated by a complex process and displays inhomogeneous, irregular temporal organization. Several studies have indicated that the physiological mechanism of this cardiac control is an autonomous, low-dimensional chaotic system under certain experimental conditions (Lefebvre et al. 1993; Yamamoto et al. 1993; Ivanov et al. 1996). Chaos theory was also applied to the study of heart rate dynamics of patients with heart disease (Guzzetti et al. 1996;

Poon & Merrill 1997; Meyer et al. 2003).

In the study of electro-physiology of single neurons, evidence of chaos was first found in the giant neuron of Onchidium (Hayashi et al. 1982), and later in the pacemaker neuron (Hayashi et al. 1983; Hayashi & Ishizuka 1992). Recently, chaotic response was also found in neural systems of vertebrates. For examples, neurons of the hippocampus (Hayashi & Ishizuka 1995; Ishizuka & Hayashi 1998) and cortex (Ishizuka & Hayashi 1996, 1998) showed chaotic response when they were periodically stimulated. Furthermore, the post synaptic membrane potential, also known as post synaptic "noise", was commonly considered to be stochastic (Softky & Koch 1993; Shadlen & Newsome 1994). Faure and Korn (1997), however, found deterministic components in it, suggesting that the mechanism of post synaptic potential might have chaotic dynamics.

Chaos theory has also been applied to analyze the electroencephalogram (EEG). Early studies had led to quite different conclusions. While some authors reported that EEGs are generated by nonlinear dynamical systems of low dimension (Babloyantz 1985; Röschke et al. 1993; Takigawa et al. 1994), others showed that EEGs are more likely the production of stochastic processes (Osborne and Provenzale 1989; Achermann et al. 1994). Later works concentrated on the comparison between EEGs recorded from healthy human subjects and from epileptic patients. It was shown that the EEG from epileptic patients possessed highly significant non-linearity (Lehnertz & Elger 1995; Casdagli et al. 1997; Röschke et al. 1997; Jing & Takigawa, 2000).

The early years of chaos theory in psychology can be traced back to catastrophe theory. Catastrophe theory originated from the works of Thom (1975). It provided interesting mathematical concepts for many phenomena in biology and social science (for an introduction see: Castrigiano & Hayes 1993). After a period of waning in the later 1980s, the application of non-linear dynamic systems approaches extended to the fields of psychological

theory in an extensive way. The concept of chaos can be found, for example, in the study of psychophysics (Gregson 1995, 1998, 1999), perception (Stewart & Peregoy 1983; Ta'eed et al. 1988; Guastello 1995), learning (Guastello 1995, 1998) and response time (Heath 2000; Heath et al. 2000; Kelly et al. 2001). In a special issue of the "Journal of the Experimental Analysis of Behavior" in 1992, several groups presented results of using the concept of nonlinear dynamic systems in behavioral experiments. For example, operant behaviors of pigeons under different reinforcement schedules were analyzed using phase diagrams reconstructed from inter-response time (IRT) data (Palya 1992). A hypothetical, deterministic model of operant responding under fixed-interval (FI) reinforcement schedules was also presented (Hoyert 1992).

These efforts marked only the beginning of the application of chaos theory in the study of life sciences. There remains a host of open questions in the study of non-linear properties of living organisms. For example, the application of the return map (RM), a tool used to reconstruct the multi-dimensional phase space out of one dimensional inter-response time data, in the study of operant behaviors of pigeons has only led to limited success (Weiss, 1970; Palya, 1992), encouraging the author to modify the RM, and to invent a new analyzing tool, the Extended Return Map (ERM, Li & Huston 2002). The application of the ERM in the analysis of operant behavior of rats under the fixed-interval (FI) reinforcement schedules, the dynamical mechanisms governing this behavior as well as the application of this new analyzing tool to behavioral pharmacological studies are the central topics of the present work.

1.3 Tools for nonlinear dynamical systems' analysis

1.3.1 Phase space

From one point of view, Lorenz's discovery implies the end of any hope for long-term prediction of non-linear dynamical systems. From another point of view, his works showed

us a new way to deal with systems with irregular appearances. If we look at the time series of any of the three variables in Lorenz's equations, we will fail to find any regularity. However, if we use the three variables as coordinates to construct a 3-dimensional Euclidean space, that is, the phase space, we will find that Lorenz's system is bounded, and its trajectory has a distinct form. The phase space of a dynamical system is a mathematical space with orthogonal coordinate directions representing each of the variables needed to specify the instantaneous state of that system. The bounded structure of a trajectory in the phase space is the "attractor" of the system. Within the basin of the attractor, no matter where the system initially starts, its time evolution will eventually fall into this bounded area.

The structure of attractors reflects the mechanism that governs the dynamics of the system. Simple dynamical systems, such as linear oscillators, or idealized pendulums, have simple geometrical forms, such as closed loops. Non-linear dynamical systems, for example, Lorenz's system, have very complex structures. The construction of phase space can be regarded as the first step in the nonlinear dynamical systems approach, and the ultimate goal is to find a theoretical model of the dynamical mechanism.

1.3.2 Reconstruction of a phase space from one-dimensional time series

To construct a phase space, the position of each variable must be known with infinite precision through time. Unfortunately, in most behavioral experiments, only few of the variables involved in a particular experimental situation are known. Even less understood is how these variables change over time. In order to circumvent this problem, we can reconstruct a multi-dimensional space with delay-coordinate vectors, which are vectors of time series measurements of one observable of a system. Analyses of this type were suggested in physics (Packard et al. 1980) and their validity has been demonstrated mathematically (Takens 1981). The delay-coordinate method is widely used in all fields of studies employing nonlinear dynamics.

The Skinner box experiment faces another problem when applying the delayed-coordinate method. The data set recorded here, the inter-response-times (IRT), is in fact a time series with time itself as the observable, and it is sampled in irregular time intervals along the time-axis. This problem is common for all systems that can be classified as "point processes", such as the inter-spike-interval of neuronal firing (e.g. Suzuki et al. 2000), or the R-R interval from electrocardiogram (ECG) studies (e.g. Guzzetti et al. 1996). Although it is possible to first convert the IRT data into response rates, thus making it uniform along the time axis, there are many settings where it is more interesting to analyze the IRT data directly (Kantz & Schreiber 1997 pp. 145-148). Instead of the time-coordinate, the basic idea of a delayed-coordinate method can be extended to the order-coordinate. A diagram drawn in this manner is the so-called "Return Map (RM)" (e.g. Shaw 1984; Braun & Lisbôa 1994).

In some early applications to operant experiments the same tool was in use, and was called "recurrent plots" (Weiss 1970; Palya 1992). Such diagrams were said to show the sequential dependence of IRTs. If IRTs are bounded by some kind of dynamic mechanism with low dimensionality, the variation of IRTs should be deterministic and the RM should be able to capture the structure of the function that describes the dynamic mechanism (Kantz & Schreiber 1997 pp. 145-148). However, these applications of the RM in Skinner-box experiments achieved only limited success (Palya 1992). It seems that the adjacent IRT data might not possess a low-dimensional, deterministic relationship. However, it is still possible that there is a "long term" relationship in the sequence of a IRT data set, and its assessment demands improvement of the analyzing ability of this tool. Therefore, we modified the original definition of the RM and developed the "Extended Return Map (ERM)" (Li & Huston 2002). Formal definition of the ERM will be introduced later in section 2.

1.3.3 Fractals and fractal dimension

Attractors of nonlinear dynamical systems possess complex geometrical structures.

Direct interpretation is usually very difficult. It is often advantageous to first run simulation studies of theoretical models, and then compare the simulated attractors with the experimental results. Thus, a complete nonlinear dynamical system's approach should include both experimental and simulation studies. Nevertheless, there are some geometrical properties of the attractors that don't need simulations. These properties could be helpful in the study of nonlinear dynamics of the system.

The geometrical structures of chaotic attractors belong to a special class of geometrical forms called "fractals". As the magnification of a fractal object increases, more fine structures will be revealed. Furthermore, the shape of the finer structures looks similar under different scales. This property is called the "self-similarity", and it can be quantitatively measured using the fractal dimension. Unlike the topological dimension, which is always an integer, the fractal dimension can be an integer or a fraction. It describes how an object fills up space.

Several mathematical definitions of fractal dimension have been suggested. According to the works of Grassberger (1983) and of Hentschel and Procaccia (1983), the correlation dimension of a point set $\{X_1, X_2, ..., X_M\}$ is defined through the following equation:

$$\nu = \lim_{\varepsilon \to 0} \frac{\ln C(\varepsilon)}{\ln (\varepsilon)} \quad . \qquad (1)$$

Here $C(\varepsilon)$ is defined as

$$C(\varepsilon) = \lim_{M \to \infty} M^{-2} \times \{ \text{number of pairs } (X_i , X_j) \text{ with } | X_i - X_j| < \varepsilon \}.$$

M is the amount of data in the time series; ε is a value predefined to calculate $C(\varepsilon)$.

In practice, several ε values between the resolution of measurements and the size of attractors are chosen. Then the corresponding $\ln C(\varepsilon)$ are calculated and plotted against $\ln(\varepsilon)$.

The slope of the resulting regression line is taken as the correlation dimension ν. In the present work, the resolution of the IRT data is 0.01 sec, and the size of ERM-patterns is in the order of 10 sec. Although it is not certain, whether or not the extended return map is a topologically equivalent reconstruction of the phase diagram, it is still possible to calculate the fractal dimension, because the mathematical definition in equation (1) is applicable to any point sets. The only constraint is the number of data points. Theoretically, infinitely many data points are required in order to obtain an exact value. In practice, the amount of data should be reasonably large (Ott et al. 1994). For Skinner-box experiments, this condition is relatively easy to fulfill.

Even if the meaning of this value calculated from the ERM differs from the dimension of attractors found in a real phase space, it is still interesting to determine, whether or not it can serve as a quantitative measure of behavioral patterns in animals receiving different reinforcement schedules and/or physiological treatments. In the present studies, the correlation dimension serves as a quantitative measure of the geometrical features of the ERM-patterns, and enables a quantitative comparison between experimental ERMs and ERMs of surrogate data sets (see below).

1.3.4 Study with surrogate data sets

Since experimental data is always contaminated with noise, the differentiation of information of a system's dynamics from disturbance by noise becomes a critical point in a non-linear analysis. We wish to determine whether our findings in the extended return map really reflect the system's dynamical properties, or whether they are simply caused by the analyzing procedure. One way to clarify this, is to test the results with surrogate data sets which have the same statistical properties as the original data, such as mean, variance and power spectra, while the deterministic dynamical information is destroyed.

As mentioned in section 1.2, a deterministic dynamical process correlates the present

state of the system to its history. Mathematically it can be expressed by the following general form: $\mathbf{X}(t) = \boldsymbol{f}[\mathbf{X}(t-1)]$. Here $\mathbf{X}(t)$ and $\mathbf{X}(t-1)$ are two sets of measurements of the system's state variables that are observed at time t and at a previous time t-1. The function $\boldsymbol{f}$ represents the deterministic dynamical process. In other words, if we assume that there is deterministic dynamics in our system, the time series data recorded in the experiment should possess sequential dependences described by $\boldsymbol{f}$. Randomly shuffling the sequential order of the time series data will destroy this correlation. Now, if the patterns in the reconstructed phase space somehow represent the deterministic dynamical correlation $\boldsymbol{f}$, these patterns will also be different after changing the sequential order of the time series data. If, however, the patterns remain unchanged in the phase space reconstructed using the surrogate data set, then we can say that the original time series data does not have sequential dependence.

It was found that random shuffling the sequence of time series data is a very severe method to generate surrogate data, since it will destroy all the sequential correlation. Theiler suggested that, for the testing of deterministic relationships in dynamical processes, it might be sufficient to generate surrogate data sets which have the same first order correlation as the original one, but all higher order correlations are removed (Theiler et. al. 1992; Liebovitch 1998 pp. 220-221). For simplicity, and in order to avoid achieving false positive results for the test of the newly developed method ERM, we applied only the random shuffling method to generate the surrogate data sets.

In the present study, 9999 surrogate data sets were generated. Together with the experimental IRT data, 10000 values of correlation dimension can be calculated. Thus a frequency distribution of the surrogate dimensions could be established. The location of the experimental fractal dimension on the diagram of the surrogate distribution quantitatively estimates the probability of acquiring the experimental IRT data by chance. This value will

be called the "by-chance-probability" throughout the present work.

1.4 The Extended Return Map (ERM)

1.4.1 The delayed-coordinate method

Suppose that there is a set of one-dimensional time series data $\boldsymbol{X} = \{X(\mathbf{t}) \mid \mathbf{t} = \text{time}\}$ whose elements $X(\mathbf{t})$ are results of a scalar measurement on a system at time $\mathbf{t}$. Then the $\mathbf{d}$-dimensional reconstruction of phase space using the delayed coordinate method with a time lag $\mathbf{L}$ is given by

$$\{ (X(\mathbf{t}), X(\mathbf{t} + \mathbf{L}), \ldots, X(\mathbf{t} + (\mathbf{d}\text{-}1)\mathbf{L}) \} \qquad (2)$$

Takens (1981) was able to show that if $\mathbf{d} = 2\mathbf{D} + 1$, here $\mathbf{D}$ is the dimension of the original phase space**,** and if the measurement $\boldsymbol{X}$ fulfilled some conditions, then the attractor in a delayed-coordinate-reconstruction would have the same topological properties as the attractor in a real phase space. Takens' work is known as the "delayed embedding theorem". Sauer et. al. (1991) were able to generalize this theorem to conditions with $\mathbf{d} > 2\mathbf{D}_{\mathbf{box}}$, where $\mathbf{D}_{\mathbf{box}}$ is the box counting dimension, a kind of fractal dimension, of the attractor. They call this theorem the "fractal delay embedding prevalence theorem".

1.4.2 The Return Map (RM) and the Integrate-and-Fire model

In the embedding theorem the time series $\boldsymbol{X}$ is the measurement of one of the system's variables. In some situations, the recorded signal itself is quite uninteresting and the relevant information is contained in the time intervals between certain characteristic events. Such a system is known as a "Point Process". The R-R intervals obtained from electrocardiograms, or the inter-response time (IRT) data from Skinner-box experiments are examples of such systems. This kind of "time" series is, in fact, a "sequence" series, since the indices of data are the sequential orders of the events, and the data itself are the "true" times.

Although it is theoretically possible to convert such time series to frequencies of

events at different instances, hence making the data uniformly spaced along the time axis, it is often more interesting for non-linear dynamical analysis to reconstruct a multi-dimensional space using the inter-event intervals directly. The **d**-dimensional reconstruction with time lag **L** of a series of inter-event-times: { $IET_{\mathbf{n}}$ } will be given by the following point set:

$\{(IET_{\mathbf{n}}, IET_{\mathbf{n-L}}, \ldots IET_{\mathbf{n-(d-1)L}}) \mid$ where **n** indicates the sequential order of events$\}$ (3)

A reconstruction of this kind is the "Return-Map (RM)", and it is widely used in many fields, for example, in the study of physical systems (Shaw, 1984), heart rate (Guzzetti et al., 1996), and neuronal firing (Hayashi & Ishizuka, 1995). It was also applied in the study of operant responses in a Skinner-box (Palya, 1992).

From a mathematical point of view, it is not sure whether or not the RM fulfills the requirement of Taken's embedding theorem. This implies that the attractor in a RM might be topologically different from that in the original phase space. In the studies of non-linear dynamical models of neuronal firing Sauer (1994) introduced an "Integrate-and-Fire" model. It was assumed that a time series *S(t)* from the dynamical system is integrated with respect to time, and when it reaches a threshold θ, a spike is generated. He showed that if the firing times T_i and the neuronal signal *S(t)* satisfy the relationship,

$$\int_{Ti}^{Ti+1} S(t)\,dt = \theta \qquad \text{i = 1 to end of the data set} \qquad (4),$$

then the embedding theorem can be applied to RMs constructed by interspike intervals ISI(i) = $T_{i+1} - T_i$. However, it was suggested both in the study of real neuron-firing and in the study of computer simulations, that the conditions stated by the "Integrate-and-Fire" model are very difficult to fulfill. Even if it is possible to build a RM using the inter-spike interval of neuronal firing, the reconstructed attractors might have an appearance different from the one in the real phase space (Suzuki et al., 2000).

Previous application of the RM in Skinner-box experiments achieved only limited success (Palya, 1992). Apparently such operant behaviors cannot be fitted into Sauer's "Integrate-and-Fire" model. In fact, the frequency distributions of most of the IRT data from Skinner-box experiments resemble exponential curves (see figure 21), which suggested that the IRT-data might be created by a Poisson process. In other words, it seemed better to describe the operant behavior by using a probability function of occurrence rather than using a deterministic function that computes the length of IRTs. On the other hand, animals do show some kinds of behavioral rhythms under certain experimental conditions, such as under the control of FI-schedules. Can the non-linear dynamical analyzing tools extract information about the dynamic of this rhythmical behavior? In order to accomplish this task, we modified the original RM, and invented the "Extended Return Map (ERM)".

1.4.3 Formal definition of the Extended Return Map (ERM)

Data suitable for the application of the ERM is the same as for the original RM, and consists of sequences of time intervals between events, the inter-event-time (IET), or, in the case of Skinner-Box experiments, the inter-response-time (IRT). The first step in the construction of an ERM was to calculate a new data set consisting of the moving average of the original IRTs according to the following equation (Li & Huston, 2002):

$$^{\mathbf{f}}MV_{\mathbf{n}} = \sum_{k=n}^{n+f-1} IRT_{\mathbf{k}} / \mathbf{f} \qquad (5)$$

The parameter **f** specifies the range within which the moving average is computed. In the nomenclature of traditional time series analysis, parameter **f** would be called the "window" of the moving average. A **d**-dimensional ERM is constructed using the following point set:

$$\{(^{\mathbf{f}}MV_{\mathbf{n}}, ^{\mathbf{f}}MV_{\mathbf{n-L}}, ^{\mathbf{f}}MV_{\mathbf{n-2L}}, \ldots ^{\mathbf{f}}MV_{\mathbf{n-(d-1)L}}) \mid \mathbf{n} \text{ indicates the time order of data points}\} \qquad (6)$$

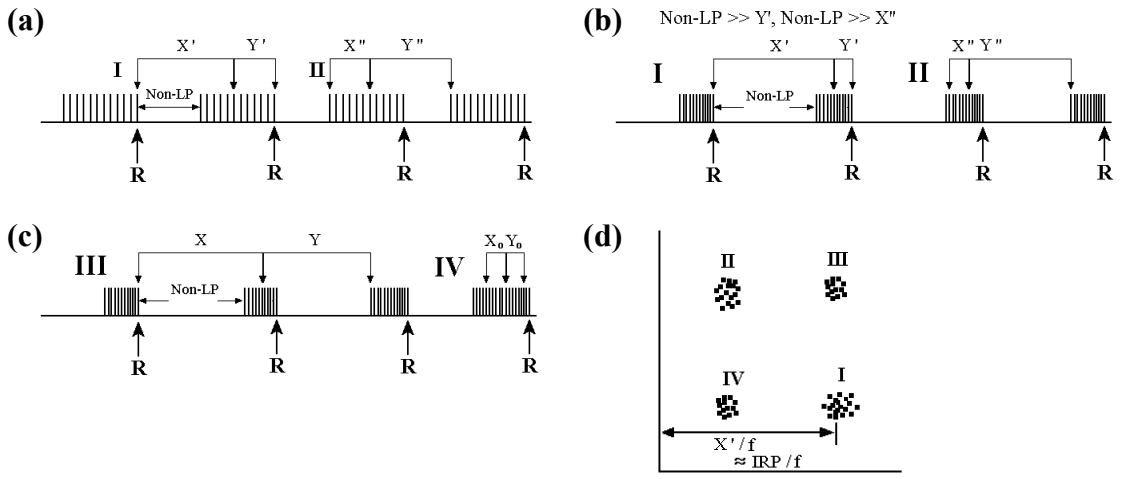

Figure 2
Choice of suitable parameters **f** and **L**. (a) The basic pattern of FI-responding is the switch between "Non-LP" and "LP" state. The parameters **f** and **L** are chosen so that the pairs of moving average windows X'Y' and X"Y" fill up the inter-reinforcement period. (b) IRTs within the LP-state are usually much shorter than the length of the Non-LP state. (c) Since the number of responses within an inter-reinforcement period varies, sometimes both of the moving average windows cross a Non-LP state (III), or sometimes they both stay within a LP-state (IV). (d) Situations in (a)-(c) will produce four clusters I, II, III and IV.

The parameter **L** is called the "lag" of the ERM. It defines the delay of the Y-coordinates in comparison with the X-coordinates. Both **f** and **L** must be integers.

1.4.4 Choice of the parameters f and L

The patterns seen in the ERM change with parameters **f** and **L**. In the special case where the parameter **f** =1, the ERM becomes identical with the original RM. In a simulation study we found that the dynamics of FI-responding is characterized by an abrupt switching between lever-pressing (LP) and non-lever-pressing (Non-LP) states during the inter-reinforcement period (see section 3.1.2). This can be demonstrated using the example in figure 2a, in which the number of lever presses (LP-number) per inter-reinforcement-period (IRP) is constant and has a value of 12. Now, if we choose a set of parameters **f** and **L**, so that they equal one half of the LP-number in an IRP (in this example: **f** = **L** = 6), the windows X' and Y' of the moving average will cover exactly one IRP as shown in situation I in figure 2a.

The total width of the moving-average-windows (X+Y) will be equal to the length of an IRP. This relationship remains true even if the moving-average-windows move forward; for example the windows X"Y" in situation II in figure 2a. Here the symbols X, X', X'' and Y, Y', Y" refer sometimes to the moving average windows themselves, sometimes to the "width" of the windows. However, it is usually clear which meanings the symbols shall have. Unless under ambiguous situations, the exact meanings of the symbols will not be specifically noted.

Usually the Non-LP behavioral state is much longer than the averaged lengths of IRTs in an LP-state as shown in figure 2b. Thus we have conditions that X'>>Y' and X"<<Y". This results in the clusters of points I and II shown in figure 2d. Furthermore, since the coordinates of data points in an ERM are defined by "moving average / **f** ", the x-coordinate of cluster I is X'/**f**, and the y-coordinate of cluster II is Y"/**f**.

In the examples in figures 2a and 2b, we assume that the LP-number in each IRP remains constant. In real data, however, the LP-number varies from IRP to IRP, like the example shown in figure 2c. If we define the parameters **f** and **L** to be equal to the averaged LP-number per IRP, we will observe situation III in figure 2c, where the momentary LP-number in that IRP is smaller than the average. We will also observe situation IV, where the momentary LP-number in that IRP is larger than the average. Situations III and IV in figure 2c lead to the formation of clusters III and IV in figure 2d.

Furthermore, if the length of Non-LP is much larger than the width of windows Y' and X" in figure 2b (windows Y' and X" cover only shorter IRTs in the LP-state), we can neglect Y' and X", and the width of the windows X' and Y" will be approximately equal to the length of an IRP. Thus, the x-coordinate of cluster I will approximate "IRP/**f** ". The same is valid for the y-coordinate of cluster II. Under the same conditions we can also neglect the contributions of the shorter IRTs in the LP-state in the averaging windows X and Y in situation III of figure 2c. As a result, windows X and Y will both approximate the length of

an IRP. This leads to the result that the x- and y-positions of cluster III in figure 2d will approximate "IRP/**f** ".

We can make use of this property and adjust the maximal scale of ERM-diagrams in such a way that the cluster III always remains in the same position in the image. For example, if the IRP is 60 seconds, and the averaged LP-number per IRP is 20, then we can define **f** = **L** = 10, and the position of cluster III will be 6 seconds. Then we can set the maximal scale of the ERM-diagram to be 12. This setting results in an image, in which cluster III is located in the center. Now if another animal (or the same animal in another session) produces on the average 10 LPs per IRP under a reinforcement schedule of FI-40s, we can define **f** = **L** = 5 and scale the ERM-diagram to have maximally 16 seconds in both axes. This setting will also produce an image with the cluster III located in the center. The advantage of this setting is that we can easily compare ERMs of different animals, or different sessions run on one animal, even if the structures in the ERMs are different from that shown in figure 2d.

Throughout the present work we follow this choice of parameters and define **f** as one half of the averaged number of lever presses per IRP in a session. Usually, the averaged LP-number per IRP is not an integer. In that case, we round the value to the closest integer. Parameter **L** is set to be equal to **f**. The maximal scale of ERM-diagrams is adjusted to be approximately three and a half times the value of "IRP/**f** ".

1.5 Organization of the present work

The application of the newly developed analyzing tool, the ERM, to analyze the dynamics of operant behavior of rats under the fixed-interval (FI) reinforcement schedules is the central topic of the present study. Since the ERM is a modification of the widely used return map (recurrent plot), and since previous application of the return map did not achieve fruitful results, we were first interested in whether or not the ERM can reveal distinct patterns that cannot be seen in the original return map. If the ERM can really reveal distinct patterns,

we have to test the relationship of these ERM-patterns and the dynamics of our experimental data by using the studies with surrogate sets. Furthermore, we wished to study the process of acquisition of these "FI-dynamics". This process can be regarded as a learning process, and is by definition a dynamical process, since it expresses how the behavior adapted to a change in environmental parameters. We set out to assess this process by use of the ERM.

The ERM-patterns alone are not sufficient to understand the FI-dynamics, since we have to somehow interpret the patterns in terms of behavioral, and, if possible, physiological terms. To accomplish this task, we need to combine the experimental results with analytical as well as simulation studies. This part of our work is summarized by a comprehensive dynamical model of FI-responding. In addition to pure behavioral studies, we also wished to use this method in practical applications. For example, using the ERM-patterns as dependent variables might be very interesting in a behavioral pharmacological study. To test this possibility, we chose a well known substance, amphetamine, and observed changes of the ERM-patterns after animals received IP-injection of this drug. Furthermore, we tried to interpret this effect by using the dynamical model we proposed for FI-responding.

2 Experimental studies on the dynamics of FI-responding

2.1 Introduction to Skinner-box experiments

2.1.1 Operant behavior and Skinner-box

The origin of the study of operant behavior can be traced back to the works of Thorndike (1911). In his experiments, cats had to learn to escape from a small cage by operating a particular mechanism to open a door. In the beginning animals needed a lot of time to try out numbers of different ways, until finally the correct response was found by chance. After repeated training the time the animals required to escape from the cage became shorter. What the animals apparently learned was to drop out unsuccessful behaviors until little or nothing remained except the necessary response for operating the door-opening mechanism.

Later B. F. Skinner trained rats to press a lever in a small box, now known as the Skinner-box, to acquire food. Unlike Thorndike's cat, the rats in the Skinner-box exhibited little unnecessary behaviors prior to the beginning of learning, because Skinner adjusted the experimental conditions in such a way that unnecessary behaviors were reduced to a minimum. What Skinner observed was an increase in the rate of responding that led to food reward. Initially Skinner formulated his theory in terms of the "conditioned reflexes" originating from Pavlov (Skinner 1935). Later he left this line of stimulus-response conception and emphasized the fact that food delivery, as a stimulus, did not elicit the lever pressing behavior, but increased the frequency of it. Thus, instead of "conditioning", he used the term "reinforcement" to designate the effect of foods in strengthening the lever pressing behavior. Stimuli having similar effects like food were called "reinforcers". Instead of "reflex", he used the term "operant" to emphasize that lever pressing behavior need not be elicited by a stimulus. However, the presence of certain stimuli could influence the rate of lever pressing (Skinner 1937, 1938).

2.1.2 Fixed-Interval (FI) reinforcement schedules

One of the most important variables that influences operant behavior is the schedule by which the reinforcers are made available. In the original conception of operant, "right" behaviors are always rewarded and "wrong" ones remain always un-rewarded. This kind of reinforcement schedule is called "continuous reinforcement (CRF)". This is, however, quite untypical in a natural environment, where most reinforcements are available intermittently. In Skinner's early studies, the effects of different intermittent reinforcement schedules, including the fixed-interval (FI) schedule of reinforcement, were examined (Ferster & Skinner 1957).

In a FI-schedule the first response after a designated interval of time, the inter-reinforcement period (IRP), is followed by the delivery of a reinforcer. The first effect caused by this setting is the extinction of non-rewarded operant responses during the IRP. In addition to extinction, several contingencies are taken into consideration in the building of theoretical models: 1) Length of inter-response time. Since reinforcement is programmed by elapsed time in a FI-schedule, the longer the interval since the last response, the more likely the next response will be reinforced. This contingency leads to the differential reinforcement of low rates. 2) Responding rate. After a long time of training under the control of FI-schedules, animals usually show higher rates of responding before each food delivery (figure 1). This leads to differential reinforcement of relatively higher rates of responses. 3) Total number of responses per reinforcement. The average number of responses during a IRP could also be differentially reinforced, so that animals would be conditioned to emit a certain number of responses.

2.2 Traditional analysis of FI-responding

2.2.1 The cumulative record

In the early studies by Skinner (Ferster & Skinner 1957), cumulative records played an important role for the analysis of responding dynamics of operant behavior. In a cumulative

record, a pen is installed on a band of constantly rolling paper. Each time when an operant response is registered, the pen shifts one unit along the vertical direction. Thus, the course of operant responding is charted cumulatively over time on the paper. The cumulative record can be regarded as a plot of "number of responses" versus "runtime"; hence, it is a kind of "time series" data set.

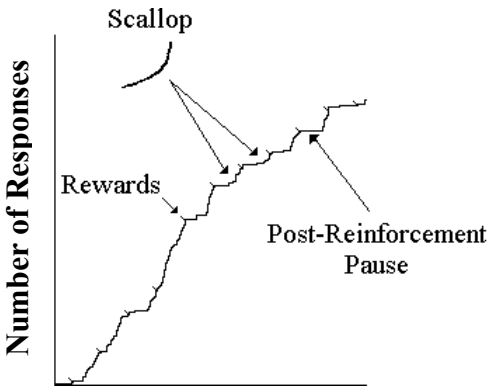

Figure 3: An example of cumulative records of FI-responding.

After several sessions of training under the control of FI-schedules, it is often found that animals make a short pause after the delivery of a reinforcer, which is called the post reinforcement pause. After the post reinforcement pause, the rate of responding increases gradually, and arrives at a constant "final-speed" before the delivery of the next reinforcer. This type of responding dynamic can be seen in a cumulative record as a concave-upward curve, which is often called the "scallop-curve" (see an example in figure 3). However, the regularity is constantly interrupted by variability in the length of the pause, the degree of acceleration, the total number of responses in the inter-reinforcement period, etc.. The whole picture of operant behavior found under the control of FI-schedules is, thus, a mixture of periodicity and irregularity. Variability can be seen not only between different individuals, but also within the same animal between different sessions, or even during different inter-reinforcement periods within a session.

2.2.2 The averaged scallop-curve

In the traditional analysis, an averaging process is usually applied to overcome the problem of variability. The inter-reinforcement period is first divided into several time-blocks with constant width. Then the number of responses in each block is counted throughout the whole session, and subsequently divided by the number of food rewards animals received in

the session. The final result is a plot of averaged rate of responses versus time after reinforcements, which shows the typical "scalloped-curve" (figure 1). The appearance of this curve suggests a sigmoid-like function, and constitutes the basis of several theoretical studies on FI-responding (Gibbon, 1977; Killeen & Fetterman 1988). However, several authors indicated that the averaged scalloped-curve might be created by dynamical mechanisms other than a continuous sigmoid-function (Schneider 1969; Dews 1978; Shull 1991). Nevertheless, it is still a convenient way to get an overview of the dynamics of FI-responding, and has played an essential role in the works by Machado and his co-workers (Machado 1997; Machado & Cevik 1998).

2.2.3 Summary of the traditional analysis

In conclusion, the traditional analysis can roughly reveal the following picture of operant responses under the FI-schedules: After intensive training of the FI-schedules, animals will learn to cease responding after receiving a reinforcer. Then the probability of responding will gradually increase, and arrive at its maximum before the onset of the next reinforcer. Exactly how the response probability varied with time, is still under study.

Although the analyzing tool and the conception of the nonlinear behavior dynamics are very different from those of the traditional analysis, the experimental setups remain almost the same. The non-linear dynamical analysis provides simply a different point of view.

2.3 Materials and methods

2.3.1 Animals and apparatus

Experimentally naive white Wistar rats obtained from the TVA (Tierversuchsanlage) at the University of Düsseldorf were used in the present study. They were 2 months old and weighed between 220 and 260 g at the beginning of the experiment. They were housed in individual cages with free access to water. Illumination was controlled artificially under a 12 hours day/night period. During the experiments, the amount of food was restricted to

maintain the animals' weight at about 85~90% of their free-feeding levels. The food pellets consumed during trials in the Skinner-Box were also taken into account.

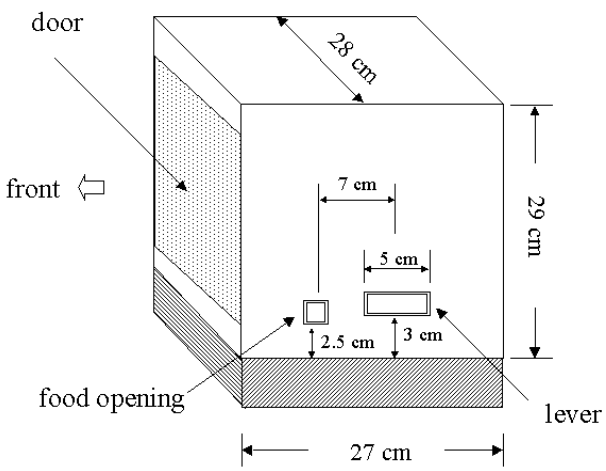

Figure 4: Sketch of a Skinner-box used in our experiments.

Three Skinner-Boxes (28 cm × 27 cm × 29 cm) made of metal were placed separately into wooden sound attenuating chambers (130 cm × 59 cm × 103 cm). A 5 cm wide, 1 cm thick lever of metal was installed about 3 cm above the floor. It was located in the middle of the wall to the right of the door. The opening of the food-delivery machinery was about 2.5 cm above the floor, and was located at the right side of the lever, with a distance of 7 cm measured from the center of the lever (see figure 4 for a sketch). A 40 W bulb was used in each chamber as a source of light. Luminance measured in the middle of the Skinner-Boxes was about 12 LUX. Experiments were executed and controlled by a personal computer. A program running under MS DOS 6.2 was developed to control the hardware and to record data. The program was written and compiled with the programming language Turbo Pascal 7.0.

2.3.2 Time schedules of experiments

Experiments for the study of non-linear dynamics of FI-responding were conducted in four blocks (A ~ D). Each block consisted of at least three phases: shaping-, CRF-, and schedule-controlled phases. Blocks B, C and D included an additional treatment-phase in which amphetamine or saline were applied. Detailed description of amphetamine treatments will be described later in the section concerning pharmacological studies. The numeration of animals as well as the summary of experimental phases can be found in table 1 and 2.

Table 1 Time schedules of experiments

Experimental Phases	A	B	C	D
Shaping	5 x 20 min	5 x 20 min	5 x 20 min	5 x 20 min
Pause	3 days	3 days	3 days	3 days
CRF	1 x 90 min	1 x 90 min	1 x 90 min	1 x 90 min
FI-Schedule Control	15 x 90 min	15 x 90 min	15 x 90 □in	26 x 90 min
Drug Treatment	---	2 x 90 min	2 x 90 min	5 x 90 min

Table 2 Numeration and groups of animals

FI-Schedules	A	B	C	D
FI-20s	A1, A6	---	---	D3, D4, D8
FI-40s	A2, A4	B3, B5	C2, C4	D2, D6, D7
FI-60s	A3, A5	B2, B4	C1, C6	D1, D5, D9
FI-90s	---	B1, B6	C3, C5	---

The operant response in the present work is the pressing of a lever, which is not a natural behavior of rats. As a result, the probability was very low that animals pressed the lever before they had learned the connection between lever pressing and food-delivery. In order to accelerate the speed of learning, it is advantageous to install a so-called shaping phase in the beginning of each experiment. The detailed procedure of shaping used in the present work was similar to that described in the original work of Skinner (1938, pp. 61). The shaping phase lasted five days. Each rat stayed at least 20 minutes in the box every day. If an animal had learned the operant response and received 100 food pellets as reinforcement, the session was interrupted before the 20-minute runtime ran out.

After the end of shaping, the animals were subjected to a CRF-phase, in which they had to complete one 90-minute session under the continuous reinforcement schedule (CRF). The CRF-phase ensured the success of shaping, and allowed the animals to adjust to the extended duration (90 minutes) of the sessions in the schedule-controlled phase as well as in the treatment-phase of blocks B, C and D.

In the schedule-controlled phase the animals were assigned to one of the following groups: FI20s, FI40s, FI60s, and FI90s, and they had to complete a 90-minute session under the control of one of these FI reinforcement schedules every day. The designation of each group also specified the length of the inter-reinforcement period, namely 20, 40, 60 and 90 seconds. Each animal received the same FI-schedule during the whole schedule-controlled phase, but the length of the inter-reinforcement period differed between groups. In blocks A, B and C, the schedule-controlled phase lasted 15 days, and in block D it lasted 26 days.

For blocks B, C and D the schedule-controlled phase was followed by an additional treatment-phase, in which IP-amphetamine and/or saline injection was applied. Detailed descriptions of the time schedule of the treatment-phase will be described in section 4.2.

2.4 Results

2.4.1 Comparison between the RM and the ERM

Figures 5~8 show both the original "Return Maps" (upper panel) and the "Extended Return Maps" (lower panel) of all the groups from session 15. The parameters **f** and **L** of the ERMs are outlined in table 3. The choice of these parameters follows the rules discussed in section 1.4.4.

In the RMs, most of the data points are located near the zero point and along the two axes. In some RMs a slightly higher concentration of data points at position near the inter-reinforcement-period (IRP) along both axes can be seen. For example, in the RM of rat D3 (FI20s-group) the distribution of data points is denser between 10 and 20 seconds along both axes. Similar results can be seen at position from 25 to 40 seconds in RMs of rat A2, B3, C2, D6 and D7 (FI40s-group), at position from 30 to 60 seconds in RMs of rat B2 and D9 (FI60s-group) as well as at position from 50 to 90 seconds in RMs of rat C5 (FI90s-group). These data points might correspond to the first lever pressing after the post-reinforcement pause. Except for this, no other distinct structures can be identified.

Table 3 Parameters f, L and the "by-chance-probability" of experimental ERMs

Abbreviation: IRP/f = inter-reinforcement period / f; ExpD = experimental correlation dimension; MSurD = mean surrogate correlation dimension; ChP = by-chance-probability.

Schedule	Number	Response	Reward	f & L	IRP/f	ExpD	MSurD	Ch. P.
FI-20s	A1	7704	243	16	1.3	0.7011	0.9166	0.01%
	A6	2243	250	4	5	1.4358	1.5259	0.09%
	D3	1762	253	3	6.7	1.3035	1.3945	0.01%
	D4	5616	263	11	1.8	1.1417	1.4064	0.01%
	D8	1686	254	3	6.7	1.2419	1.1856	3.86%
FI-40s	A2	1386	122	6	6.7	1.3878	1.4431	1.22%
	A4	7179	90	40	1	0.4365	0.8022	0.01%
	B3	838	129	3	13.3	1.2977	1.3443	1.86%
	B5	3413	132	13	3.1	1.5097	1.5796	1.32%
	C2	1039	127	4	10	1.2921	1.3744	0.02%
	C4	2252	132	9	4.4	1.5272	1.7054	0.01%
	D2	2492	131	10	4	1.3572	1.6046	0.01%
	D6	1697	131	6	6.7	0.7778	1.0015	0.01%
	D7	1465	131	6	6.7	1.3480	1.4190	0.23%
FI-60s	A3	1635	87	9	6.7	1.0424	1.2229	0.01%
	A5	1072	86	6	10	1.3570	1.3130	6.12%
	B2	3136	88	18	3.3	0.9341	1.0828	0.81%
	B4	4222	89	24	2.5	1.5886	1.3881	0.01%
	C1	2585	87	15	4	1.6202	1.5631	2.93%
	C6	5904	89	33	1.8	1.1203	1.2159	11.60%
	D1	2642	88	15	4	1.3133	1.5046	0.01%
	D5	1813	87	10	6	1.6039	1.6398	5.31%
	D9	765	87	4	15	1.0069	1.0654	5.75%
FI-90s	B1	1521	58	13	6.9	0.9857	1.3009	0.01%
	B6	636	55	6	15	0.8404	1.1036	0.01%
	C3	788	58	7	12.9	1.0218	1.2544	0.01%
	C5	1224	58	11	8.2	1.0281	1.1845	0.03%

The ERMs of the FI20s-group are shown in the lower panel in figure 5. The five ERMs can be roughly classified into three types according to their patterns. The ERMs of rats A1 and D4 show a big cluster near the left-bottom corner with approximately a triangle form. In the ERM of rat D4 there is an additional "center cluster" at the position X=Y=1.8 seconds.

FI20s Session 15

Return Maps

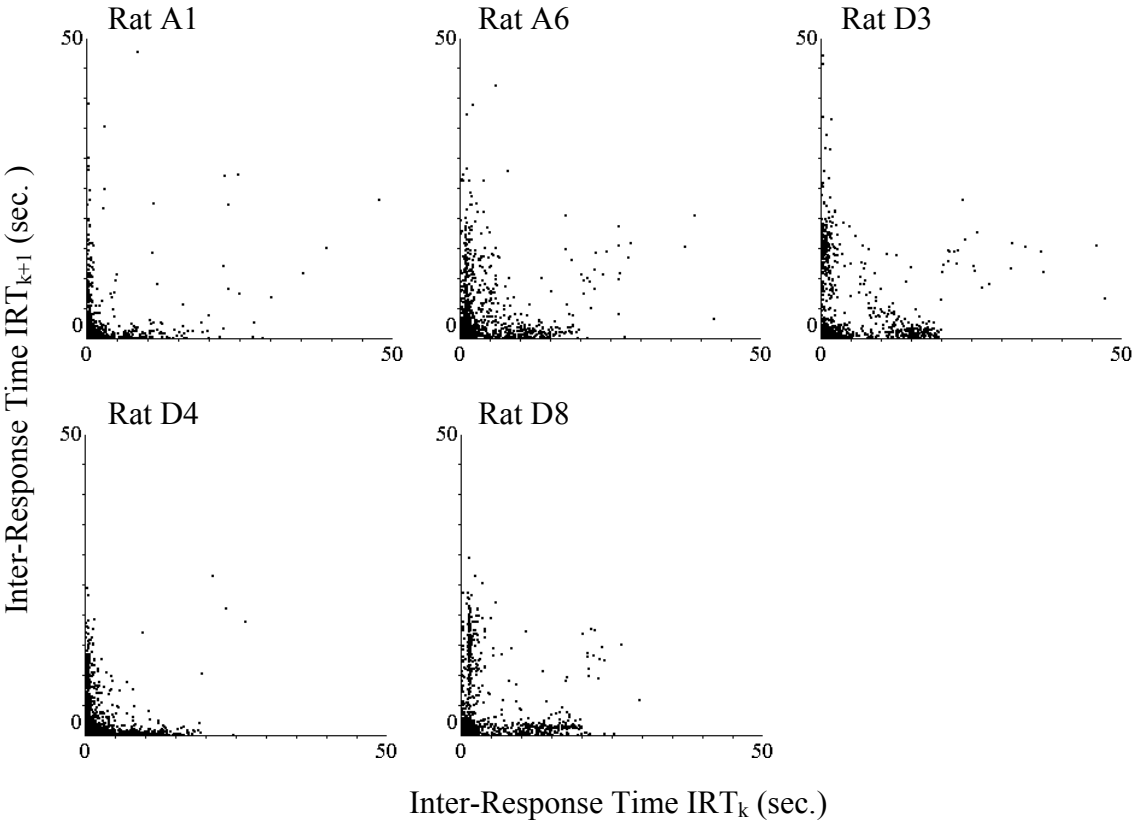

Extended Return Maps

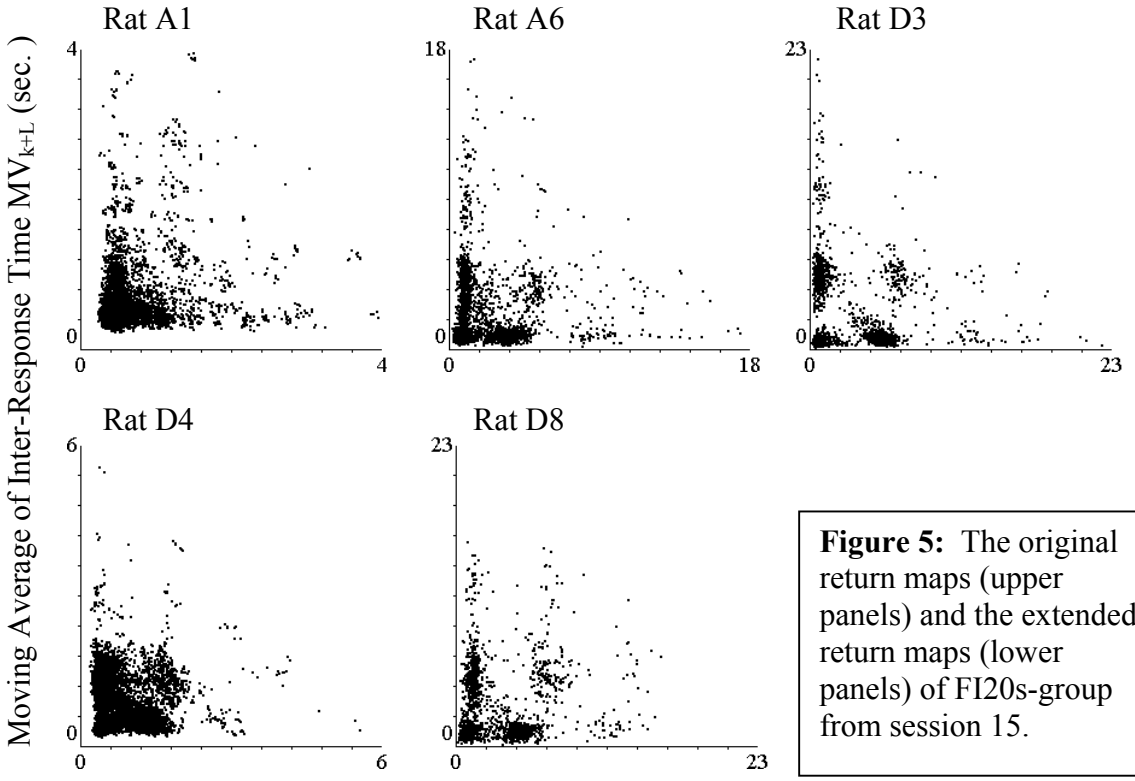

Figure 5: The original return maps (upper panels) and the extended return maps (lower panels) of FI20s-group from session 15.

FI40s Session 15

Return Maps

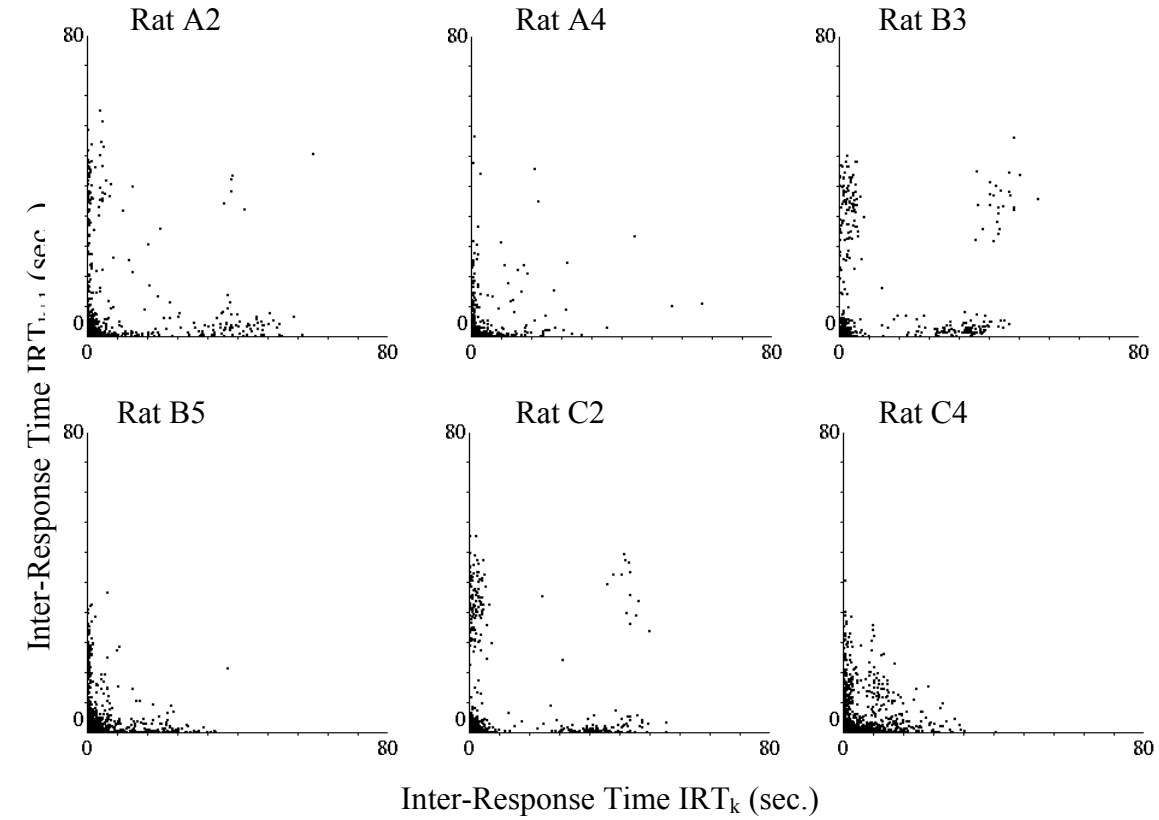

Extended Return Maps

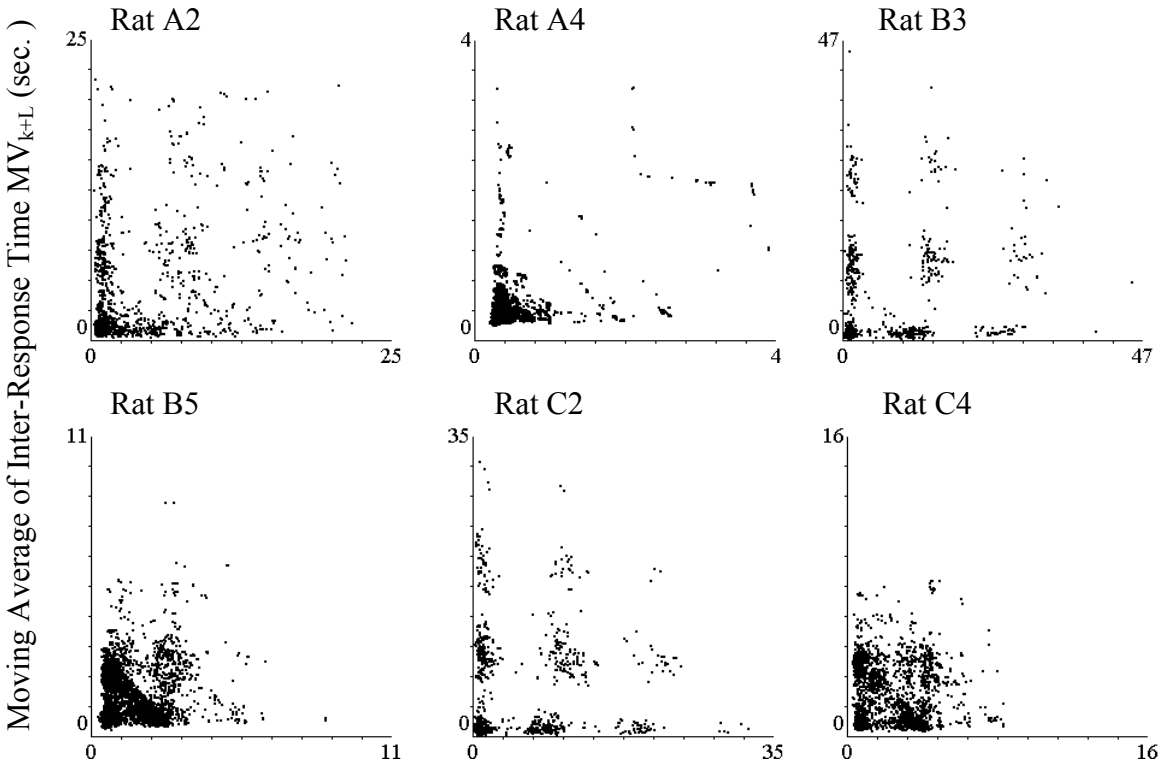

Figure 6: the original return maps (upper panels) and the extended return maps (lower panels) of FI40s-group from session 15. (continued in next page)

FI40s Session 15 (continued)

Return Maps

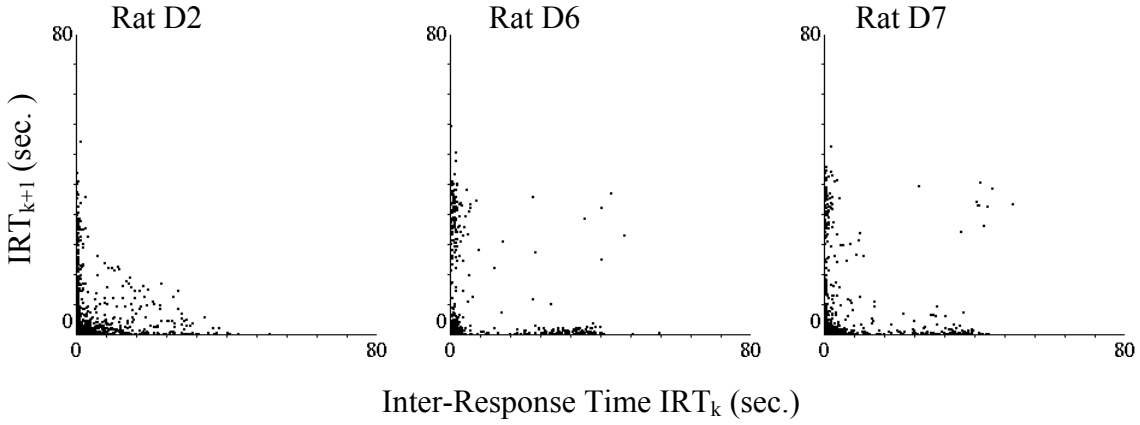

Extended Return Maps

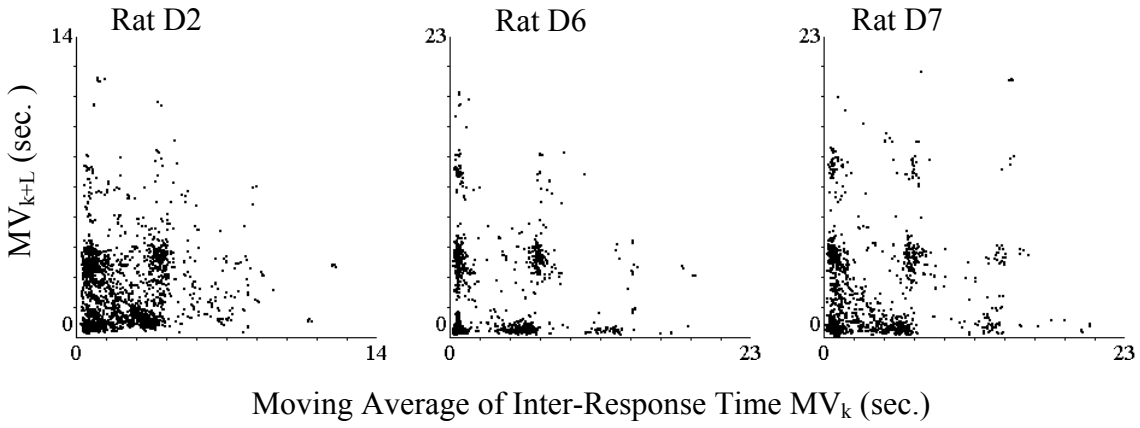

Figure 6: (continued from the previous page) The original return maps (upper panels) and the extended return maps (lower panels) of FI40s-group from session 15.

This value is about equal to the term IRP/**f**. This "center cluster" is analog to the cluster III in ERM of rat D4 there is an additional "center cluster" at the position X=Y=1.8 seconds. This value is about equal to the term IRP/**f**. This "center cluster" is analog to the cluster III in figure 2d. The point density and clearance of this central cluster play an important role in the dynamics of FI-responding. Detailed explanation will be discussed in section 3.2. The ERMs of rats A6 and D8 represent another type, in which a L-form cluster near the left-bottom corner, and the "center cluster" at the position X=Y= IRP/**f** can be identified. The ERM of rat D3 can be classified as the third type. Here several clusters are clearly separable and they form together a lattice structure. Again, the term IRP/**f** plays an important role in the

FI60s Session 15

Return Maps

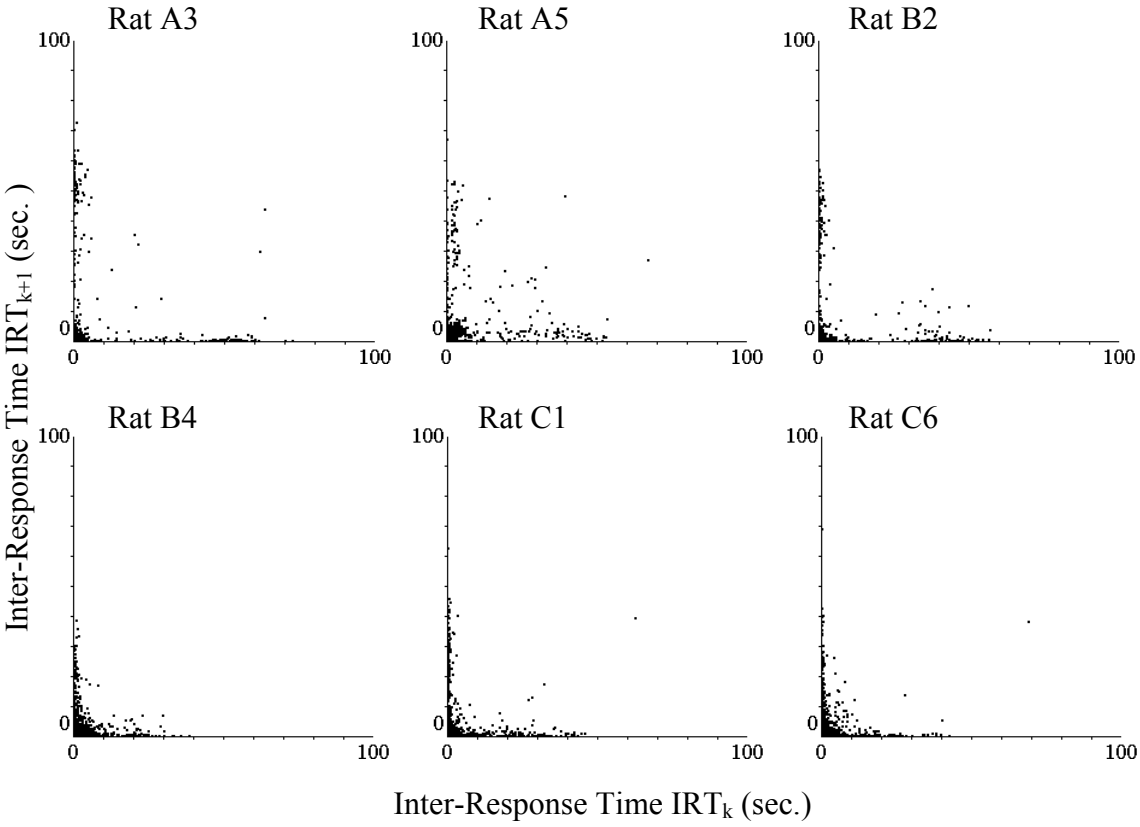

Extended Return Maps

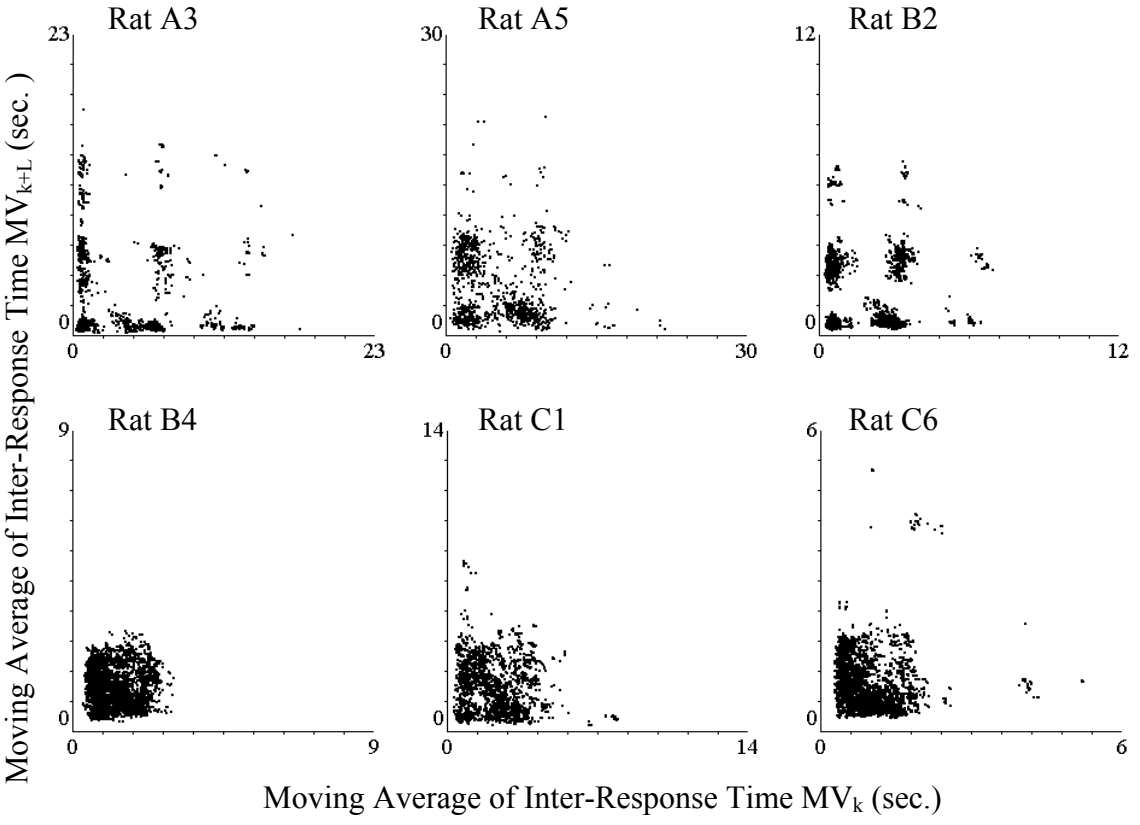

Figure 7: the original return maps (upper panels) and the extended return maps (lower panels) of FI60s-group from session 15. (continued in next page)

FI60s Session 15 (continued)

Return Maps

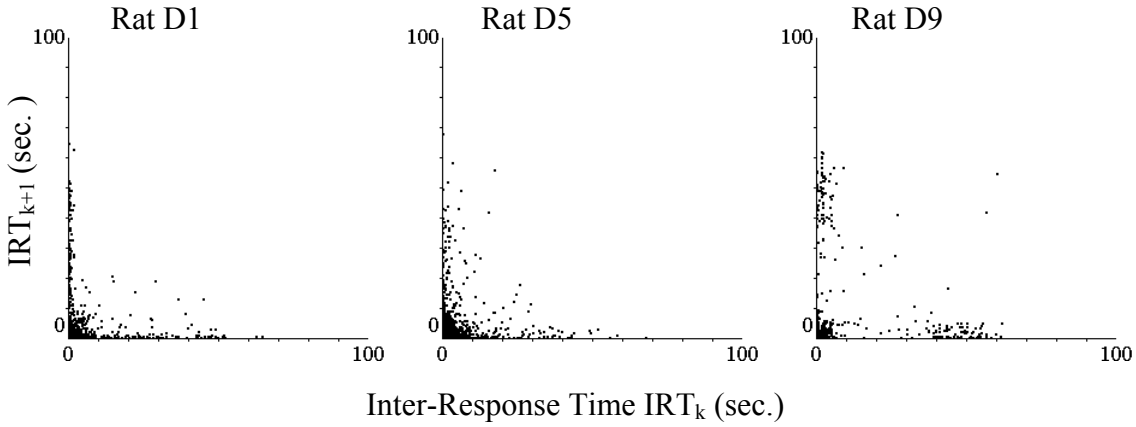

Extended Return Maps

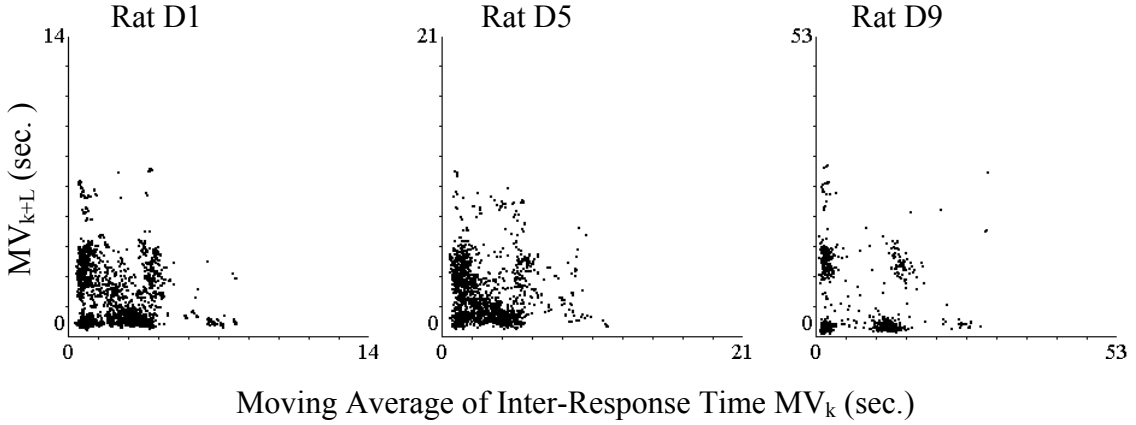

Figure 7: (continued from the previous page) The original return maps (upper panels) and the extended return maps (lower panels) of FI60s-group from session 15.

positioning of the clusters. Firstly, the "center cluster" at position X=Y= IRP/f can be identified. Secondly, the distance between clusters approximately equals the term IRP/**f**. In addition to the position of the clusters, the geometrical form of the cluster is also important. Especially the cluster at position X=IRP/**f**, Y~0 (analog to the cluster I in figure 2d) shall be examined with more care. Here the point-density along the diagonal direction plays an important role in the dynamics of FI-responding (see section 3.2 for detail).

Figure 6 shows the results of the FI40s-group. The ERM-patterns also have some distinct structures similar to those of the FI20s-group: 1) a triangle (number A4, B5, C4, D2 and D7) or L-form (number A2 and B3) cluster near the left-bottom corner, 2) a center cluster

FI90s Session 15

Return Maps

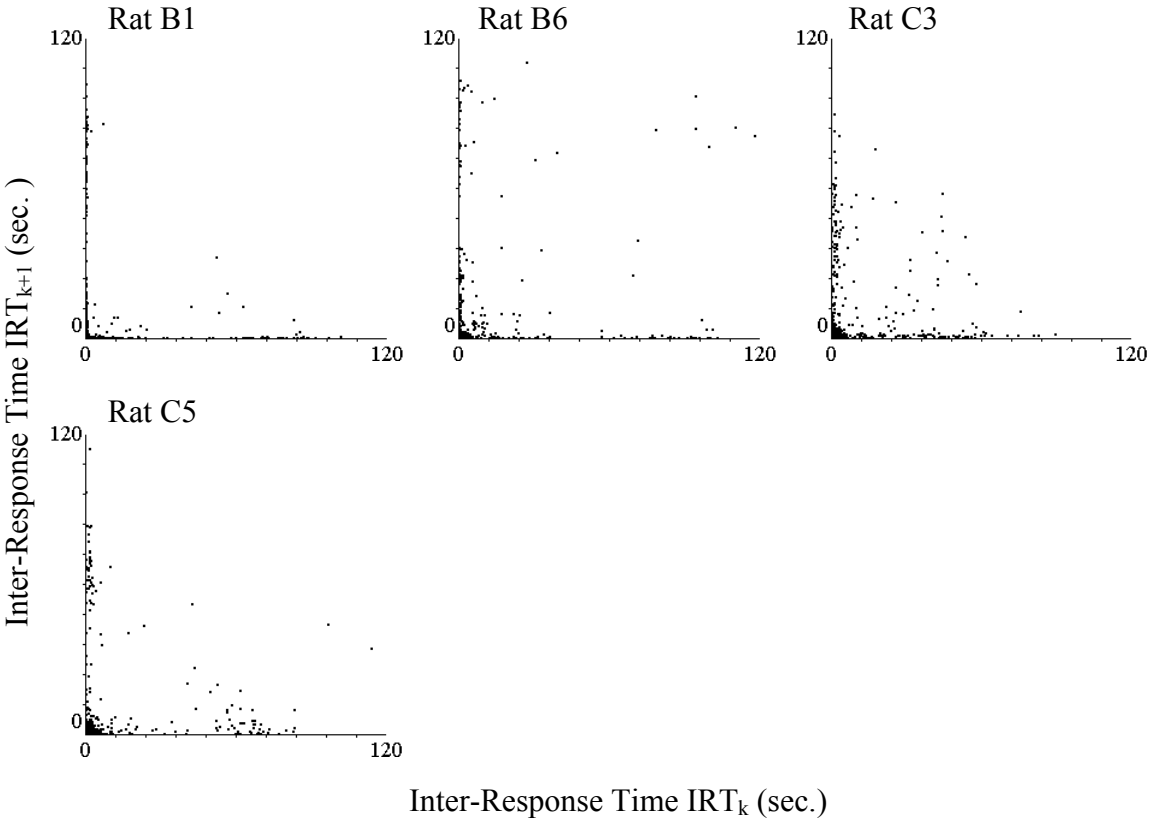

Extended Return Maps

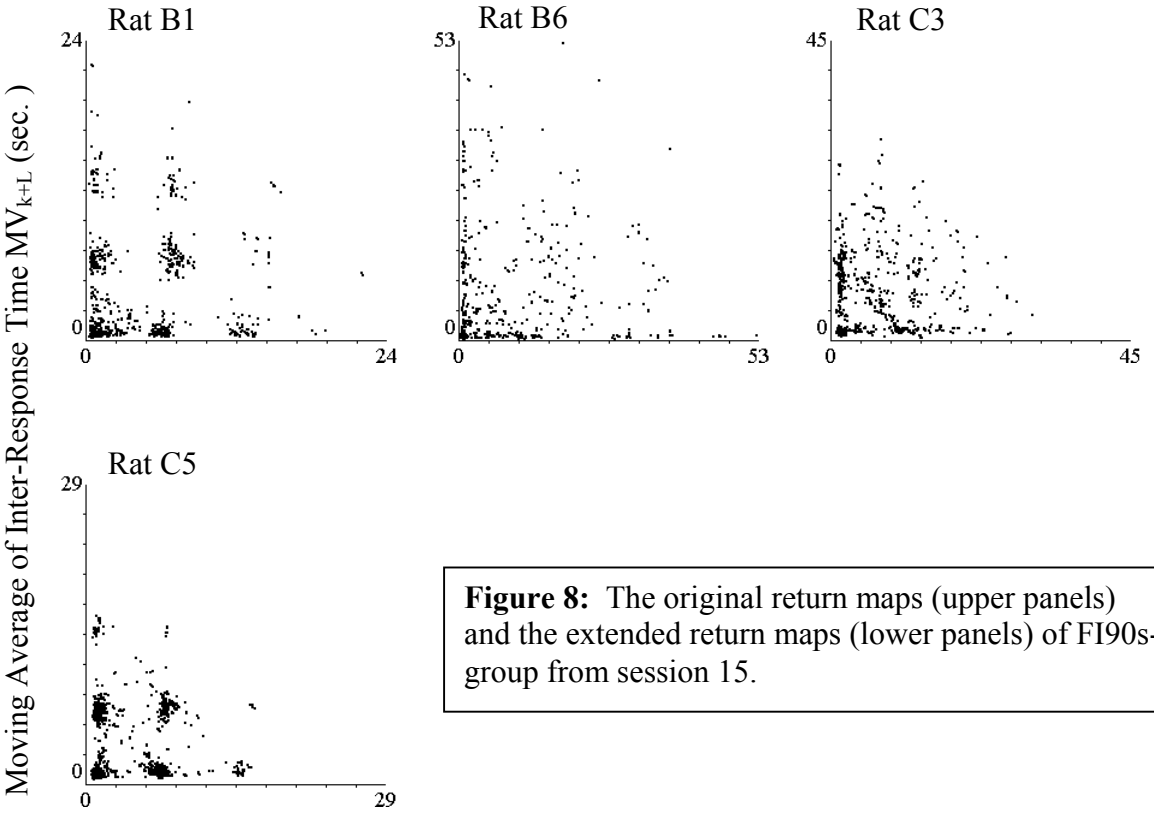

Figure 8: The original return maps (upper panels) and the extended return maps (lower panels) of FI90s-group from session 15.

at position IRP/f (all rats except number A4), and 3) lattice structure formed by several clusters with distance ≈ IRP/**f** (number B3, C2, D6 and D7). The separation between types has no clear-cut boundary. For example, data points in the ERM of number A2 are very diffuse and form only a very diffuse L-form cluster. The ERM of number D7 shows both a triangle cluster at left-bottom corner, and the lattice structure. The result of number A4 can be regarded as an exception, because of the lack of the "center cluster", and because of the extreme concentration of data points in the cluster near the left-bottom corner.

The lower panels in figure 7 show the ERMs of the FI60s-group. Similarly, a triangle cluster at left-bottom corner can be found in ERMs of rats B4, C1, C6, D1 and D5. However, the triangles of rats C1 and D1 look different from those of rats B4, C6 and D5. The former are empty triangles, and the later are solid ones. The center cluster at position IRP/**f** can be found in ERMs of all other rats, but their form and density differ slightly. In the ERM of rat B4, the large cluster at the left-bottom corner almost fuses with the "center cluster", so that they look together more like a square. A L-form cluster can be seen in the ERM of rat A3. However, it is difficult to separate it from a lattice structure. In addition to rat A3, distinct lattice structures can be found in the ERMs of rat A5, B2 and D9. The lattice structure in the ERM of rat B2 is particularly clear and dense, especially when it is compared with the ERM of rat A5. The distance between clusters is again equal to the value of the term IRP/**f**.

The ERMs of the FI90s-group are shown in the lower panel of figure 8. The "center cluster" at position X=Y=IRP/**f** can be found in the ERMs of B1 and C5. These show also a clear lattice structure. The ERMs of rats B6 and C3 are very different. In general, the distributions of data points are very diffuse in comparison with the ERMs of all the other rats, and the "center cluster" at position IRP/**f** cannot be definitely identified. Nevertheless, an empty triangle cluster can still be recognized in the ERM of C3.

2.4.2 ERMs of the surrogate data sets

The comparison between RMs and ERMs in section 2.4.1 clearly shows that distinct patterns can be seen only in the ERMs. Do these patterns really reflect dynamical properties of the IRT-data from the Skinner-box experiments? To answer this question, we compared the experimental ERMs with ERMs created from surrogate data sets. The surrogate data sets in the present study are generated by randomly reorganizing the sequential order of the experimental IRT-data. We applied a pseudo-random-number-generator called Mersenne Twister (Matsumoto & Nishimura 1998) in the generation of surrogate data sets. The same generator was also applied in all the simulation studies. Figure 9 right column shows four typical examples of the surrogate ERMs. The left column shows the corresponding experimental ERMs. They are all created by using IRT-data from session 15.

The first surrogate ERM comes from rat B2. The original ERM shows a clear lattice structure consisting of 6 clusters. The cluster at position X = IRP/**f**, Y≈ 0 (analog to the cluster I in figure 2d) shows some data points along the diagonal direction. In the surrogate ERM the clusters are interconnected with each other. The "center-cluster" at position X=Y=IRP/**f** becomes very diffuse and extends along vertical direction. The distribution of data points along the diagonal direction vanishes. The second example comes from rat A6. The original ERM shows a L-form cluster with relatively clear-cut boundary near the left-bottom corner and a "center-cluster" at position IRP/**f**. In the surrogate ERM the "center-cluster" disappears, and the edge of the "L"-cluster becomes more diffuse. It now looks triangle-formed. The third and fourth examples come from rats D1 and B5 respectively. Both experimental ERMs have a large triangle cluster near the left-bottom corner, and a "center-cluster" at position X=Y=IRP/**f**. The ERM of rat D1 has an empty triangle cluster- a lot of data points are distributed along the diagonal direction. The triangle cluster in the ERM of rat B5 is a solid triangle and has a very clear-cut boundary. In both of the surrogate ERMs the

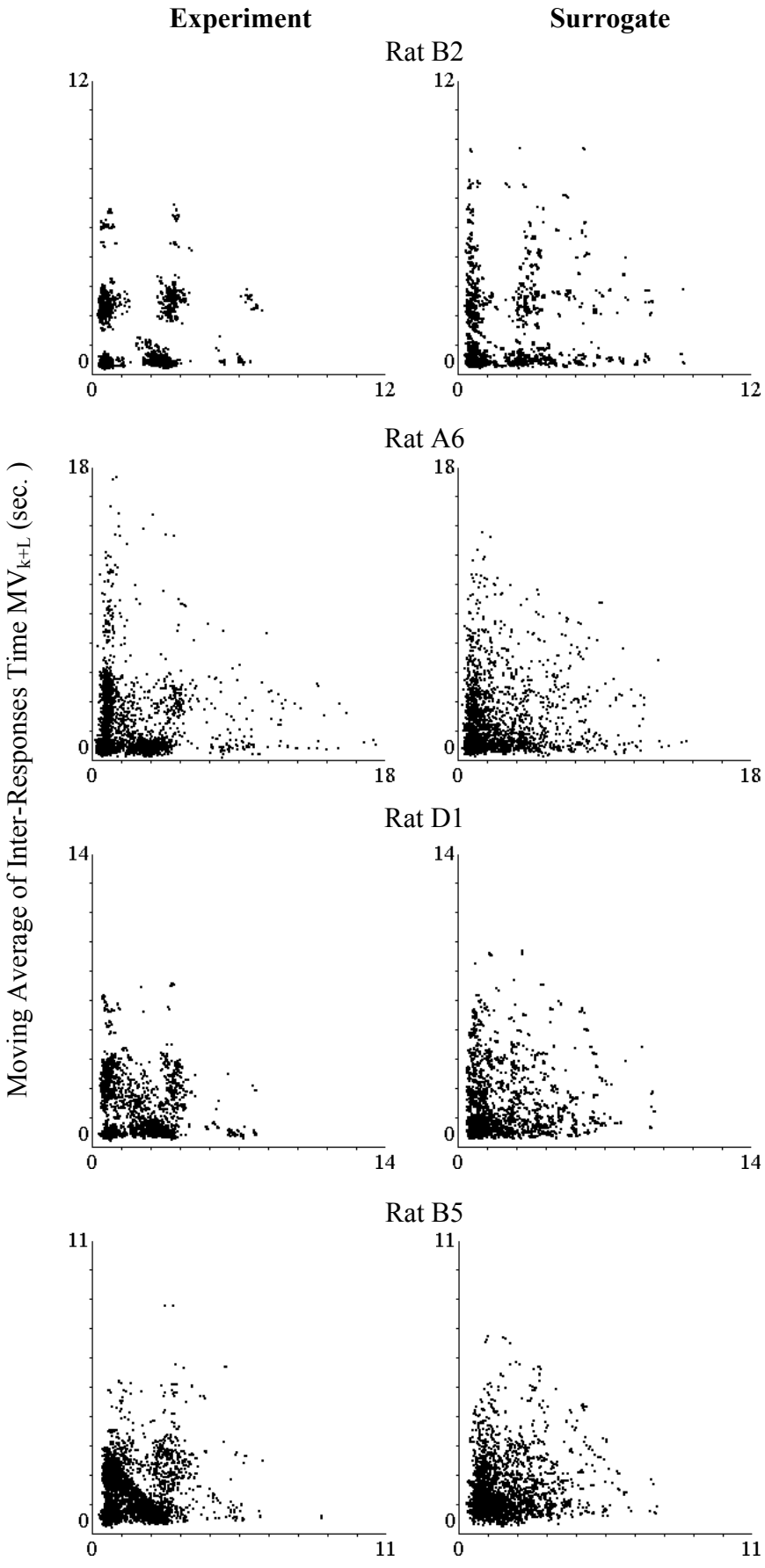

Figure 9: Comparison of the experimental (left) and the surrogate (right) ERMs. The four animals are chosen to represent the four typical geometrical structures of ERM-patterns: (from top to bottom) lattice, L-type, empty triangle and solid triangle.

center cluster disappears. The distribution of data points along the diagonal direction also decreases, so that the empty triangle almost completely vanishes. The boundary of the solid triangle becomes very diffuse.

These results suggest that: 1) the separation of clusters, 2) the form and density of the "center-cluster", and 3) the data points distributed along the diagonal direction are important elements that reflect the dynamical properties of the IRT-data. The meaning of the large cluster near the left-bottom corner, both L- and triangle form, on the other hand, might be relatively unclear. The randomization of the sequence of the IRT-data does not destroy this cluster completely. However, the clear-cut boundary becomes more diffuse and the form might be changed. These examples demonstrate qualitatively what kind of changes can be caused by the randomization of the sequential order of the experimental IRT-data. They suggest that, the ERM-patterns can indeed reflect dynamical properties of the FI-responding. Particularly, the "center-cluster", the data points along the diagonal direction, and the clear separable lattice structure are important elements in the ERM-patterns of FI-responding.

2.4.3 Distribution of the surrogate correlation dimension

The direct comparison between the surrogate and the experimental ERMs in figure 9 cannot tell us quantitatively how much change is caused by the process of randomization. Theoretically, the process of randomization is capable of producing exactly the same, or even better "structured" ERM-patterns. We need a quantitative measurement of the probability that the experimental, "well structured" ERM-patterns are acquired simply by chance. To accomplish this goal, we repeated the process of randomization and generated a distribution of surrogate correlation dimensions out of 10000 values. Comparing this distribution with the experimental correlation dimension gives us the probability of acquiring the experimental ERM-patterns simply by chance (the "by-chance-probability"). The definition and meaning of the correlation dimension have been discussed earlier in section 1.3.3.

The results are summarized in table 3 (page 35). If the experimental correlation dimension is smaller than the mean of the surrogate dimension, then the "by-chance-probability" is defined by the percentage of surrogate data sets that have a correlation dimension no larger than the experimental value. If the experimental correlation dimension is

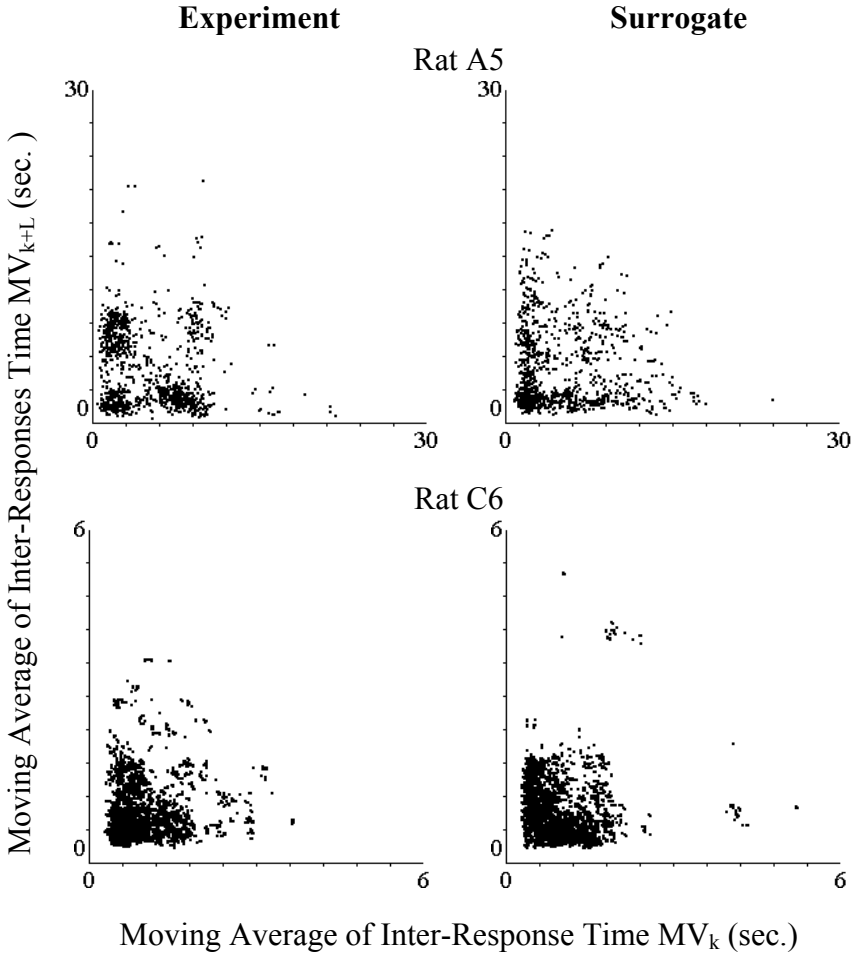

Figure 10: Comparison of the experimental (left) and the surrogate (right) ERMs of rats A5 and C6. Their "by-chance-probabilities" acquired in the study using the distribution of surrogate correlation dimension are 6.12% and 11.60% respectively.

larger than the mean of the surrogate dimension, then the "by-chance-probability" is defined by the percentage of surrogate data sets that have a correlation dimension no smaller than the experimental value. Most of the data have a quite small "by-chance-probability". There are, however, some exceptions. The "by-chance-probability" of rats A5 and C6 reveal values of 6.12% and 11.6% respectively. For these two animals, especially rat C6, the "well structured" patterns shown in their ERMs maybe do not reflect the dynamics of their operant behavior, but are acquired simply by chance. A qualitative comparison between the experimental and

the surrogate ERMs of these data are shown in figure 10.

2.4.4 Comparison between ERMs from session 15 and 26

The animals in block D have completed 26 sessions under the FI-schedules. We can compare results from sessions 15 and 26, and find out, whether or not there are some changes of behavioral dynamics after the animals have completed 11 more sessions under the FI reinforcement schedules. The results are shown in figure 11. Clearly the main features of the ERMs from session 15 are preserved in session 26. For example, the big cluster near the left-bottom corner, the center cluster and the lattice structures can be found in ERMs from both session 15 and 26. In addition to the appearance of these structures, the similarity in their geometrical forms and density distribution of data points also indicate the stability of behavioral dynamics. Nevertheless, minor differences can be seen in ERMs of rat D8 (FI20s-

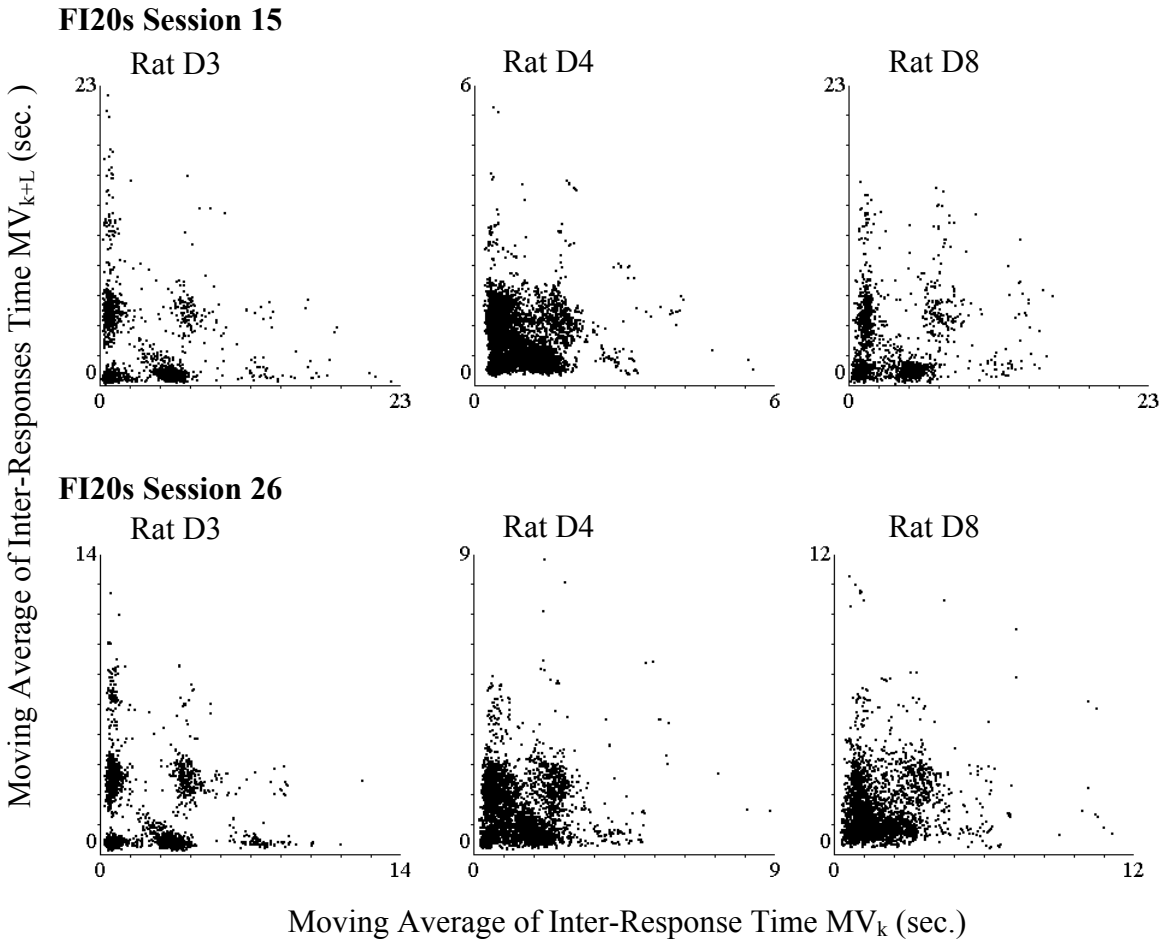

Figure 11: Comparison of ERMs from session 15 and session 26. (continued in the next page). The ERM of rat D8 showed a L-type structure in session 15, and the patterns changed to a solid triangle in session 26.

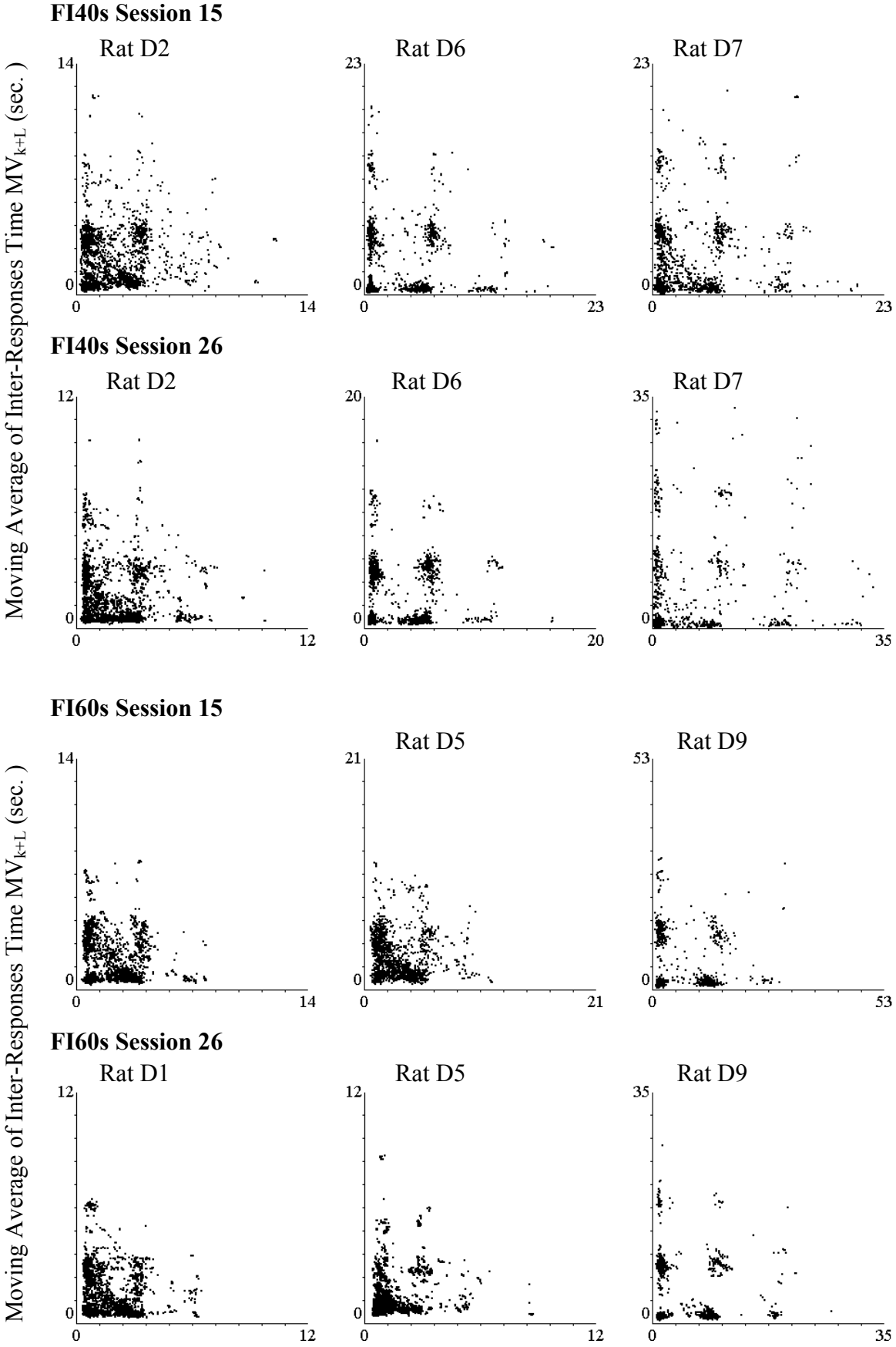

Figure 11: (continued from the previous page) Comparison of ERMs from session 15 and session 26. Except for rat D8, there are few changes in the ERM-patterns

group), D2, D7 (FI40s-group), D1 and D5 (FI60s-group).

In the ERM of rat D8 there are more data points in session 26 than in session 15. That implies increased overall operant activities in session 26. The big cluster near the left-bottom corner in the ERM from session 26 is much bigger than the L-form cluster at analog position in the ERM from session 15, and it looks now like a mixture of L-form and solid triangle. In the ERMs of rats D2 and D7 the point density in the big cluster near the left-bottom corner decreases slightly in session 26. The basic structures of the ERM-patterns do not change. In the ERMs of rats D1 and D5 the distribution of data points along the diagonal direction shifts slightly toward the left-bottom corner, so that in the ERM of rat D1 the empty triangle cluster near the left-bottom corner now looks more like a solid triangle.

In conclusion, these results suggested that the behavioral dynamics might have arrived at a steady state after the animals received 15, 90-minute sessions of FI-schedules.

2.4.5 Investigating the process of development of FI-responding

The process of acquisition of these specific behavioral dynamics can be assessed using ERMs. The ERMs of the experimental block "D" from sessions 1, 2, 3, 6, 9, 12, 15, 18, 21, 24, 25 and 26 are shown in figures 12-20. Sessions 1, 2, 3 and 24, 25, 26 are chosen because they represent the beginning as well as the end of the schedule-controlled phase. The other sessions are chosen in constant distance, namely 3 sessions. Initially, all animals show similar behavioral dynamics, as indicated by the similar ERM-pattern of session 1. Some also share similar intermediate stages, such as session 9 for rats D1, D3, D6 and D9. Gradually each rat develops its individual dynamics of FI-responding. A careful examination on the ERMs of sessions in the end-phase of this process (sessions 24-26) reveals that even the fine structures seen in the ERM-patterns are preserved from session to session, which is indicative for the stabilization of the behavioral dynamics of the animals under the given experimental conditions.

Figure 12 Rat D1 FI60s

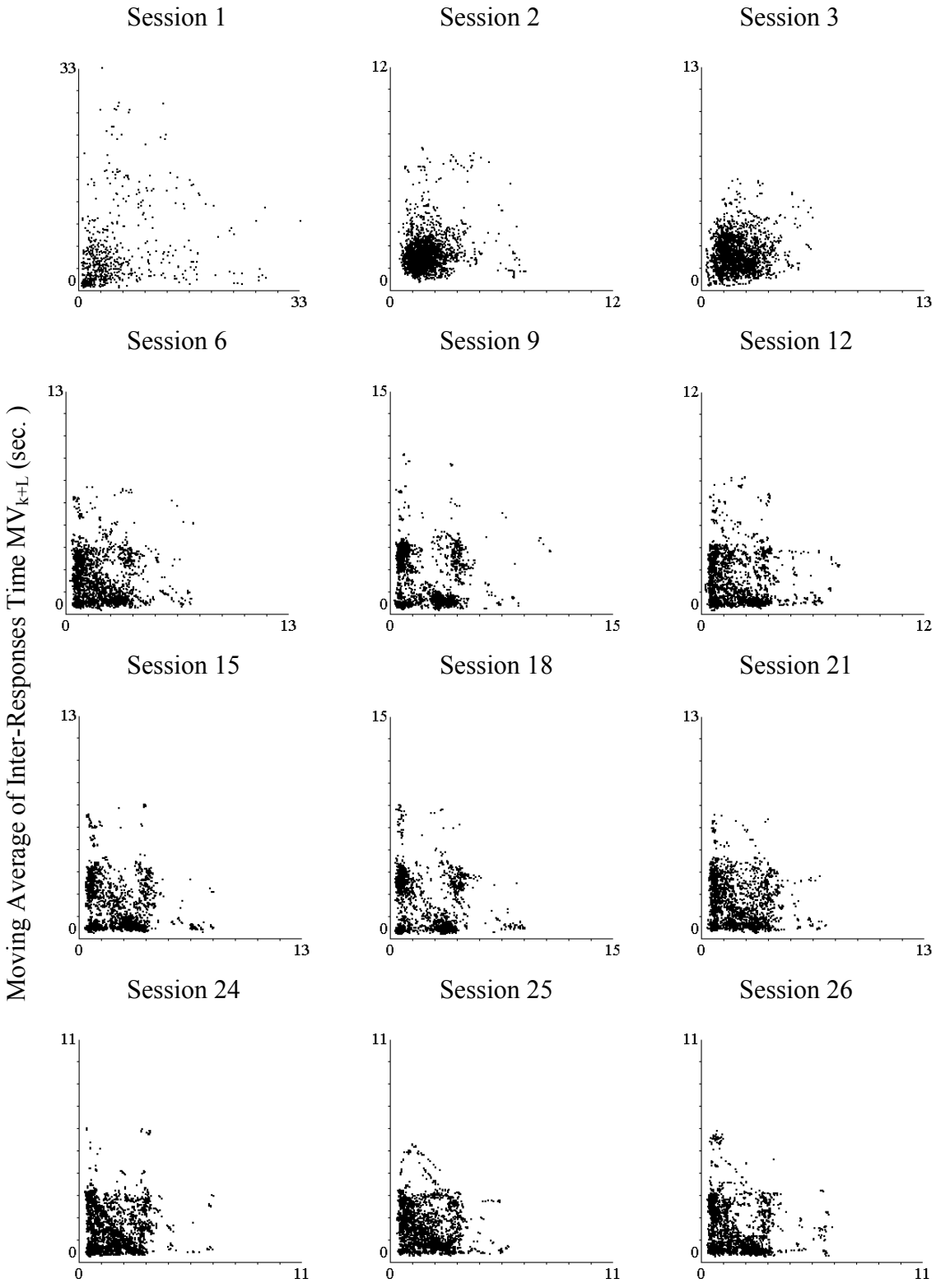

Figures 12-20 (pages 50-58): Using ERMs to assess the process of acquisition of the specific behavioral dynamics under the control of the FI-schedules. ERMs of animals in group D from sessions 1, 2, 3, 6, 9, 12, 15, 18, 21, 24, 25, 26 are shown. The patterns of ERMs of all animals looked similar in the beginning sessions (1, 2, and 3). Individual characters of ERM-patterns gradually developed, and the patterns stabilized in the last few sessions.

Figure 13 Rat D2 FI60s

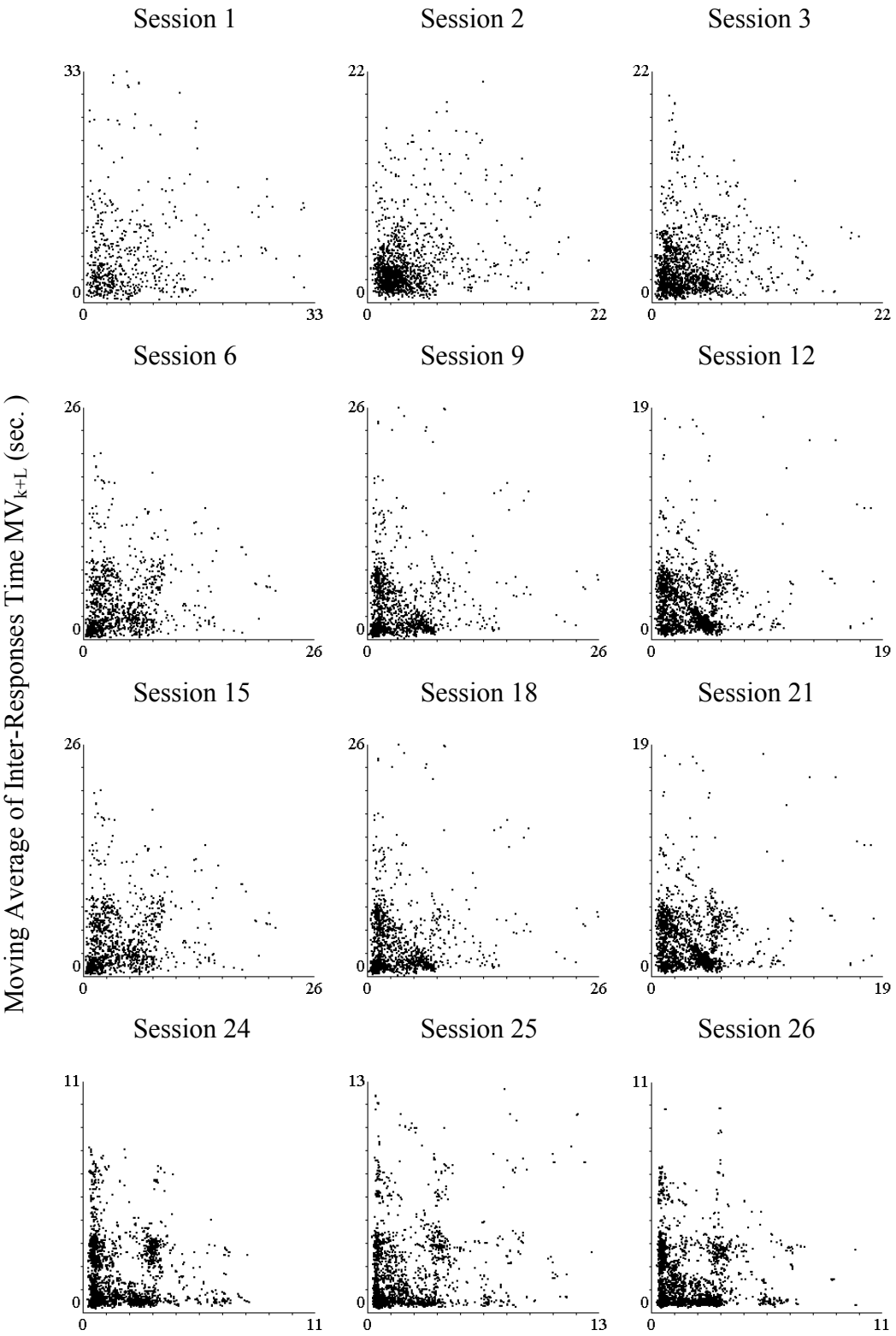

Figure 14 Rat D3 FI60s

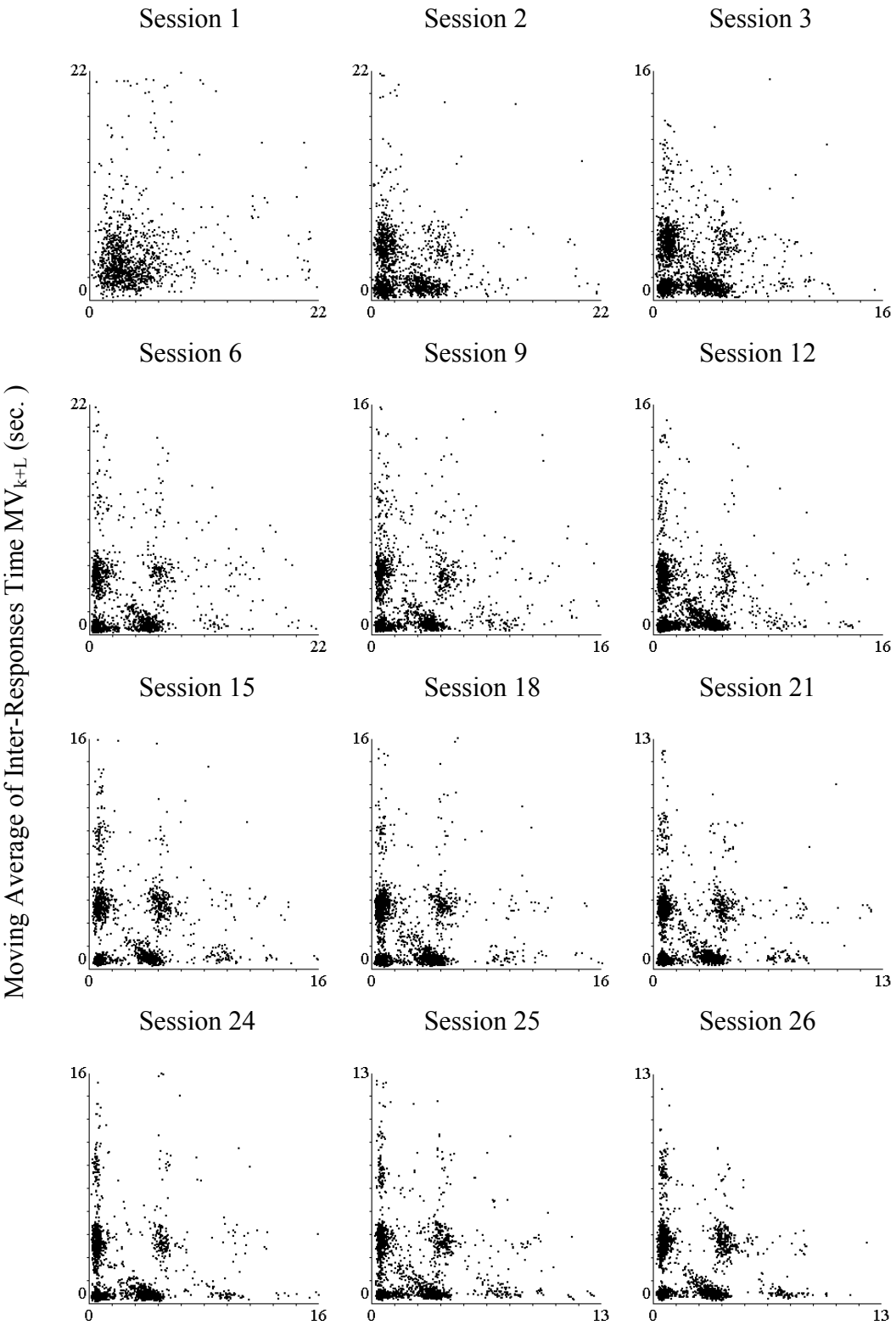

Figure 15 Rat D4 FI60s

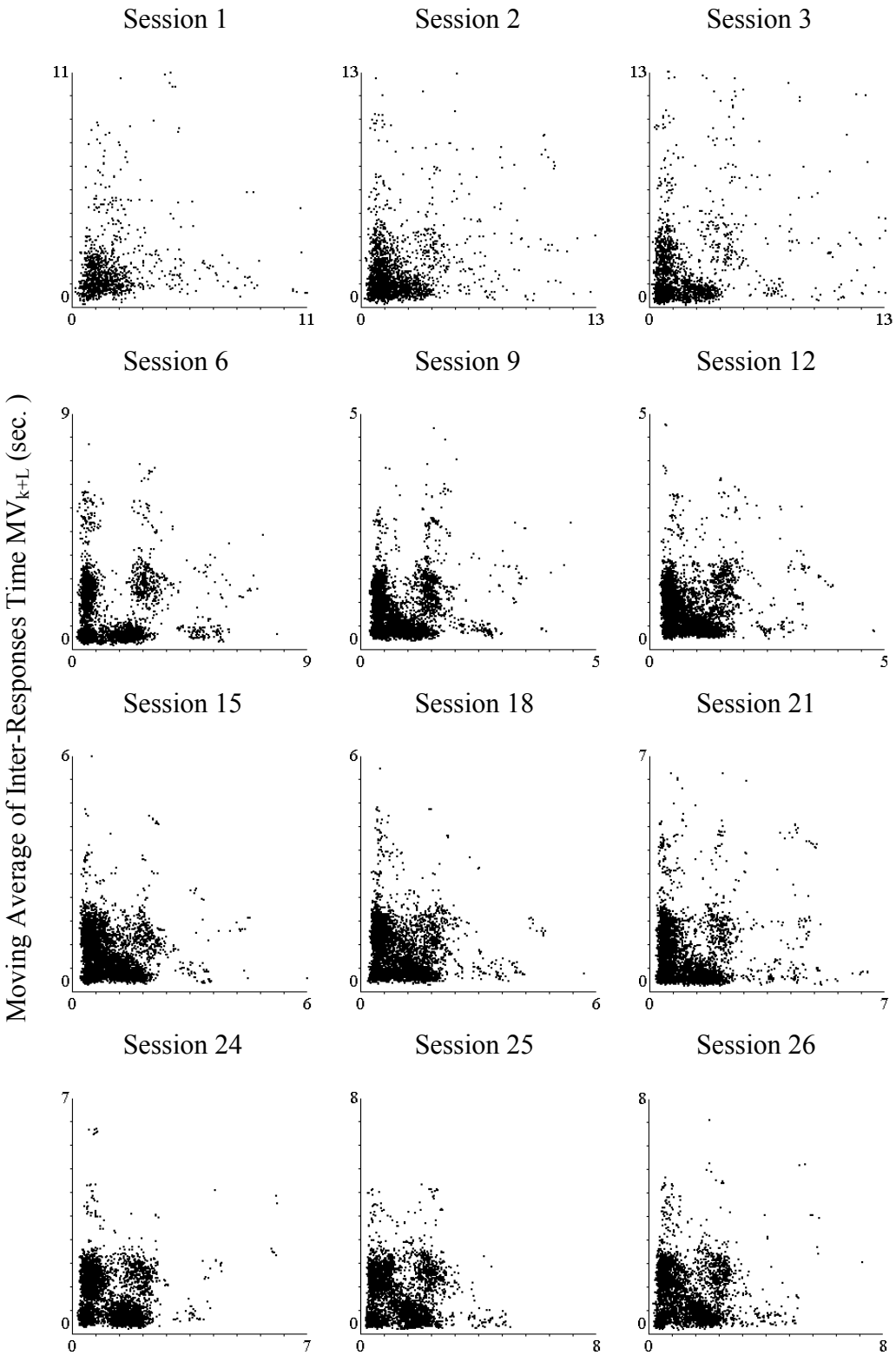

Figure 16 Rat D5 FI60s

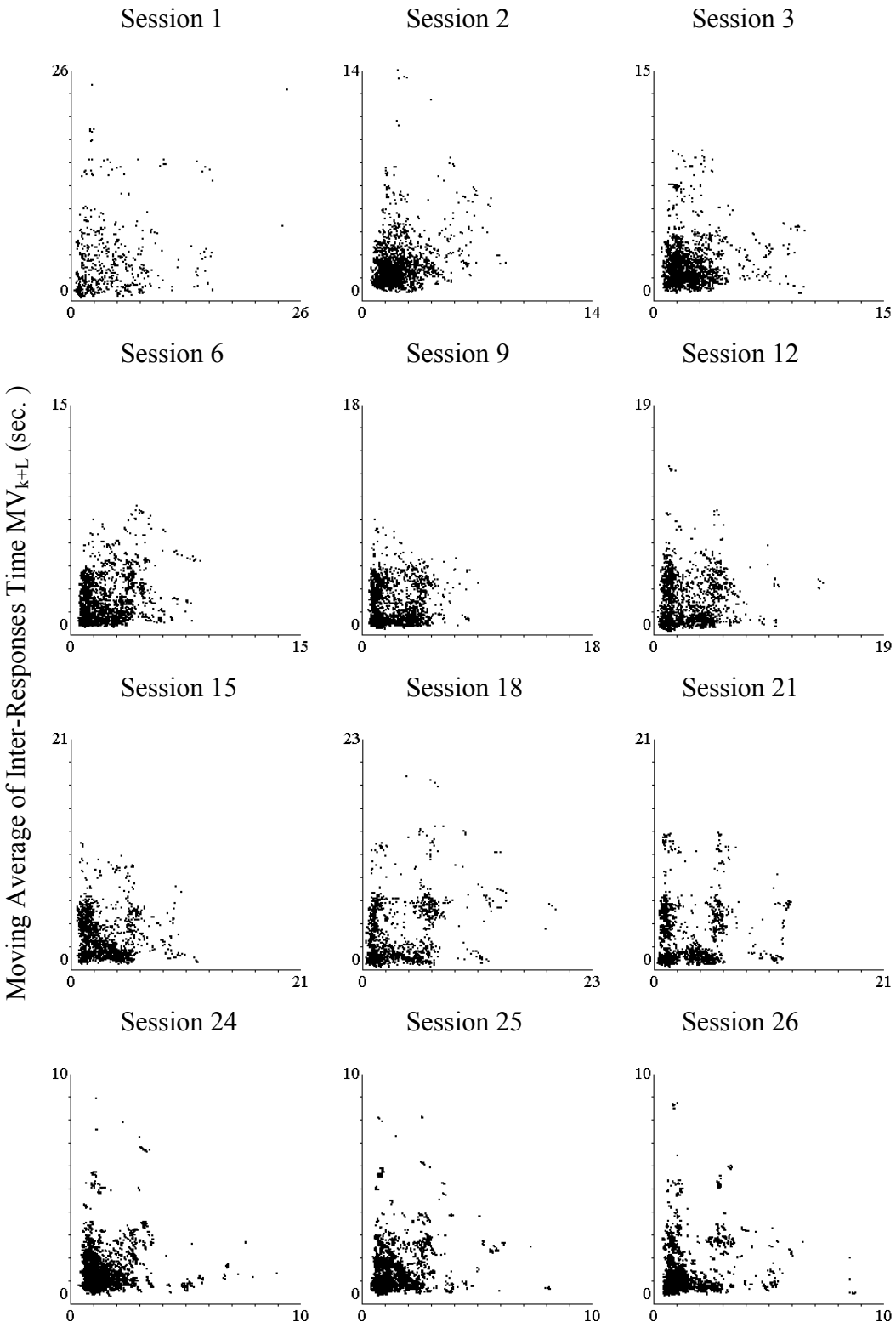

Figure 17 Rat D6 FI60s

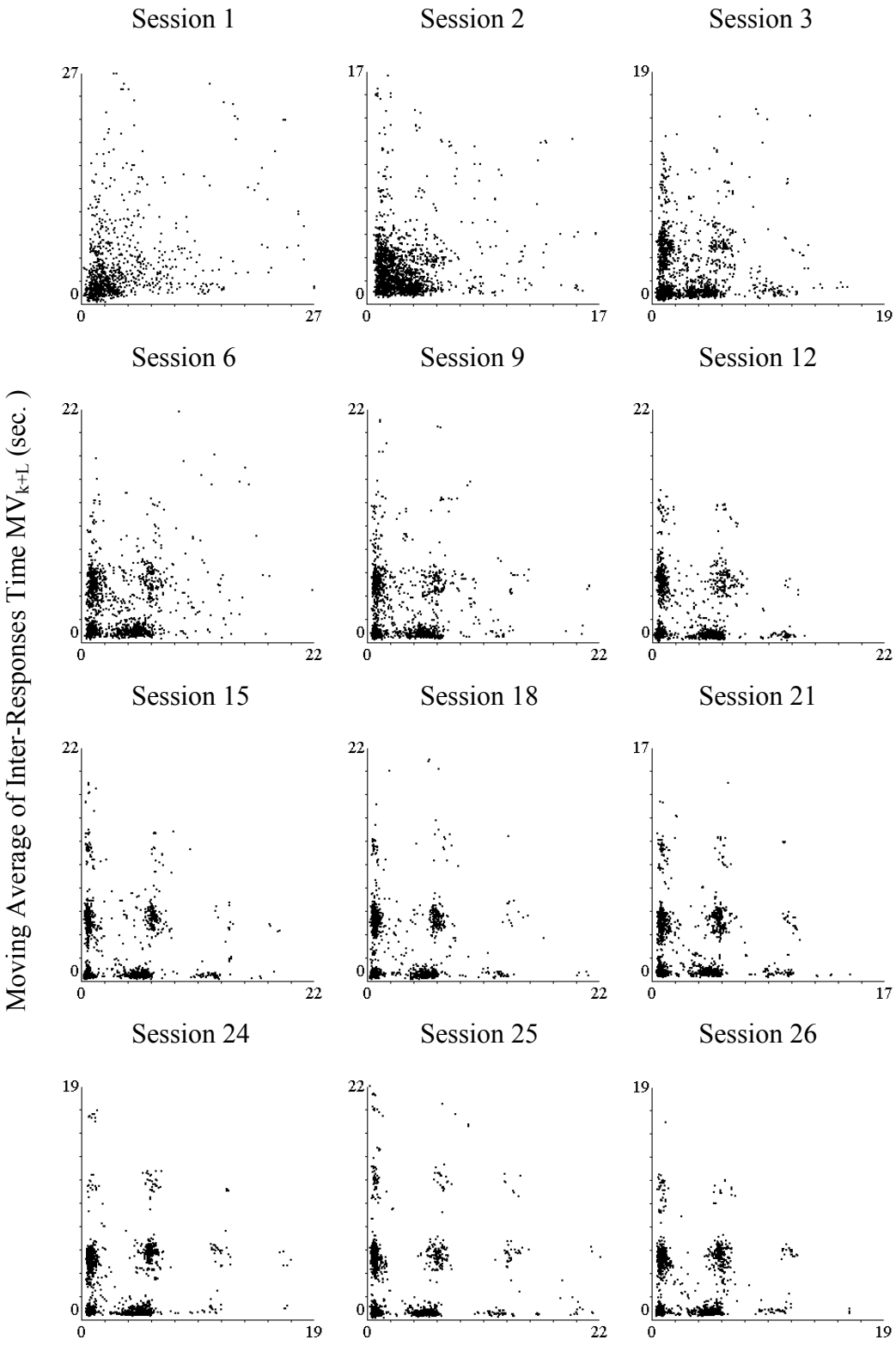

Figure 18 Rat D7 FI60s

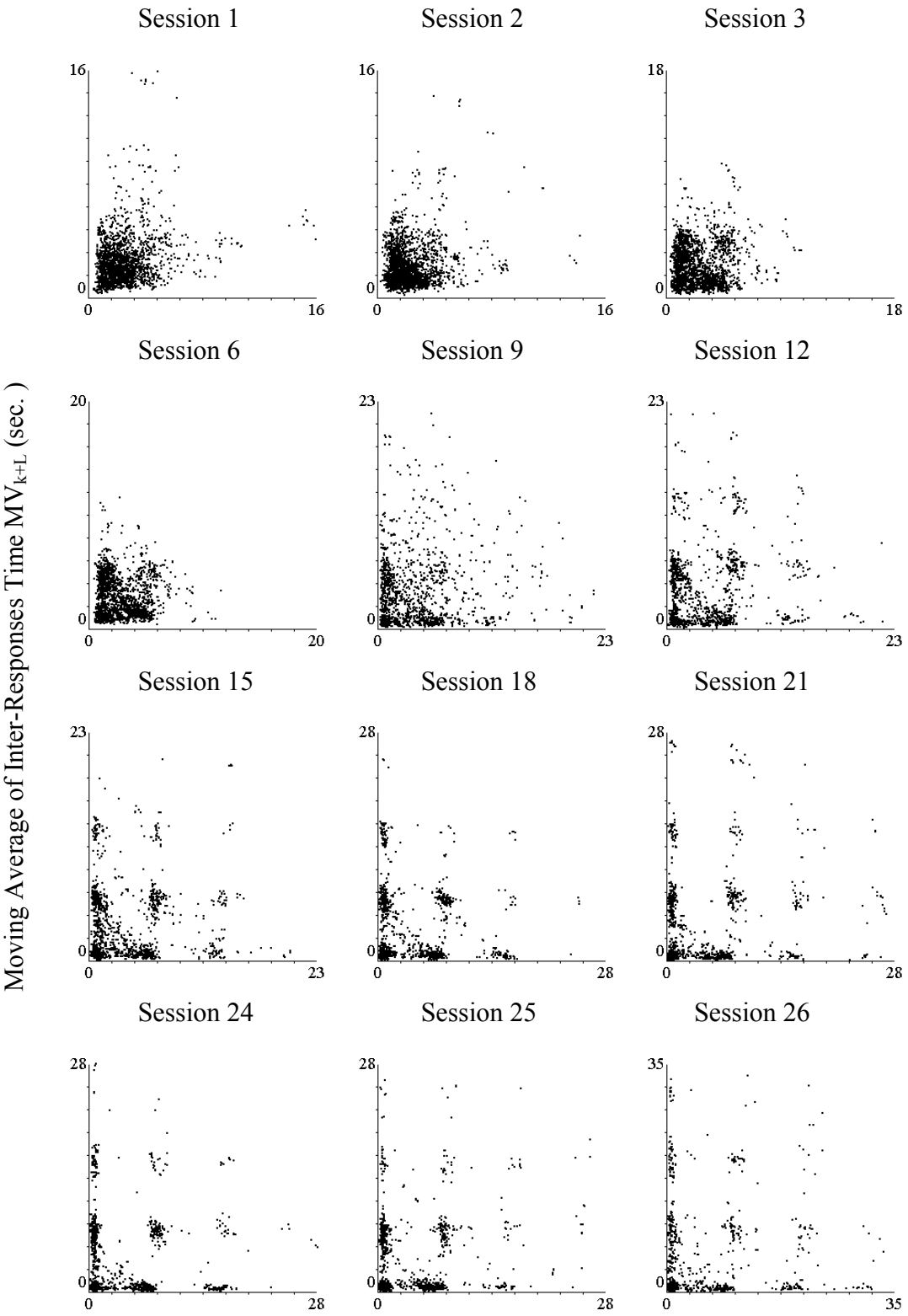

Figure 19 Rat D8 FI60s

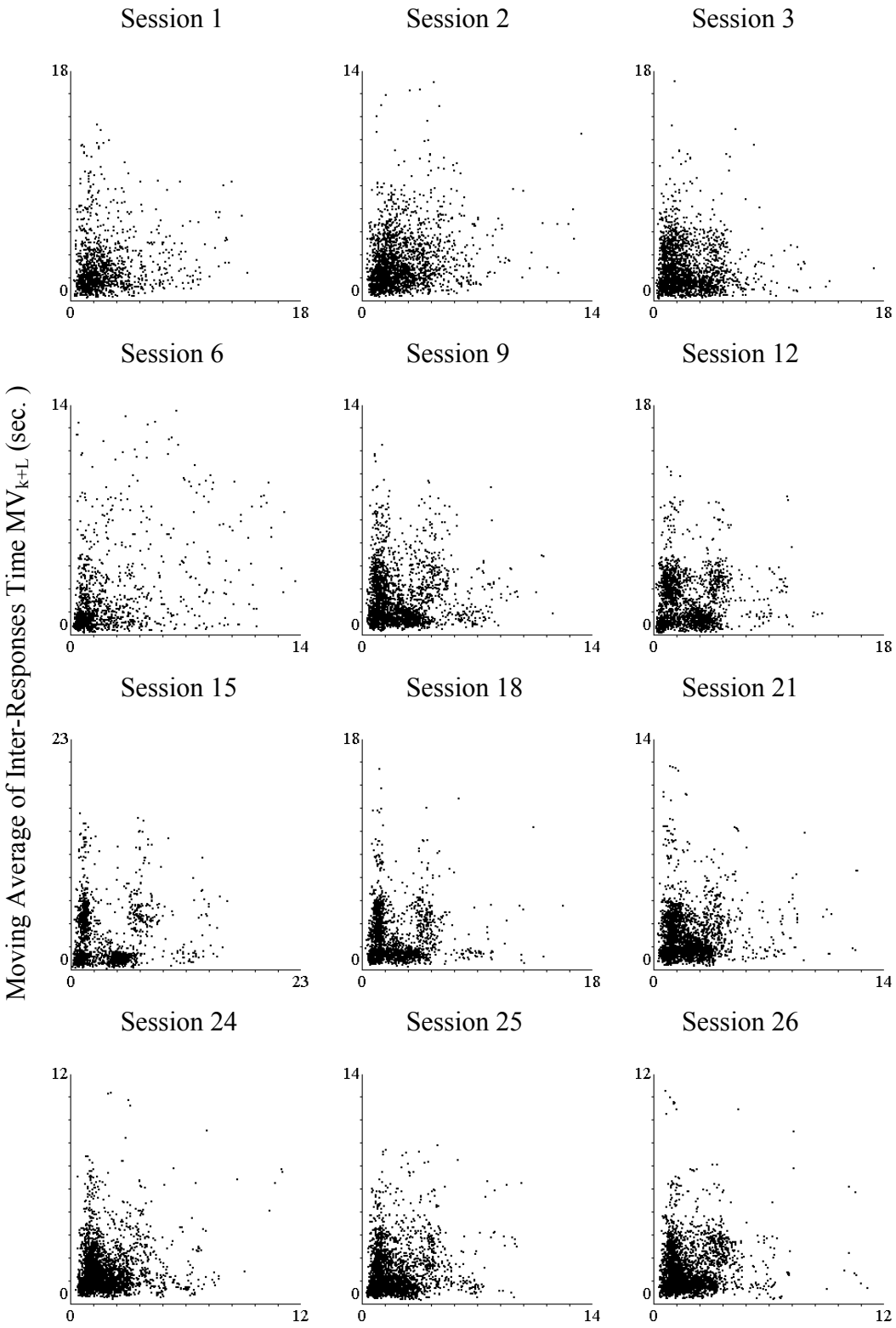

Figure 20 Rat D9 FI60s

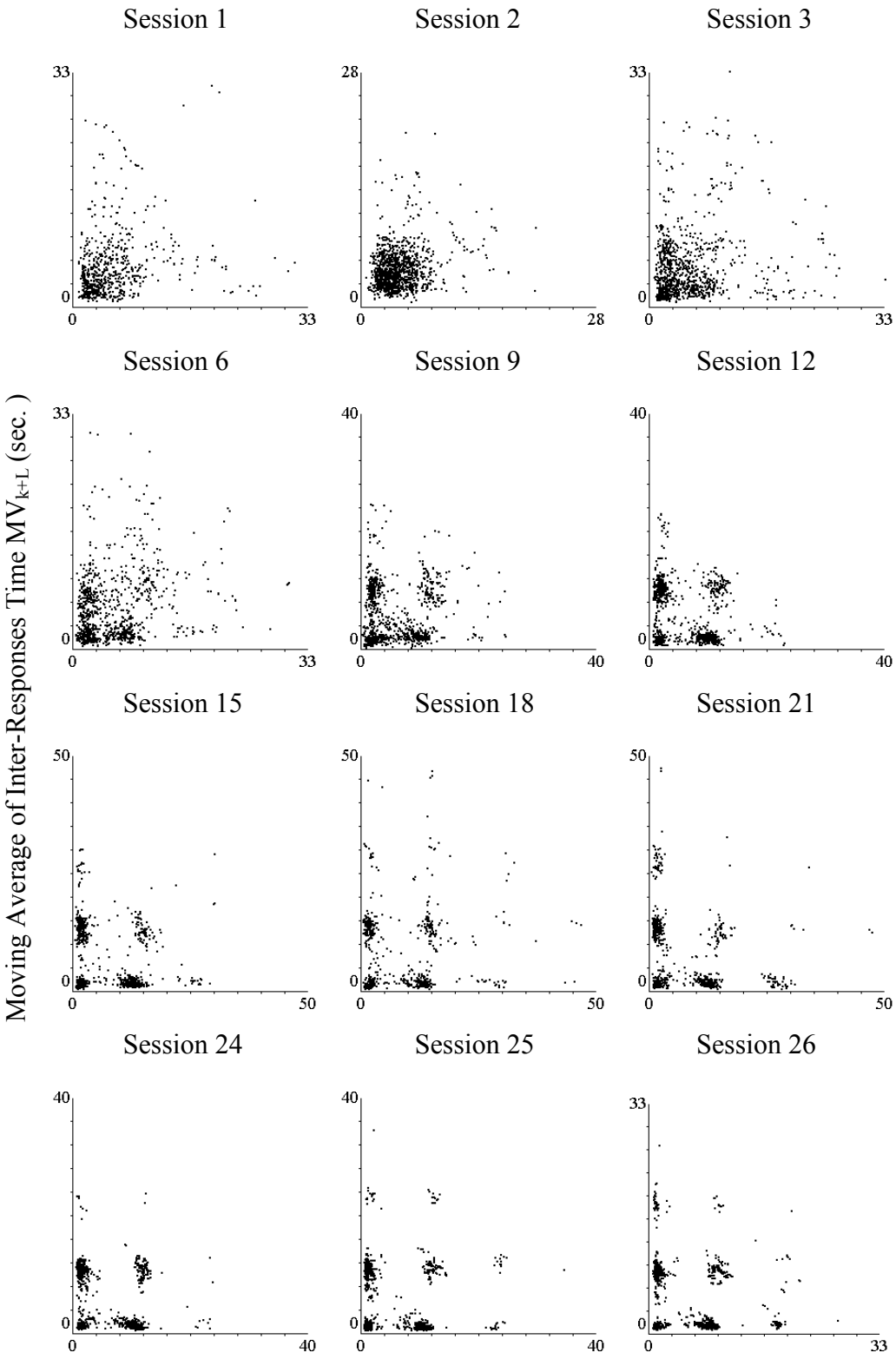

3 Simulation studies on the dynamics of FI-responding

3.1 Simulation I: Basic behavioral patterns

3.1.1 The strategy of the initial simulation studies

Our next step is to construct a model that can produce artificial IRTs which match the experimental results from session 15. The model is to be basically a kind of "point process"; that is, it is intended to describe the time dependent changes of the probability of emitting operant behavior. The first idea for the construction of such a model comes from the averaged scallop-curve. Similar to the lattice structures in the ERMs, this stereotypical pattern also develops over the course of the learning process (Machado, 1997; Machado & Cevik, 1998). In addition to that, the frequency distribution of IRT is another source of information. Since this model is basically a kind of point process, the frequency distribution of IRT can provide important hints for the behavior of the function that describes the probability of emitting a response.

Theoretically, there is an infinite number of different ways to build models that can generate IRTs to match such experimental cumulative records and IRT distributions. The question is, whether these two conditions are sufficient to completely describe the operant behavior under the interval-schedule. If, for example, we can build a model that can successfully simulate the cumulative records and IRT distributions, but fails to generate ERMs that can match the experimental results, then we can be sure that the ERM is able to show some properties that are not visible in the cumulative records and the IRT distributions. Furthermore, if a small modification can make this model fulfill all the three conditions, then this modification might represent a very important feature for the dynamics of the operant behavior under these conditions.

3.1.2 "Continuous scallop" versus "two state conception"

Following the strategy discussed , we have designed two models, both of which are able to generate IRT data sets that match the IRT distributions and the cumulative records. However, they differ in the way in which they generate the averaged scallop curve. The first model implements a continuous sigmoid-function, to describe the probability of lever pressing responses. Because of the form of the sigmoid function, the averaged scallop curve comes out. The second model implements the "two-state" conception of operant behavior, which has been suggested in several works (for example: Schneider 1969; Dews 1978; Shull 1991). The two-state model states that operant behavior can be viewed as alternation between two behavioral states, the "pause" and the "response (engagement)" states. When the animal is in response-state, lever pressing behavior will be emitted with an approximately constant rate, while in the pause-state no lever press can be observed. The design of both models will be now discussed in more detail.

3.1.3 Definition of the models in simulation I

The algorithms of the models can be divided into two parts. The first part $\boldsymbol{F_0}(t_a)$ depends on the time after the delivery and the consumption of food rewards.

$$\boldsymbol{F_0}(t_a) = \boldsymbol{F_0}(t_a - 1) + \mathbf{A_0} \times \boldsymbol{F_0}(t_a - 1) \times [\mathbf{M_0} - \boldsymbol{F_0}(t_a - 1)] \quad (7)$$

with initial condition:

$$\boldsymbol{F_0}(0) = \mathbf{O_0} \quad (8)$$

The second subunit consists of three sigmoid functions which are dependent on the time after each response.

$$\boldsymbol{F_1}(t_b) = \mathbf{R_1}(t_b) - \mathbf{R_2}(t_b) + \mathbf{R_3}(t_b) \quad (9)$$

The functions $\mathbf{R_1}(t_b)$, $\mathbf{R_2}(t_b)$ and $\mathbf{R_3}(t_b)$ are defined as follows:

$$\mathbf{R_1}(t_b) = \mathbf{R_1}(t_b - 1) + \mathbf{A_1} \times \mathbf{R_1}(t_b - 1) \times [\mathbf{M_1} - \mathbf{R_1}(t_b - 1)] \quad (10)$$

$$\mathbf{R_2}(t_b) = \mathbf{R_2}(t_b - 1) + \mathbf{A_2} \times \mathbf{R_2}(t_b - 1) \times [\mathbf{M_2} - \mathbf{R_2}(t_b - 1)] \quad (11)$$

$$\mathbf{R_3}(t_b) = \mathbf{R_3}(t_b - 1) + \mathbf{A_3} \times \mathbf{R_3}(t_b - 1) \times [\mathbf{M_3} - \mathbf{R_3}(t_b - 1)] \quad (12)$$

with initial conditions:

$$\mathbf{R_1}(0) = \mathbf{O_1},\ \mathbf{R_2}(0) = \mathbf{O_2} \text{ and } \mathbf{R_3}(0) = \mathbf{O_3} \quad (13)$$

Here t_a and t_b are discrete counters which represent the time after the taking of or the consumption of a reward (t_a), and the time after an operant response (t_b), respectively. When a reward is consumed, the counter t_a is reset to 0. Similarly, when an operant response is emitted, the counters t_b is reset to 0.

How these two subunits are interconnected, represents the main difference between the two models. While in the first model the two subunits are interconnected with a multiplication-operation, in the second model they are interconnected with a switch-operation. That is, after the reward is consumed and before the first operant response occurs, the final probability of an operant behavior to occur is decided by the first subunit $\boldsymbol{F_0}(t_a)$. After the first response, it is decided by the second subunit $\boldsymbol{F_1}(t_b)$. We can regard this switch between reacting modi as a switch between behavioral states. The first model, on the contrary, is defined by a continuous function.

Model I : $\boldsymbol{\Phi}(t) = \boldsymbol{F_0}(t_a) \times \boldsymbol{F_1}(t_b)$ (14)

Model II: $\boldsymbol{\Phi}(t) = \boldsymbol{F_0}(t_a)$ after the taking or consumption of a reward and before the occurrence of the first response

or $\boldsymbol{F_1}(t_b)$ after the first response (15)

Here $\boldsymbol{\Phi}(t)$ is the probability for an operant response to occur. The definitions of the two models differ only in equations (14) and (15). All other equations are valid for both models. The unit of both time counters t_a and t_b is 0.01 second.

Table 4 Parameters for simulation I

SLQ denotes the sum of least squares.

	Model I (continuous)	Model II (two-states)		Model I (continuous)	Model II (two-states)
$\mathbf{M_0}$	0.1364	0.1184	$\mathbf{M_2}$	0.2893	0.2478
$\mathbf{A_0}$	0.00153	0.000903	$\mathbf{A_2}$	0.6245	0.6654
$\mathbf{O_0}$	0.00083	0.000153	$\mathbf{O_2}$	0.0275	0.0294
$\mathbf{M_1}$	0.4613	0.2533	$\mathbf{M_3}$	0.1866	0.0505
$\mathbf{A_1}$	0.8562	0.8052	$\mathbf{A_3}$	0.0938	0.0599
$\mathbf{O_1}$	0.0221	0.0224	$\mathbf{O_3}$	0.0094	0.0103
SLQ	0,0289	0.0041			

The Levenberg-Marquardt algorithm was applied to optimize the setting of parameters $\mathbf{A_{0\text{-}3}}$, $\mathbf{M_{0\text{-}3}}$ and $\mathbf{O_{0\text{-}3}}$ (Marquardt,1963; Press et al., 1992). The averaged scallop curve and the IRT distribution were each divided into 21 columns (figure 21). The resulting 42 values of the columns were treated as a 42-dimensional vector. A 42-dimensional residual vector was calculated by subtracting the experimental vector from the simulated one. The sum of the least squares (SLQ) of the residual vector quantifies the goodness of fit of the models.

3.1.4 Results of simulation I

The results of rat B2 from session 15 are taken as target for the adjustment of parameters in simulation I. Detailed information of parameters are outlined in table 4. The experimental as well as the simulated IRT distributions, the averaged scallop curve (number of lever presses vs. time after reinforcement) and the ERMs are shown in figure 21, from which it is apparent that both models can produce simulations by which the IRT distributions and the averaged scallop curve are well matched with the experimental results. The second model (right column) produces an ERM that looks quite similar to the experimental ERM. The first model (middle column), however, produced an ERM that is quite different from that of the experimental data.

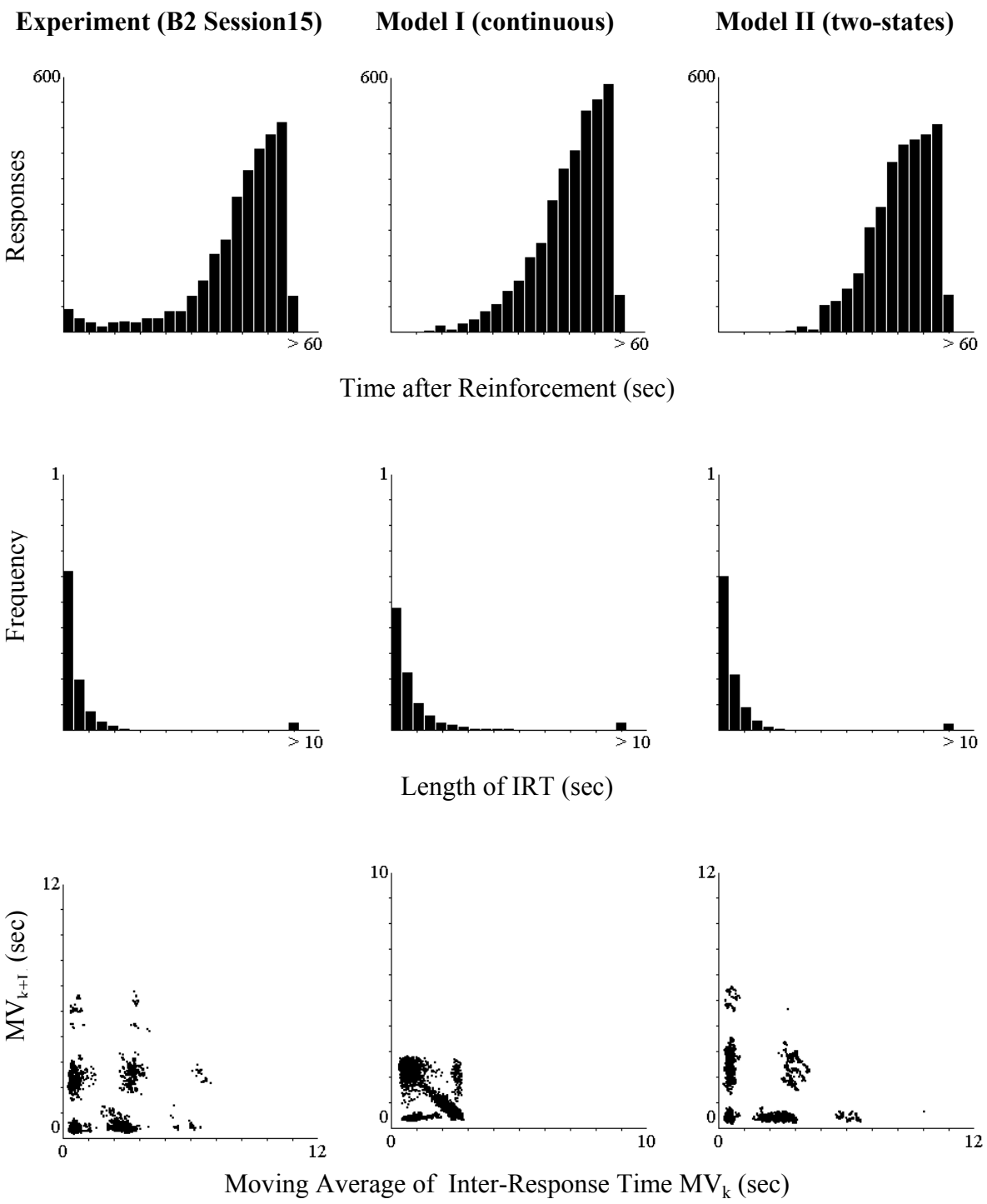

Figure 21: Results of simulation I. The averaged scallop curve, the IRT distribution and the ERM are shown. The IRT data of rat B2 from session 15 is the target. Both models I and II have similar forms of averaged scallop curve and IRT distribution. However, only model II can produce similar ERM-patterns as the experimental target does.

In summary, this simulation suggests that the averaged cumulative records and the IRT distribution alone are not sufficient to completely describe the dynamics of the operant behavior under FI-schedules, whereas the ERM accomplishes this task. Furthermore, the

simulation also suggests that a switch between two behavioral states plays an important role in the operant behavior under FI-schedules.

3.2 Analytical explanations for the ERM- patterns

The results in simulation I indicate that an abrupt switching between behavioral states during the inter-reinforcement period is essential for the lattice patterns to appear in the ERMs. This finding is consistent with our precious work (Li & Huston, 2002). Employing this idea as a starting point, we now present some analytical explanations for the formation of the lattice, L-type and triangle structures seen in the ERMs shown in figures 5-8.

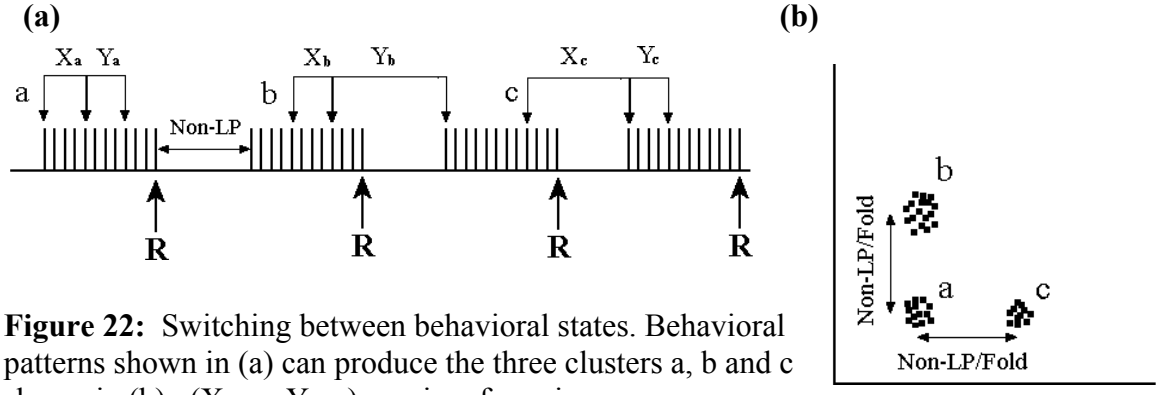

Figure 22: Switching between behavioral states. Behavioral patterns shown in (a) can produce the three clusters a, b and c shown in (b). (X_{a-c} , Y_{a-c}) = pairs of moving average windows; **R** = reinforcements.

3.2.1 Lattice structures

We begin our discussion with a regular alternation between the non-lever-press (Non-LP) and the lever-press (LP) sections, as shown in figure 22a. For simplicity, we also initially presume that the rate of lever pressing within the LP-sections is approximately constant, and the length of Non-LP sections is much longer than the averaged IRTs within LP sections. Under these conditions, and using parameters f and L smaller than one half of the averaged number of lever presses per reinforcement, we obtained three clusters of points in the ERM, as shown in figure 22b. The points in the cluster "a" have both X- and Y-coordinates within the LP-sections (windows X_a and Y_a). If either the X- or the Y-window crosses a Non-LP-

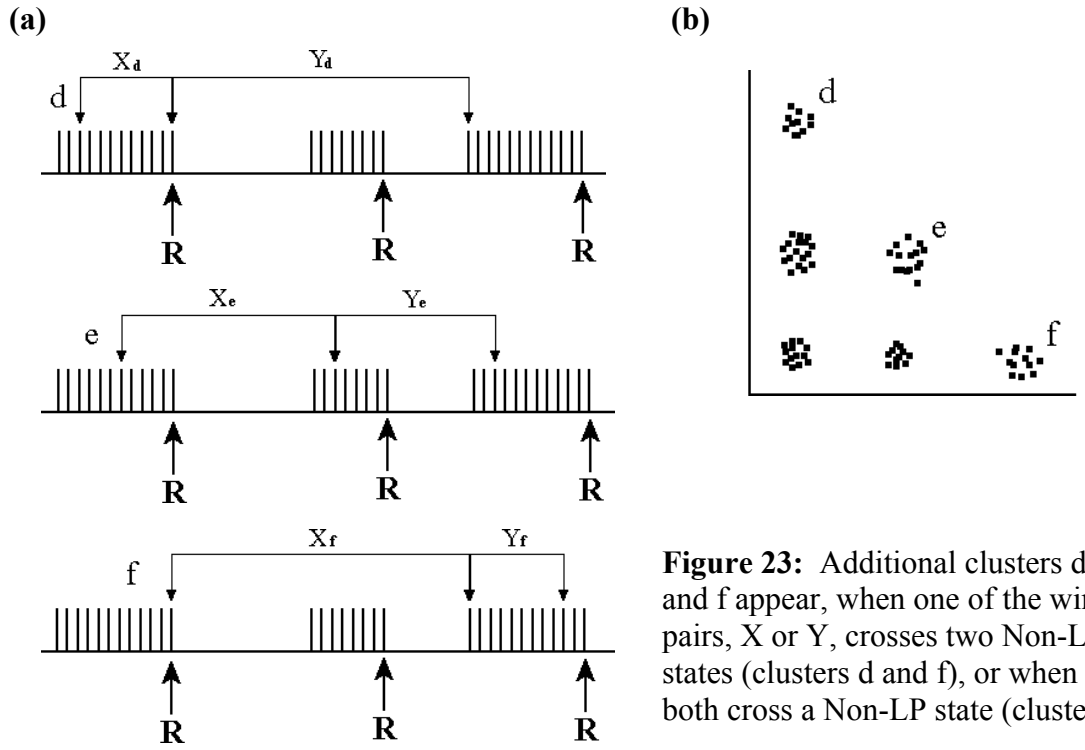

Figure 23: Additional clusters d, e and f appear, when one of the window pairs, X or Y, crosses two Non-LP states (clusters d and f), or when they both cross a Non-LP state (cluster e).

section, clusters "b" (with windows X_b,Y_b) and "c" (with windows X_c,Y_c) appear (figure 22b).

Now we must further consider the situation that some data points have Y- or X-windows across two or more Non-LP-sections (Y_d and X_f in figure 23a), or that both X- and Y- windows cross at least one Non-LP-section (X_eY_e in figure 23a). Since the length of Non-LP sections is usually much longer than the averaged IRTs in LP-sections, the resulting magnitude of one of the coordinates (X or Y) in the former cases will be about twice that of the situations Y_b and X_c discussed in figure 22a. In the latter case, the magnitude of both X- and Y-coordinates (X_e and Y_e) will be about the same as that of the situations Y_b and X_c. As a consequence, additional clusters "d", "e", and "f" will appear in the ERM (figure 23b). They form, together with the clusters "a", "b", "c" in figure 22b, a lattice structure (figure 23b).

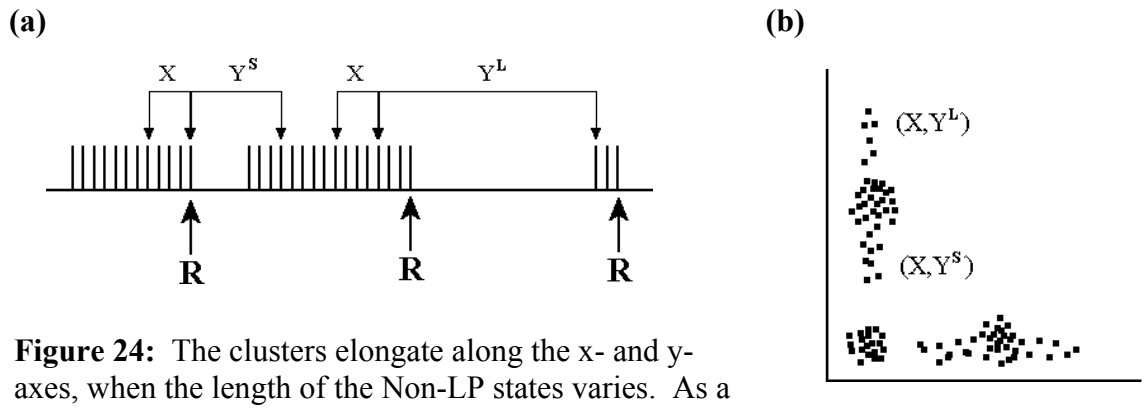

Figure 24: The clusters elongate along the x- and y-axes, when the length of the Non-LP states varies. As a consequence, the L-type structure appears.

3.2.2 L-structures

The distance between clusters has a value of Non-LP/**f** (figure 22b), so it is proportional to the length of Non-LP-sections. In most of the IRT-data, the length of Non-LP varies from IRP to IRP, as indicated by the windows Y^{S} and Y^{L} in figure 24a, where Y^{S} covers a shorter and Y^{L} a longer Non-LP section. This variation results in an elongation of clusters, as shown in figure 24b. In extreme cases all three clusters are interconnected and a L-type structure appears. This type of ERM-patterns can often be found in earlier sessions in the experimental data, for example rat D1 session 9 (figure 12), rat D3 session 2, 3, 12 (figure 14), rat D4 session 3, 6 (figure 15), rat D6 session 3, 6, 9 (figure 17) and rat D9 session 9 (figure 20). It is sometimes found in ERMs from session 15, for example rat A6, D8 (figure 5), A2 (figure 6), A3 and D5 (figure 7).

3.2.3 Acceleration-state and triangle structures

We now consider the situation in which the rate of lever pressing is not constant, but accelerates in the beginning of the LP-sections, as shown in figure 25a. This results in smaller Non-LP-sections followed by some relatively longer IRTs in the LP-sections. When the averaging windows $X_{\mathbf{g}}$ and $Y_{\mathbf{g}}$ move forwards, the resulting Y-coordinates of data points in the ERM increase gradually, while the X- coordinates remain approximately constant and small. This corresponds to the elongated cluster “g” along the Y-axis shown in figure 25b.

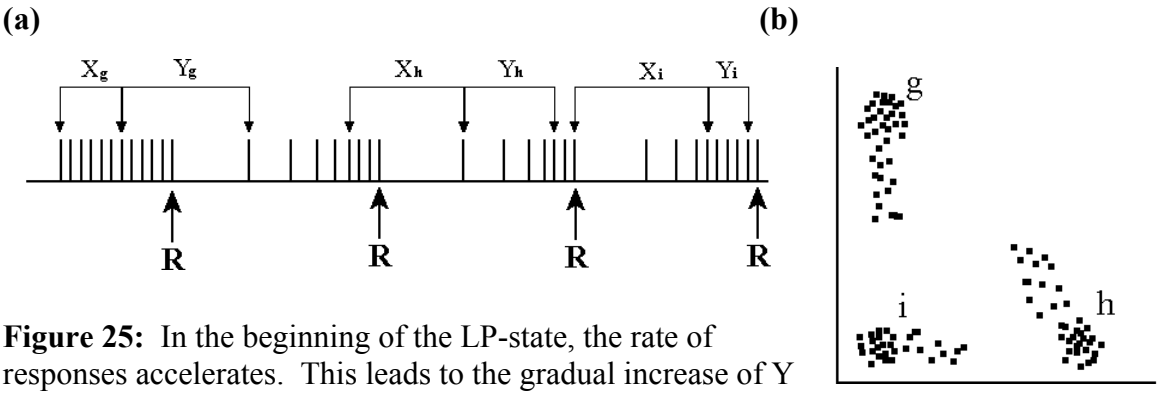

Figure 25: In the beginning of the LP-state, the rate of responses accelerates. This leads to the gradual increase of Y in situation "g", the gradual decrease of X in situation "i", and the simultaneous increase of X and decrease of Y in situation "h". The result is a broken triangle in diagram (b).

Next we consider what will happen when the averaging windows X_h and Y_h move forwards. In this case the X-coordinates of data points in the ERM increase, while the Y-coordinates decrease. The result is the cluster "h" in the ERM shown in figure25b, which elongates along the diagonal direction. Finally, we consider the case of windows X_i and Y_i, where the X-coordinates decrease gradually and the Y-coordinates remain approximately constant and small when the averaging windows move forwards. This leads to the cluster "i" in the ERM, which elongates along the X-axis (figure 25b). Thus, there appears an empty triangle-pattern in the ERMs. Sometimes the distribution of data points along the diagonal direction does not completely interconnect the clusters g and h, so that only a short "tail" stretched out from the cluster g along the diagonal direction can be seen. This kind of ERM-patterns can be found, for example, in rat D3 (figure 5) and B2 (figure 7).

3.2.4 Multiple-switches during the inter-reinforcement-periods

The triangle-structure in the ERMs can also be explained by an alternative behavioral pattern shown in figure 26. In this pattern, multiple switches between Non-LP and LP states exist during the inter-reinforcement period. We first consider the moving of windows X_g and Y_g in figure 26a. Similar to the situation "g" in figure 25, Y-coordinates of data points in the ERM increase gradually when the windows move from the range marked by solid line and

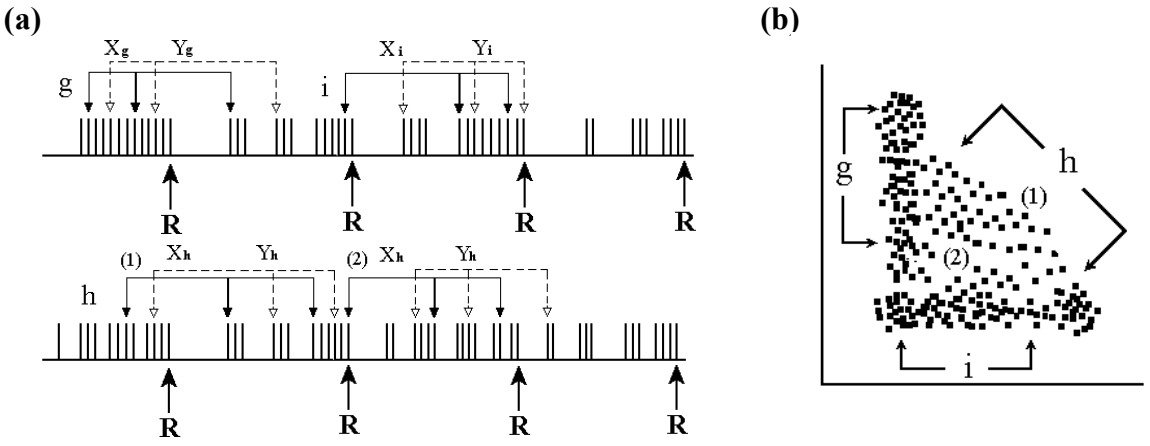

Figure 26: Multiple-switches between behavioral states during the inter-reinforcement periods. Under this condition, there are complicated lengthening and shortening of the window pairs X and Y. As a result, the triangle structure appears. Dashed lines indicate the new situations when the window pairs drawn in solid lines move forward.

filled arrowhead, to the range marked by dashed line and empty arrowhead, while the X-coordinates remain approximately constant and small. Thus, the cluster "g" in the ERM will appear (figure 26b). Similar consideration for the moving of windows X_i and Y_i from the range marked by solid line and filled arrowhead, to dashed line and empty arrowhead will reveal the cluster "i" in the ERM shown in figure 26b. The situation for the moving of windows X_h and Y_h is more complicated. In situation "h" both averaging windows X_h and Y_h include some Non-LP-states. The resulting data points have comparable X- and Y-coordinates, thus, they locate between clusters "g" and "i". Depending on the location of the averaging windows and on the distribution of Non-LP-states, we might have situation (1), in which X-coordinates increase while Y-coordinates decrease, or situation (2), in which X-coordinates decrease while Y-coordinates increase. The resulting points could uniformly distribute between X- and Y-axes as in the cluster "h" (1) and (2) in the ERM shown in figure 26b, or it could be more concentrated along the diagonal direction. The resulting ERM-patterns will look like a solid or an empty triangle.

3.3 A dynamical model of FI-responding

3.3.1 Overview

We now propose a comprehensive dynamical model for the operant behavior under the control of FI-schedules. It is not a purely deterministic model, as in most of the studies implementing the concepts of chaos theory. Nor is it a purely stochastic model, since the conception of the model bases on the findings in simulation I and the analytical discussion in section 3.2, in which some kinds of dynamical patterns play an important role. In fact, the failure to find distinct patterns in the original return map (recurrent plot) suggests that the IRT data might not possess a "short-ranged", low-dimensional, deterministic dependence. However, it is still possible that there is a "long term" dependence in the sequence of a IRT data set. In previous sections, the results of the application of ERM in the analysis of experimental data also support this idea.

Most of the contemporary theories of operant behavior deal with the rate of responses (for example: Killeen & Fetterman 1988; Hoyert 1992), and, thus bypass the problem of the generation of the events of operant behavior itself. Our model, however, is designed to generate the IRT data sets. To overcome the gap between the "rate" and the actual "events" of responses, there must be a mechanism for emitting operant events with a certain "rate". On the other hand, most of the IRT distributions from the experimental data show, except the region near the zero point, an exponential-like curve. This is an indication for a Poisson process. It seems plausible to assume that the mechanism of emitting operant events is a stochastic process with complicated probability functions.

The goal of this part of the simulation study is to find out these functions, and to generate the "correct" IRT data sets that can reproduce the main geometrical characters seen in the experimental ERM-patterns, namely, the lattice, the L-type structures, and both the empty and solid types of triangle structures. These patterns can be regarded as representing

the steady state behaviors of the animals, after they have been well trained under the given reinforcement schedules (see sections 2.4.4 and 2.5.5).

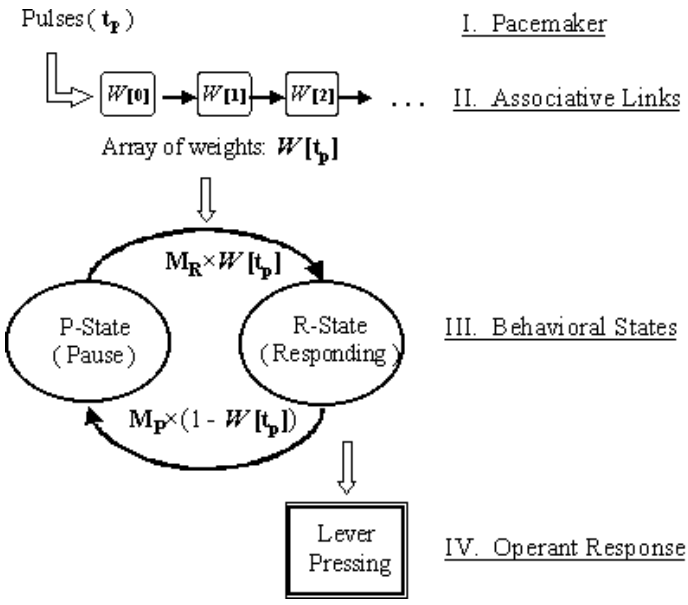

Figure 27: Overview of the dynamical model. It consists of four major parts: a pacemaker, the associative links (weights array), behavioral states and the mechanism for emitting operant responses.

The basic organization of the model is summarized in figure 27. It consists of four major components: 1) a pacemaker, 2) the associative links, 3) two behavioral states, and 4) a mechanism for generating operant responses. The pacemaker generates pulses $\mathbf{t_P}$ that drive forward an array of weights, which links the temporal states to the probability of switching between two behavioral states: the P-(pause) state and the R-(responding) state. Only in the R-state the mechanism for generating operant responses will be active. In the P-state, alternative behaviors are shown. Note that the word "pause" does not automatically imply quiescence, but indicates behaviors other than the operant response, in the case of the present studies, the lever pressing behavior.

3.3.2 Detailed description of the model

The existence of internal clocks that, among other functions, influence the temporal behaviors has been proposed by a number of authors (see e.g. Gibbon, 1977; Church, 1984; Killeen and Fetterman 1988; Church et. al. 1994). For convenience in describing our dynamical model, we speak of a pacemaker-like mechanism that generates pulses of signals which, in turn, drive the temporal states of the animals forward. The mathematical properties of this pacemaker is described by the following equation:

$$\mathbf{t_P} = \begin{cases} 0 & \text{if reinforcement is being delivered} \\ \mathbf{t_P}+1 & \text{if reinforcement is NOT being delivered and random(1)} < \mathbf{k_P}. \\ \mathbf{t_P} & \text{otherwise.} \end{cases} \quad (16)$$

The pseudo random number generator "random(1)" can generate a real number between 0 and 1 with constant probability. We applied the algorithm suggested by Matsumoto and Nishimura to implement the generator (1998). The pulses of the pacemaker are represented by an integer counter $\mathbf{t_P}$. Each pulse has a constant probability "$\mathbf{k_P}$" of occurring ($0< \mathbf{k_P} <1$). The delivery of reinforcement resets the counter $\mathbf{t_P}$ to zero.

The pacemaker and the probability of switching between behavioral states are linked by an array of weights, $\boldsymbol{W}[\mathbf{t_P}]$. Two constants $\mathbf{M_P}$ and $\mathbf{M_R}$ define the switching rate from one behavior state to the other. Both $\mathbf{M_P}$ and $\mathbf{M_R}$, as well as the weights array $\boldsymbol{W}[\mathbf{t_P}]$ shall have values between 0 and 1. In the present simulation studies we further assume that $\boldsymbol{W}[\mathbf{t_P}]$ is described by a sigmoid function:

$$\boldsymbol{W}[\mathbf{t_P}] = \boldsymbol{W}[\mathbf{t_P}-1] + \mathbf{A_W} \times (1 - \boldsymbol{W}[\mathbf{t_P}-1]) \qquad 0<\mathbf{A_W}<1 \quad (17)$$

where the parameter $\mathbf{A_W}$ decides how fast the weight increases with pulses $\mathbf{t_P}$. The first value of the weights array $\boldsymbol{W}[0]$ is defined by another parameter $\mathbf{O_W}$ ($0<\mathbf{O_W}<1$).

Equation (17) is chosen to simulate the behavior of animals having already received intensive training of schedule control under the FI-schedules. If a suitable learning rule for the adaptation of the weights-array can be found, the model will also be able to simulate the process of acquisition of these behavior dynamics.

Theoretically, there could be a number of different behaviors during the inter-reinforcement period (IRP). For example, eating, drinking, grooming etc. (Roper 1978). For simplification of modeling, we summarize all the non-operant behaviors into one class. Thus, we define two behavioral states during the inter-reinforcement period in this dynamical model, the P-(pause) state and the R-(responding) state. Only when the simulation program is

in the R-state, operant responses will be generated.

After the delivery of reinforcement, the pacemaker, that is, the pulse $\mathbf{t_P}$ will be reset to zero, and the model will be started with the P-state. When a new pulse comes in, the counter $\mathbf{t_P}$ will be increased by one, and at the same time the behavioral state of the model will have a certain chance to switch to the R-state. The probability of switching is defined by $\mathbf{M_R} \times \boldsymbol{W}[\mathbf{t_P}]$. If the model does switch to the R-state, the mechanism for generating operant responses will become active. Detailed description will be outlined in the next section. During the visit in the R-state and each time when a new pulse comes in, the model has also a probability to switch back to the P-state. Its magnitude is defined by $\mathbf{M_P} \times (1 - \boldsymbol{W}[\mathbf{t_P}])$. The cycles of switching back and forth between the P- and R-states are repeated until the delivery of the next reinforcement.

When the model is in the R-state, the mechanism for generating operant responses will become active. The probability $\boldsymbol{\Phi}_\mathbf{R}(\mathbf{t_R})$ is defined by the combination of two sigmoid functions:

$$\boldsymbol{\Phi}_\mathbf{R}(\mathbf{t_R}) = \mathbf{M_1} \times \boldsymbol{S_1}(\mathbf{t_R}) - \mathbf{M_2} \times \boldsymbol{S_2}\,(\mathbf{t_R}) \tag{18}$$

Functions $\boldsymbol{S_1}$ and $\boldsymbol{S_2}$ are defined as follows:

$$\boldsymbol{S_1}(\mathbf{t_R}) = \boldsymbol{S_1}(\mathbf{t_R} - 1) + \mathbf{A_1} \times [1 - \boldsymbol{S_1}(\mathbf{t_R} - 1)] \tag{19}$$

$$\boldsymbol{S_2}(\mathbf{t_R}) = \boldsymbol{S_2}(\mathbf{t_R} - 1) + \mathbf{A_2} \times [1 - \boldsymbol{S_2}(\mathbf{t_R} - 1)] \tag{20}$$

The initial values of $\boldsymbol{S_1}(0)$ and $\boldsymbol{S_2}(0)$ are defined by parameters $\mathbf{O_1}$ and $\mathbf{O_2}$. All the parameters $\mathbf{M_{1\text{-}2}}$ and $\mathbf{A_{1\text{-}2}}$, as well as the initial values $\mathbf{O_{1\text{-}2}}$ shall have values between (0,1). Suitable values of the parameters were first found by visually matching the experimental and simulated scallop curves and IRT-distribution. Then the values were given in the Levenberg-Marquardt algorithm as starting point (Marquardt,1963; Press et al., 1992). The algorithm optimised the parameters by minimizing the sum of least squares (SLQ) of the residual vector. In the

present study, the IRT-distribution and the averaged scallop curve were each divided into 21 columns. The resulting 42 values of the columns were treated as a 42-dimensional vector. The residual vector is calculated by subtracting the experimental vector from the simulated one.

3.3.3 Results of simulation II

The experimental data of rat D6 from session 26, rat D8 from session 15, rat C1 from session 15 and rat B5 from session 15 are chosen as targets for the simulations IIa – IId. They are chosen to represent the lattice type, the L-type, the empty and solid triangle types of ERM-patterns respectively. The data of rat D8 from session 26 is additionally taken as the target for simulation IIe, since rat D8 was used in the studies on the effects of amphetamine treatment, and the results from session 26 will be compared with those on the treatment days (see section 4.3). The parameters and the SLQ of the simulations are outlined in table 5. The results are presented with three different forms of analysis: the averaged scallop curve, the

Table 5 Parameters for simulation II

SLQ = sum of least squares

Simulation	**IIa**	**IIb**	**IIc**	**IId**	**IIe**
Targets	D6 session 26	D8 session 15	C1 session 15	B5 session 15	D8 session 26
$\mathbf{k_P}$	0.0149	0.00776	0.00713	0,00594	0,00551
$\mathbf{M_P}$	0.8268	0.7646	0.8152	0,8311	0,8785
$\mathbf{M_R}$	0.8029	0.7211	0.8079	0,7818	0,7686
$\mathbf{A_W}$	0.2179	0.6369	0.2536	0,3048	0,6346
$\mathbf{O_W}$	0.0000712	0.00479	0.0101	0,0798	0,0735
$\mathbf{M_1}$	0.0597	0.2474	0.0503	0,0501	0,1608
$\mathbf{A_1}$	0.1501	0.0304	0.2875	0,2771	0,0558
$\mathbf{O_1}$	0.0202	0.00704	0.0105	0,0249	0,0188
$\mathbf{M_2}$	0.0306	0.1152	0.0418	0,0399	0,1319
$\mathbf{A_2}$	0.2963	0.0439	0.2940	0,3013	0,0668
$\mathbf{O_2}$	0.00101	0.00253	0.000993	0,00302	0,00931
SLQ	0.0160	0.0612	0.0215	0,0221	0,0158

frequency distribution of IRT, and the ERMs. They are shown in figures 28 to 32. The simulations are shown in the upper panels, and the experimental results in the bottom panels.

Roughly speaking, all four simulations can fit the experimental data quite well. This can be seen in the graphical presentation and the SLQ. Nevertheless, minor differences can be seen in the averaged scallop curve. The experimental data show clearly the so-called overshooting. That is, non-zero probability of operant responses directly after the delivery of reinforcement. In the simulations, however, the number of operant responses drops to zero after each reinforcement. Possible explanations for this phenomenon could be: delay in the delivery of food pellets due to the feeding machine, delay due to not noticing the presence of foods, or, animals' inability to stop their operant responding. Some of these factors might be depressed by changing experimental setups, for example, by installing a retractable lever.

Minor differences can also be seen in the frequency distribution of IRT, especially the

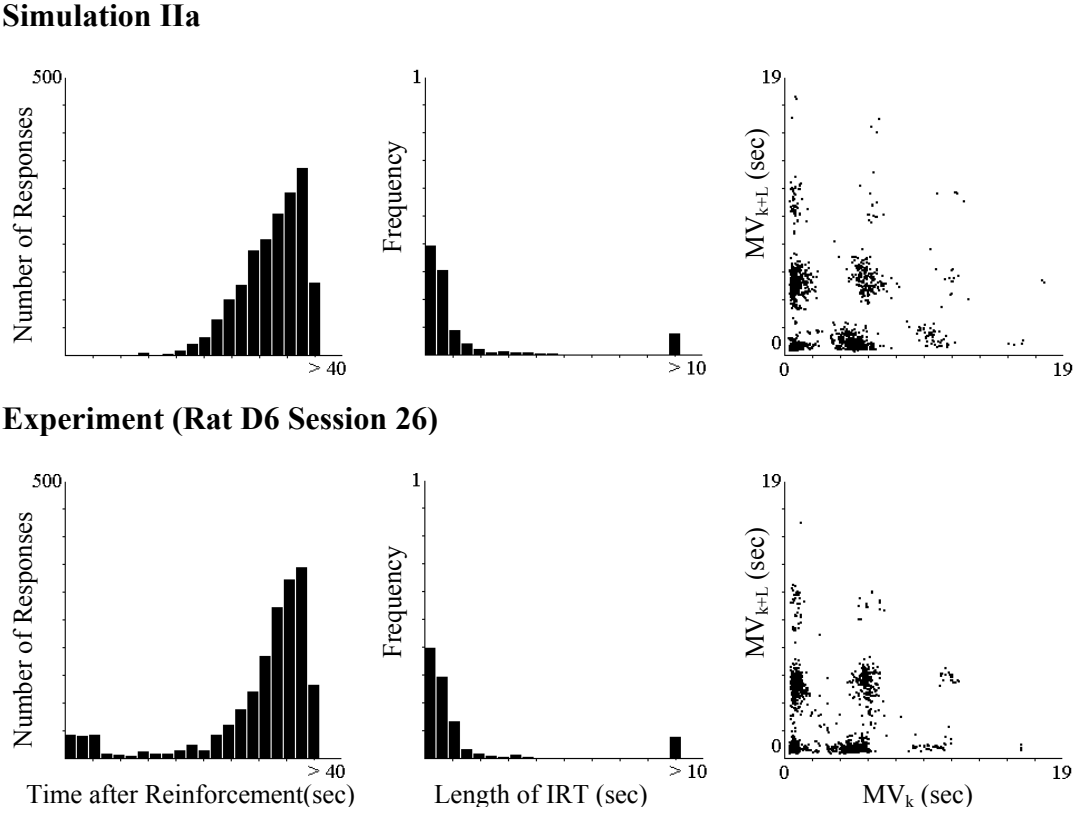

Figure 28: Results of simulation IIa. Data of rat D6 in session 26 was chosen as target. This data represents the lattice-type of ERM-patterns.

Simulation IIb

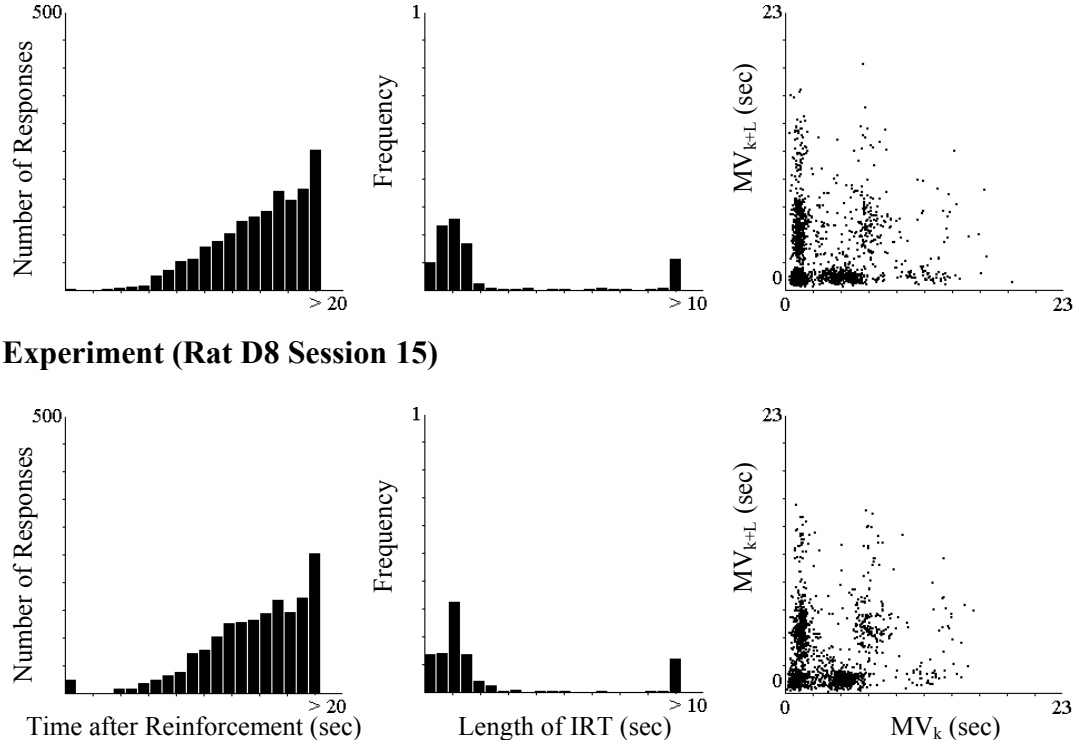

Figure 29: Results of simulation IIb. Data of rat D8 in session 15 was chosen as target. This data represents the L-type of ERM-patterns.

Simulation IIc

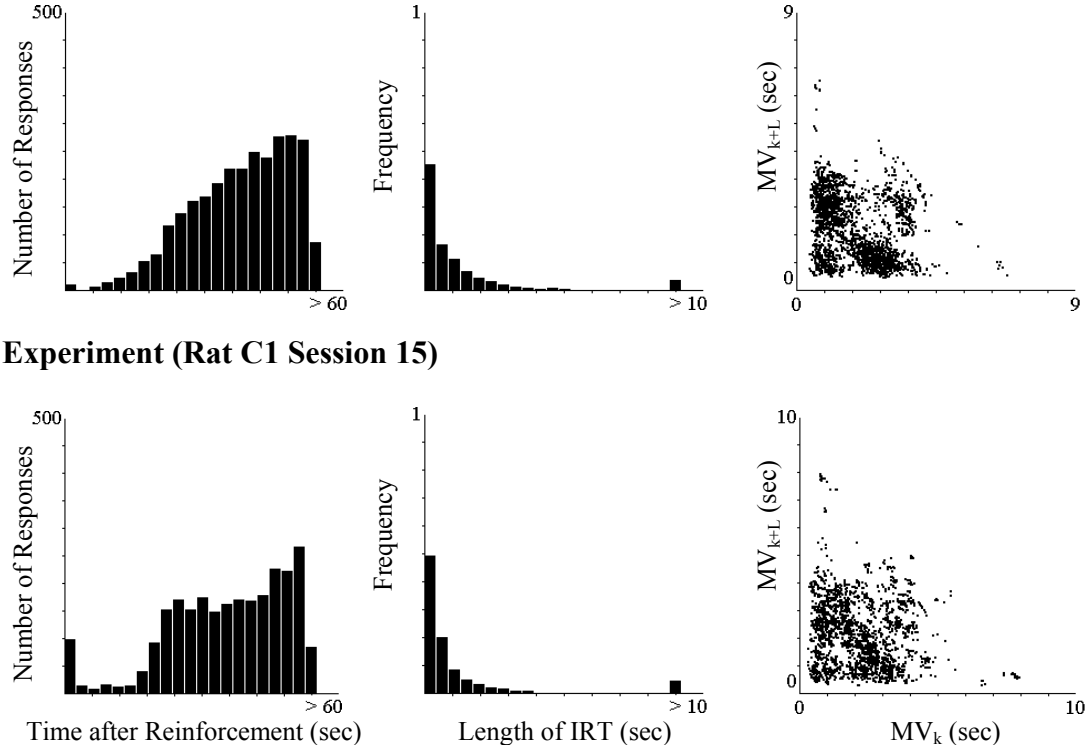

Figure 30: Results of simulation IIc. Data of rat C1 in session 15 was chosen as target. This data represents the empty-triangle-type of ERM-patterns.

Simulation IId

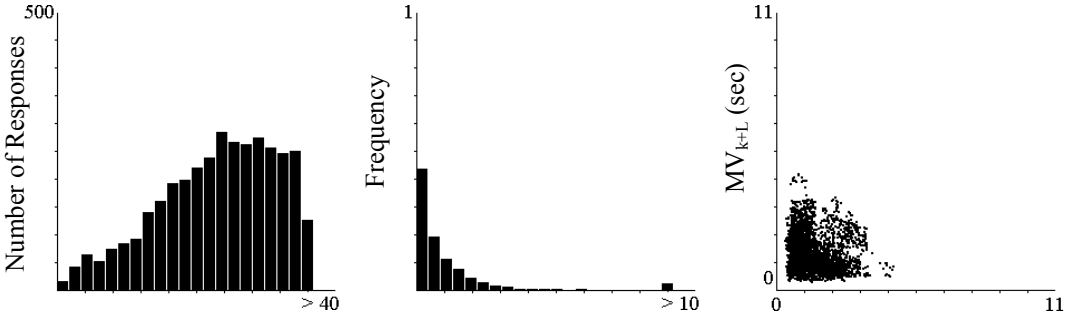

Experiment (Rat B5 Session 15)

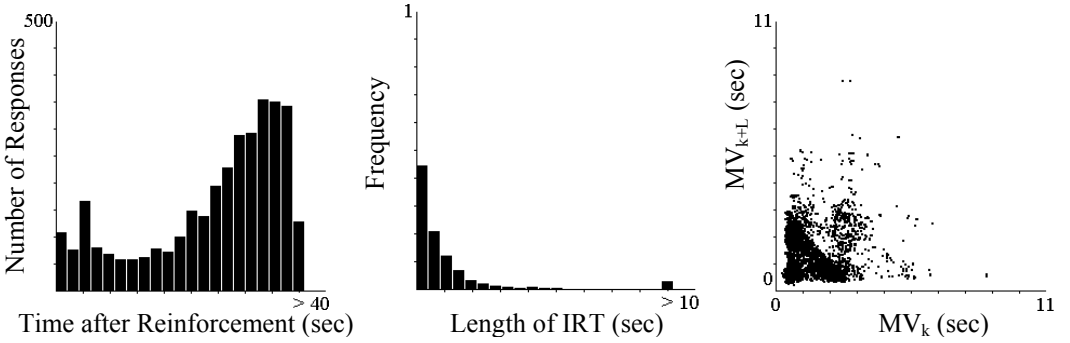

Figure 31: Results of simulation IId. Data of rat B5 in session 15 was chosen as target. This data represents the solid-triangle-type of ERM-patterns.

Simulation IIe

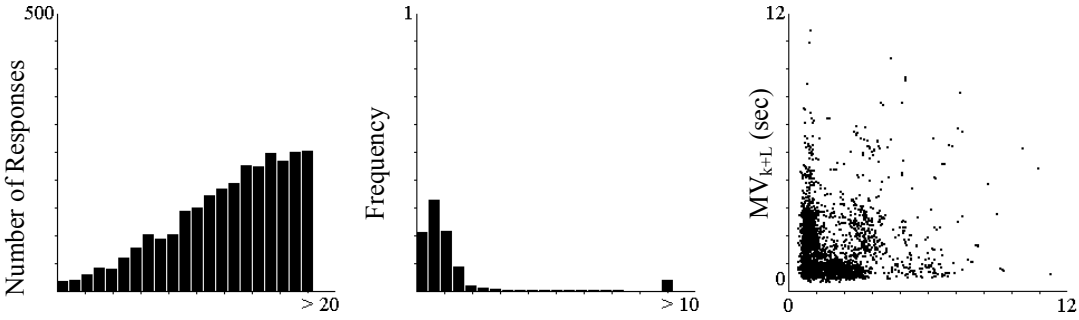

Experiment (Rat D8 Session 26)

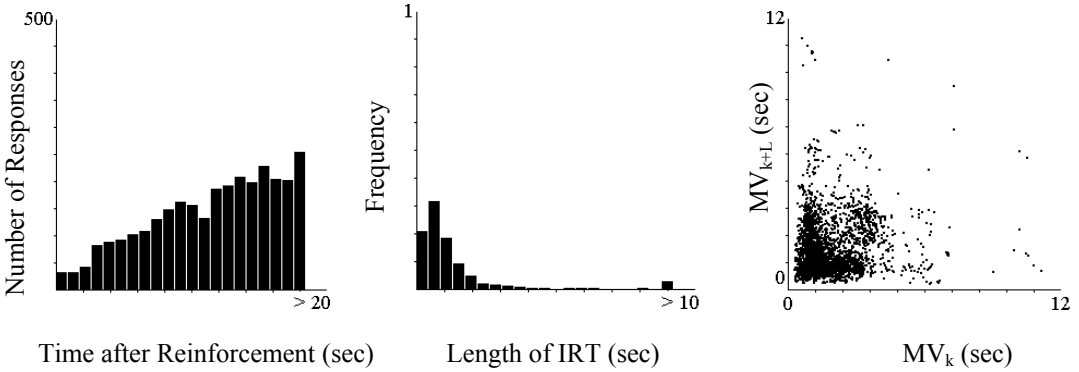

Figure 32: The IRT data of rat D8 from session 26 is additionally taken as a target of simulation. This simulation will be used to be compared with behavioral dynamics under the influences of amphetamine.

results of rat D8. While the other three distributions show roughly an exponential decrease of occurring frequency with increasing length of IRT, the peak of the IRT-distribution of rat D8 is located at a position of about 0.5~1.5 seconds. In other words, the distribution of this IRT data does not fit well to a Poisson process, which is the basic conception of the mechanism for generating operant responses in our model (see equations 18-20). The parameter setting of equations 18-20 (parameters $\mathbf{M_1}$, $\mathbf{A_1}$, $\mathbf{O_1}$, $\mathbf{M_2}$, $\mathbf{A_2}$ and $\mathbf{O_2}$) also gives hints to this particularity. While the simulations IIa, IIc and IId have very similar values for the parameters $\mathbf{M_1}$, $\mathbf{A_1}$, $\mathbf{O_1}$, $\mathbf{M_2}$, $\mathbf{A_2}$ and $\mathbf{O_2}$, the values for the same parameters in simulation IIb and IIe are located in a completely different range (see table 5 for parameters $\mathbf{M_1}$, $\mathbf{A_1}$, $\mathbf{O_1}$, $\mathbf{M_2}$, $\mathbf{A_2}$ and $\mathbf{O_2}$). Similar form of IRT distribution can be seen in the data of rat D8 from both sessions 15 and 26. The parameters $\mathbf{M_1}$, $\mathbf{A_1}$, $\mathbf{O_1}$, $\mathbf{M_2}$, $\mathbf{A_2}$ and $\mathbf{O_2}$ in both simulations are also located in the similar range.

The simulated ERMs differ also slightly from the corresponding experimental targets. Nevertheless, the essential geometrical properties of the ERM-patterns, namely, the lattice, the L-form, the empty and solid triangles, can be unambiguously recognized in the simulated ERMs. The rat D8 revealed slightly different experimental ERM-patterns in session 26 as in session 15. This difference is also quite well simulated using the present parameter settings, as indicated by the comparison between figures 29 and 32.

3.3.4 The parameters used in simulation II

The parameters used in simulation II show some interesting findings which will be discussed here. Firstly, it shall be noted that the constant $\mathbf{k_P}$ (for setting the speed of the pacemaker) and the constants $\mathbf{A_W}$ and $\mathbf{O_W}$ together decide the form of the sigmoid function that describes the weights array. Effects of decreasing the value of $\mathbf{k_P}$ can be compensated by increasing the values of $\mathbf{A_W}$ and/or $\mathbf{O_W}$. This can be seen in the results of simulation III in figure 33, in which three different sets of $\mathbf{k_P}$ and $\mathbf{A_W}$ values were used. The other parameters

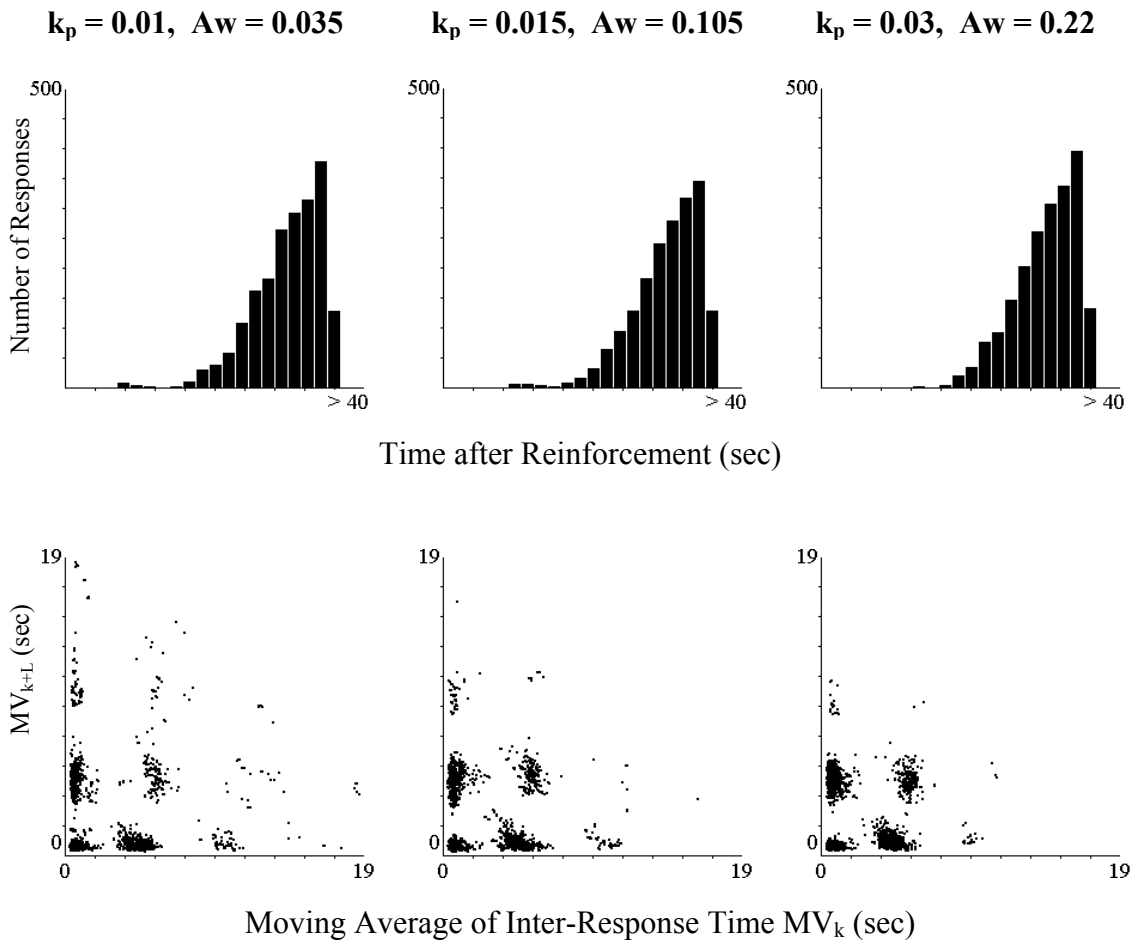

Figure 33: Effects of varying $\mathbf{k_P}$, and $\mathbf{A_W}$. The other parameters are the same as in the simulation IIa. Both the averaged scallop curves and the ERMs look similar, except that the dispersion of data points in the ERMs decreases when the values of $\mathbf{k_P}$ increase.

used in simulation III are the same as in simulation IIa. The three sets of $\mathbf{k_P}$ and $\mathbf{A_W}$ in simulation III all reveal similar "averaged scallop curves" and ERM-patterns. However, the degree of dispersion of data points in the ERMs decreases slightly with increasing $\mathbf{k_P}$.

Secondly it is remarkable that similar switching rates ($\mathbf{M_P} \approx \mathbf{M_R} \approx 0.8$) were used to simulate all the target animals in the simulations IIa-d. The effects of using smaller $\mathbf{M_P}$ and $\mathbf{M_R}$ are investigated in the simulations IV and V. In both simulations all parameters except the $\mathbf{M_P}$ and $\mathbf{M_R}$ are the same as in the simulation II. The new values of $\mathbf{M_P}$ or $\mathbf{M_R}$, as well as the results of simulations are shown in figures 34 and 35.

The averaged scallop curve and the IRT distribution are relatively insensitive to the

change of $\mathbf{M_P}$ (results not shown here). The ERMs, on the contrary, are effected by varying the value of $\mathbf{M_P}$. The degrees of the apparent changes of the ERM-patterns depend on the type of the patterns (figure 34). The main structures of the lattice and L-type ERM-patterns in simulations IIa and IIb remain almost unchanged after the value of $\mathbf{M_P}$ is reduced from 0.8 to 0.1 and 0.01. Only the dispersion of data points in the ERM decreases slightly (the first and second panels in figure 34). The same changes of parameter $\mathbf{M_P}$ transform the empty triangle ERM-patterns in simulation IIc to L-type ones (the third panel in figure 34). Also the solid triangle ERM-patterns undergo a structural change from triangle to a "thick" L-type when the $\mathbf{M_P}$ is reduced to 0.01 (the last panel in figure 34).

The decrease of $\mathbf{M_R}$ from 0.8 to 0.3 delays the onset of operant activity, and at the same time decreases its magnitude. These effects can be observed in the "averaged scallop curve" in figure 35. Increase of dispersions of data points in the ERMs can also be observed. However, the main structures of ERM-patterns, that is, the lattice, the L-type, and both the empty and solid triangles, can still be recognized (figure 35).

The forms of the averaged scallop curve and the IRT distribution seem to be controlled by two different sets of parameters. Namely, the parameters $\mathbf{k_P}$, $\mathbf{M_P}$, $\mathbf{M_R}$, $\mathbf{A_W}$ and $\mathbf{O_W}$ for the averaged scallop curve, and $\mathbf{M_{1\text{-}2}}$, $\mathbf{A_{1\text{-}2}}$ and $\mathbf{O_{1\text{-}2}}$ for the IRT distribution. This finding suggests that the mechanism for generating operant responses, that is, component IV (figure 27), seems to work, at least to a certain degree, independently from the other parts of the model (components I-III in figure 27). This impression is further supported by the simulation VI, whose results are shown in figure 36. In simulation VI the parameters are the same as in simulation IIb and IIc. However, the settings for $\mathbf{M_{1\text{-}2}}$, $\mathbf{A_{1\text{-}2}}$ and $\mathbf{O_{1\text{-}2}}$ are interchanged between the two simulations, so that simulation VIa has the same parameters $\mathbf{k_P}$, $\mathbf{M_P}$, $\mathbf{M_R}$,

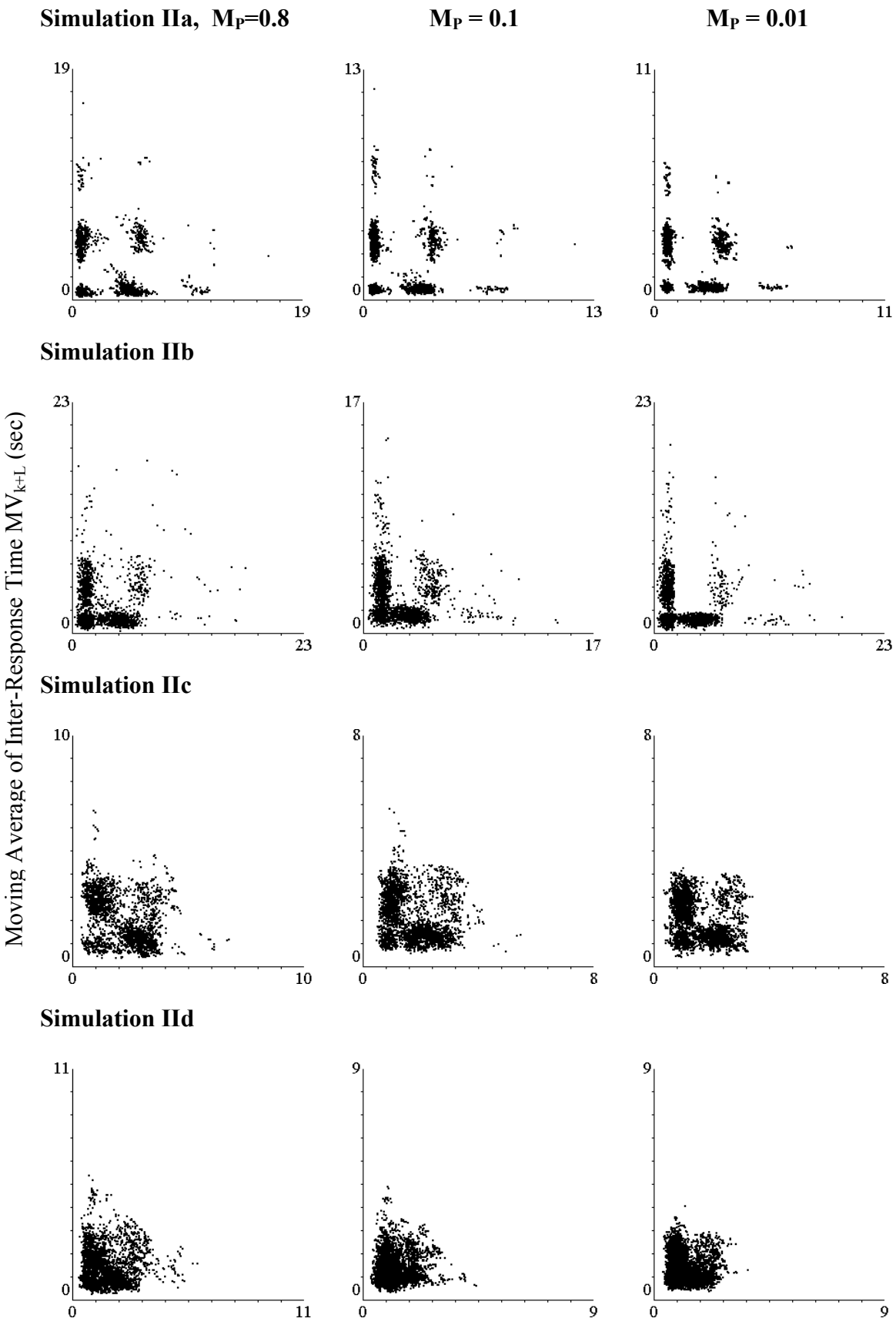

Figure 34: Effects of varying parameter $\mathbf{M_P}$. The dispersion of data points decreases with decreasing $\mathbf{M_P}$. Only the ERMs of simulation IIc show clear structural changes.

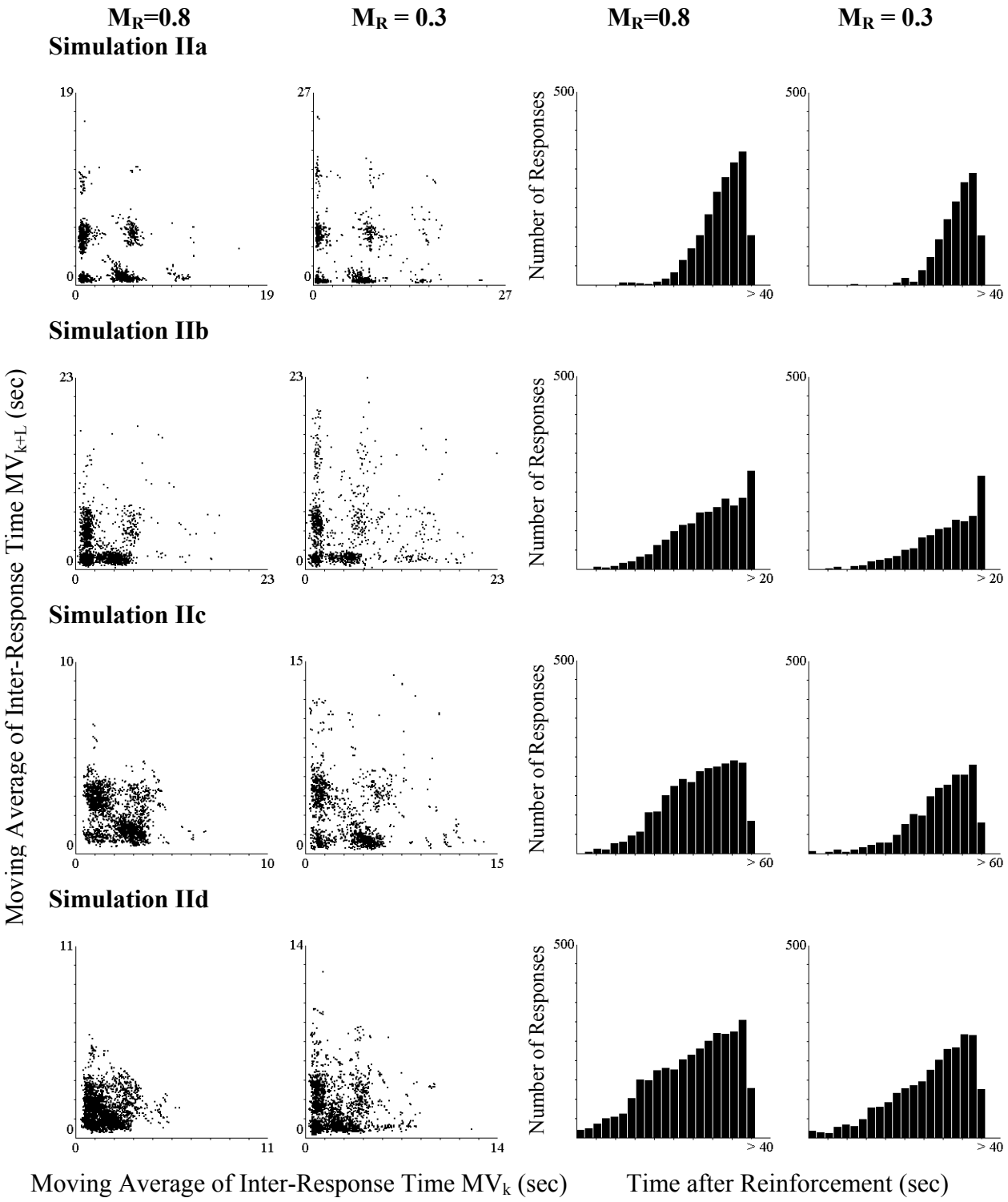

Figure 35: Effects of varying parameter $\mathbf{M_R}$. Smaller $\mathbf{M_R}$ values induce later onset of operant responses. So the averaged scallop curves shift toward right. However, the main characters of the ERM-patterns are still intact.

Simulation VIa

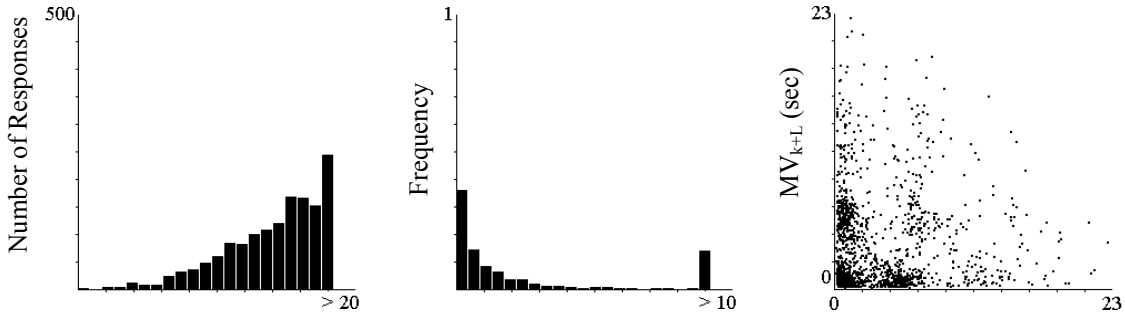

Simulation VIb

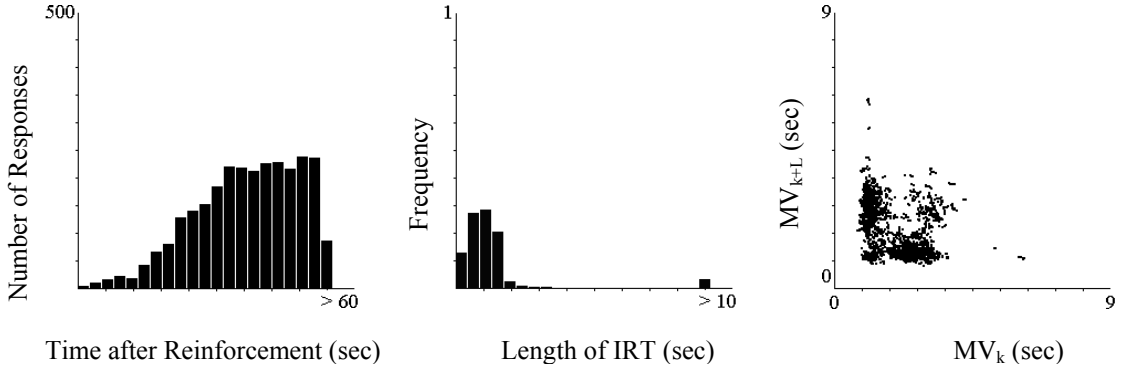

Figure 36: Effects of interchanging parameter sets. The parameters used here are the same as in simulations IIb and IIc, but the parameters $\mathbf{M_{1\text{-}2}}$, $\mathbf{A_{1\text{-}2}}$ and $\mathbf{O_{1\text{-}2}}$ are interchanged. As a result, simulation VIa has a similar form of the scallop curve as the simulation IIb, but its IRT distribution is similar to that of simulation IIc. Simulation VIb, on the contrary, has a similar form of the scallop curve as that of simulation IIc, but its IRT distribution looks similar to that of the simulation IIb.

$\mathbf{A_W}$ and $\mathbf{O_W}$ as simulation IIb, but its parameters $\mathbf{M_{1\text{-}2}}$, $\mathbf{A_{1\text{-}2}}$ and $\mathbf{O_{1\text{-}2}}$ are the same as simulation IIc. Simulation VIb, on the contrary, has the same parameters $\mathbf{k_P}$, $\mathbf{M_P}$, $\mathbf{M_R}$, $\mathbf{A_W}$ and $\mathbf{O_W}$ as simulation IIc, but its parameters $\mathbf{M_{1\text{-}2}}$, $\mathbf{A_{1\text{-}2}}$ and $\mathbf{O_{1\text{-}2}}$ are the same as simulation IIb.

In figure 36 we can see that simulations VIa and IIb have very similar averaged scallop curves. However, simulation VIa's IRT-distribution looks very similar to that of simulation IIc. Analogically, simulations VIb and IIc have very similar averaged scallop

curves, but simulation VIb's IRT-distribution looks very similar to that of simulation IIb. In the ERMs of simulation VI we can see that, although the patterns look neither like simulation IIb, nor simulation IIc, the main geometrical features, namely the L-type structure of simulation IIb and the empty triangle structure of simulation IIc, can be discovered in simulations VIa and VIb respectively. This finding implies that the parameters $\mathbf{k_P}$, $\mathbf{M_P}$, $\mathbf{M_R}$, $\mathbf{A_W}$ and $\mathbf{O_W}$ have more influence on the main structures of the ERM-patterns.

The form of the averaged scallop curve is controlled by many parameters. They seem to be able to partly compensate the effects of each others, which makes it more difficult to fit the simulated curve to the experimental data. The present work provides only some initial hints to the complete understanding of the model. Further studies in the future will be required.

4 Applications in behavioral pharmacology

4.1 Basic concepts

4.1.1 ERM-pattern as a dependent variable

After seeing the pure behavioral and theoretical sections discussed above, we now turn our interest to more practical applications of non-linear dynamical analysis. The operant behavior observed in the Skinner-box have been used in many practical applications. For example, the rate of responses can serve as a dependent variable to measure the strength of reinforcement, which might be induced or facilitated by pharmacological treatments. Furthermore, the FI-schedules can be used to study temporal behavior, or even as a diagnostic tool for diseases that are thought to be related to impairments of the temporal function of the brain. An example of these kinds of diseases is the attention deficit/hyperactivity disorder (ADHD). One of its characteristics is the earlier onset of operant activities under the control of FI-schedules (Sagvolden et al. 1998). If pharmacological treatments can lead to changes of the ERM-patterns, the ERM-patterns might be able to serve as a dependent variable to study the effects of pharmacological substances. The difference between using the rate of responses and using the ERM-patterns as dependent variable is, that the changes of ERM-patterns might provide more insight into the dynamical mechanism that leads to these behavioral changes.

One strategy to explore this possibility is to apply a well known treatment to the animals, and to see whether there are changes in the ERM-patterns. The treatment shall have been positively tested by traditional analysis. In case that there is no change in the ERM-patterns after the treatment, we can be sure that the negative result is not due to the failure of the treatment itself. To accomplish this goal we chose the intra-peritoneal injection of a medium dosage of amphetamine as our testing treatment.

4.1.2 Amphetamine and FI-responding

Considerable attention has been paid to the effects of amphetamine on operant

behavior. Evidence that amphetamine increases the rewarding property of food as well as of brain-stimulation has been reported in numerous studies (Dews 1958; Wenger and Dews 1976; Greenshaw et al. 1985; Hunt & Dale 1992). For FI-responding, the direction and magnitude of amphetamine-induced changes in rate of responses depends on the dosage of amphetamine.

When high doses of amphetamine are applied, the overall rate of responses is decreased. When a medium dosage of amphetamine is applied, the overall rate of responding increases. However, the magnitude of changes is not uniformly distributed over the inter-reinforcement period. In the segments after the delivery of reinforcements, where the rate of responses is lower prior to the treatment, the magnitude of increase is larger. In the segments before the delivery of reinforcements, where the rate of responses is higher prior to the treatment, the magnitude of increase is smaller, or sometimes the rate of responses even decreases slightly (Dews 1958; Branch & Gollub 1974; Segal et al. 1981; Tewes & Fischman 1982). As a result, medium dosages of amphetamine flatten the scallop-curve seen in the traditional analysis of FI-responding.

In the following experiment we use the ERM to observe the effect of medium dosages of intra-peritoneal amphetamine treatment. If changes of ERM-patterns appear after the treatment, we will further simulate the new ERM-patterns by setting a different set of parameters of the dynamical model. Then we can interpret the effects of amphetamine by comparing the two sets of parameters.

4.2 Experiments

4.2.1 Materials and methods

The animals from blocks B, C and D of the previous experiments described in section 2 continued to take part in the studies involving amphetamine. The animals from blocks B and C received only one injection of either amphetamine (B1, B3, B4, C1~C6) or saline (B2,

B5, B6) solution. The animals from block D received both the saline and the amphetamine injections. The detailed time schedules of the treatments will be discussed in section 4.2.2. The conditions for the maintenance of animals, including the procedure of food deprivation were the same as that described in section 2. Apparatus and software were also unchanged.

The amphetamine is obtained from the company SIGMA, and the chemical form of the compound is: d-amphetamine sulfate. For the intra-peritoneal injection, the typical range for the medium dosage is about 1 mg amphetamine per kg body weight (1mg/kg). The range of high dosage is about 10 mg/kg. In the present studies we wished to test the effects of a medium dosage of amphetamine. Thus, 1 mg amphetamine per kg body weight was applied. The solutions for the injection were prepared one day before the treatment. To prepare the solutions, 1mg amphetamine sulfate was dissolved in 1 ml saline, and the volume of injection depended on the body weight of the animals, which was measured daily during the whole experiment. The saline solution was prepared by dissolving 0,9 g NaCl in 1000 ml water.

4.2.2 Time schedule of experiments

Before the beginning of the treatment phase, the animals had been trained intensively under the control of FI-schedules. For animals in blocks B and C the training lasted 15 days, with one daily 90-minute session. For animals in block D, the training lasted 26 days.

Animals in blocks B and C received only one injection in the treatment phase. The solutions were either saline (B2, B5 and B6) or 1 mg/kg amphetamine (B1, B3 and B4, and all animals in block C) injection. After the injection they were brought back to their home cages, and could stay there for about 15 minutes to recover from the shock caused by the injection procedure. Then they were subjected to a 90-minute session under the same FI-schedules they had been trained. One day after the treatment they accomplished another 90-minute session without injections.

Animals in block D received totally two injections during the treatment phase, and these were applied on different days: the first and the third days of the treatment phase. The solutions were saline for the first injection, and 1mg/kg amphetamine for the second one. Similar to animals in blocks B and C, the animals in block D were allowed to recover after the treatment for 15 minutes, and then they were subjected to a 90-minute session in the Skinner-box. On the day between the first and second injections, as well as on the next day after the second injection, they also accomplished a 90-minute session with no injection.

4.2.3 Results and Discussions

The effects of saline injections are shown in figure 37. The comparison between treatment day and the day before reveals that the saline injection caused very little qualitative changes in the main structures, that is, the lattice, triangle and L-type structures of the ERM-patterns. Nor were the ERM-patterns considerably changed on the next day after the saline treatment. These results suggest that the saline solution as well as the procedure of injection do not noticeably alter the dynamics of the FI-responding.

The results of amphetamine injections are shown in figure 38. The effects are not uniform among the animals. Rats B4, C6, D3 and D9 showed very little changes in the ERM-patterns under the influences of amphetamine. The other animals showed at least the tendency that more data points were concentrated near the left bottom corner. Some animals showed noticeable qualitative changes in the ERM-patterns under the influences of amphetamine. The ERM-patterns of rats B3, C2, C5 and D6 had lattice structures under the drug-free conditions. On the day of amphetamine treatment, the lattice structures in the ERMs of rats B3, C2 and C5 almost completely vanished. Instead of the lattice patterns, a very dense cluster with a triangle form could be observed near the left bottom corner. The ERM-pattern of rat D6 on the treatment day still revealed lattice structures. However, a clear

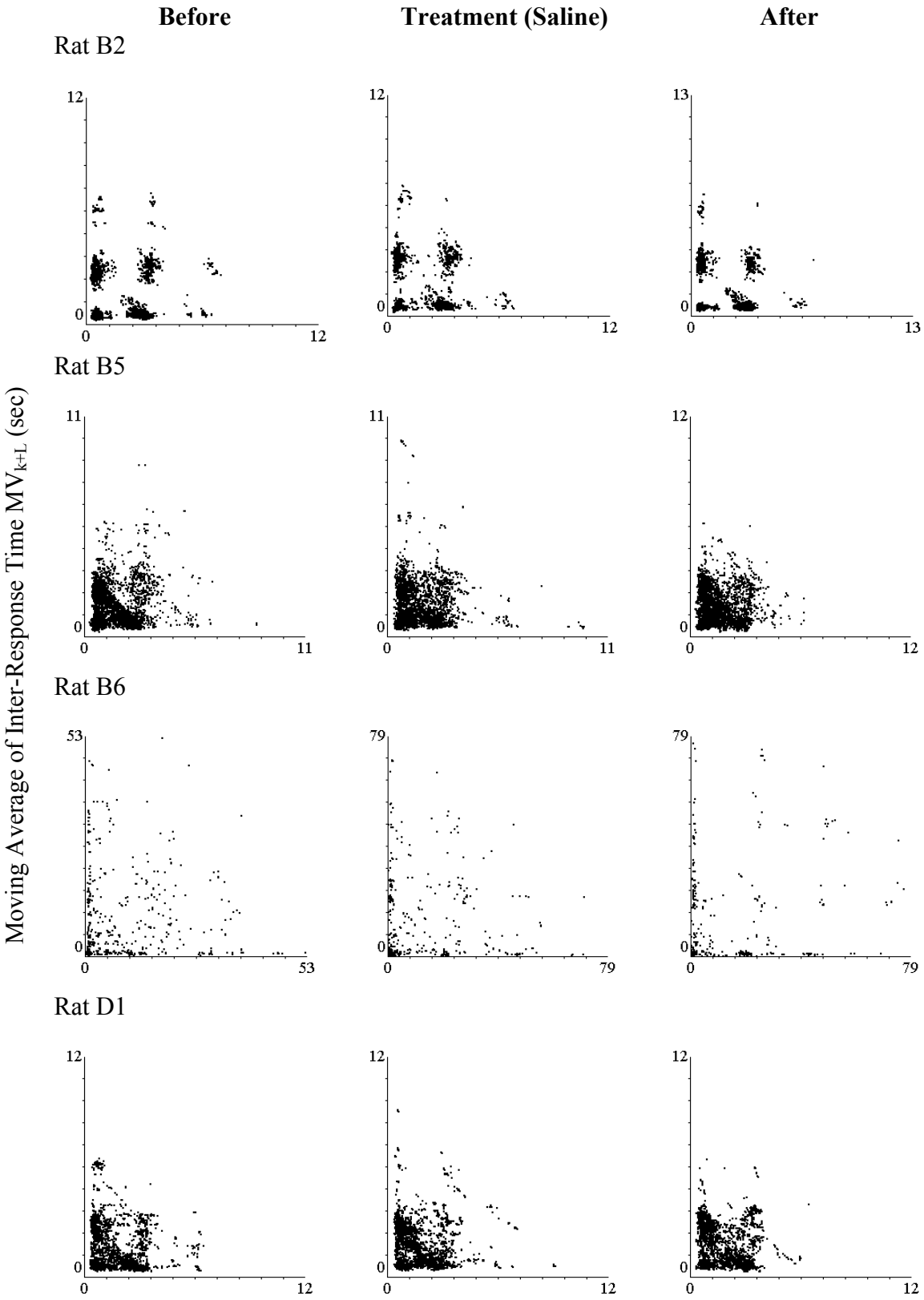

Figure 37: Effects of saline injection on the patterns of the ERMs. Injections were given at about 15 minutes before the beginning of the trials on the day of treatment. Their ERMs are shown in the middle column. The ERMs on the day before and after the treatment are shown in the left and right columns. Very few changes in the ERM-patterns can be seen. (continued in the next page)

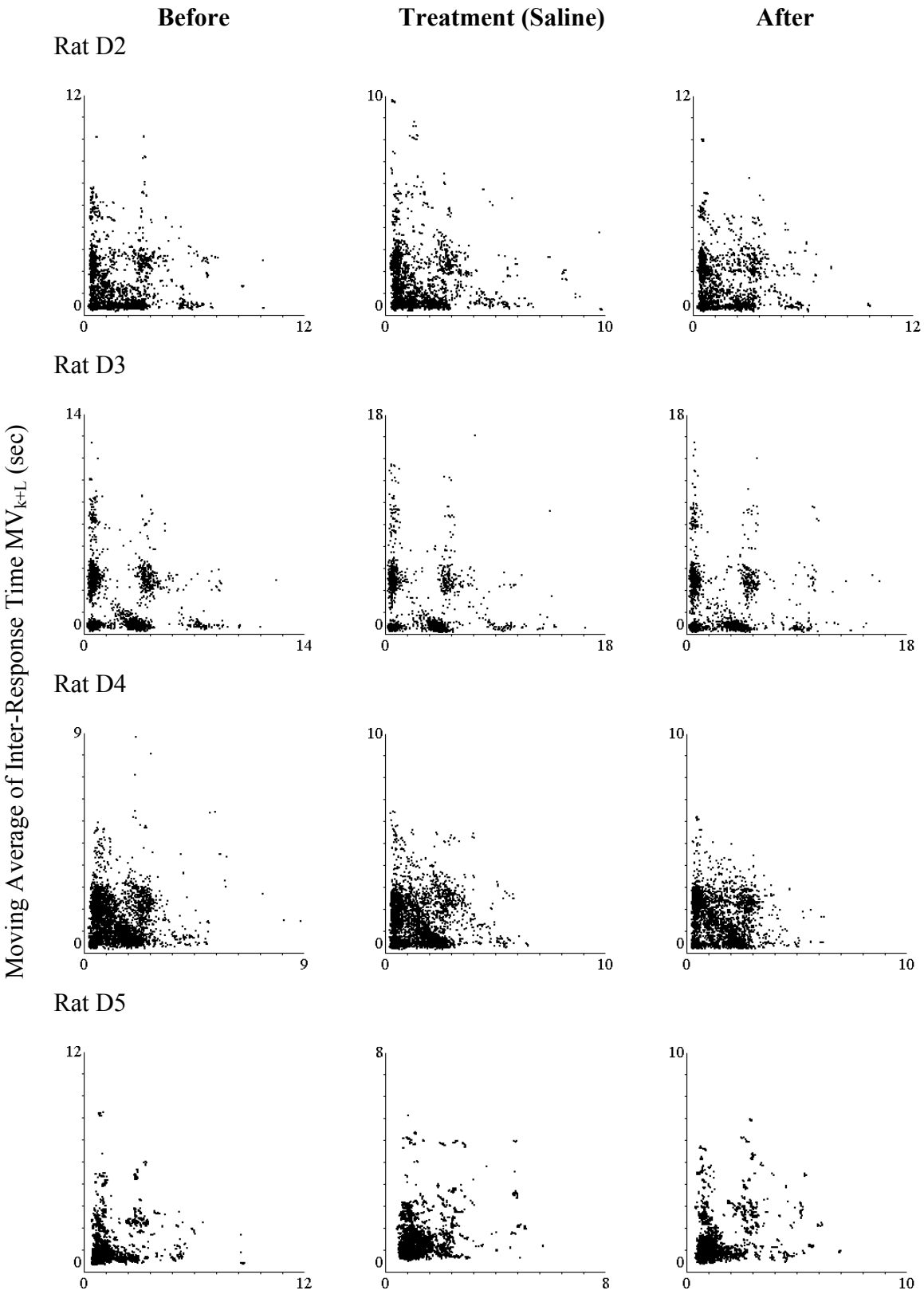

Figure 37: (continued from the previous page) Effects of saline injection on the patterns of the ERMs. The ERMs on the day before and after the treatment are shown in the left and right columns. (continued in the next page)

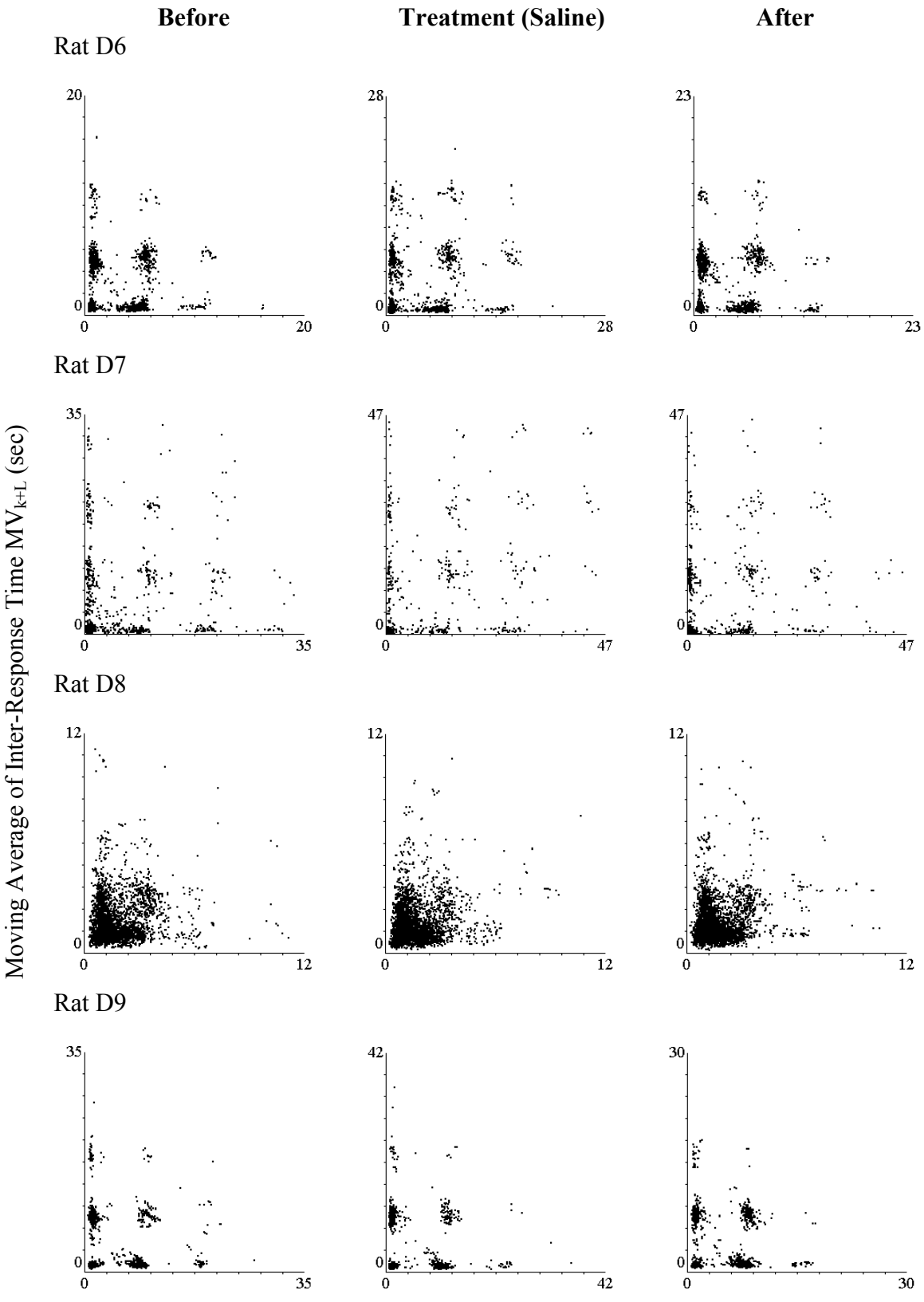

Figure 37: (continued from the previous page) Effects of saline injection on the patterns of the ERMs. The ERMs on the day before and after the treatment are shown in the left and right columns.

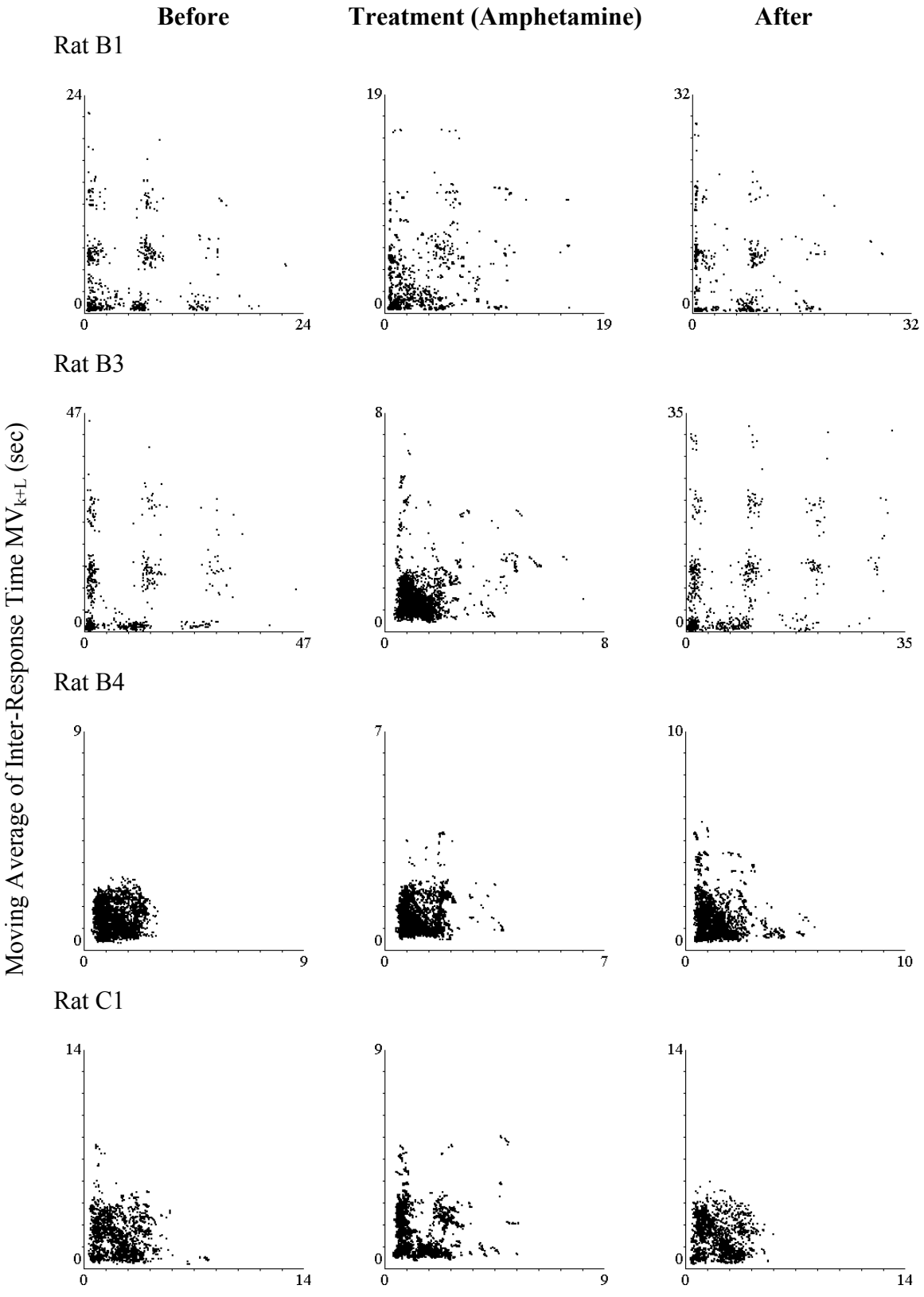

Figure 38: Effects of amphetamine injection on the patterns of the ERMs. The treatments was given 15 minutes before the trial. The ERMs on the day before and after the treatment are shown in the left and right columns. The reactions to amphetamine treatment were not the same for each animal. However, all the ERMs on the day after treatment were recovered to the original patterns on the day before treatment. (continued in the next page)

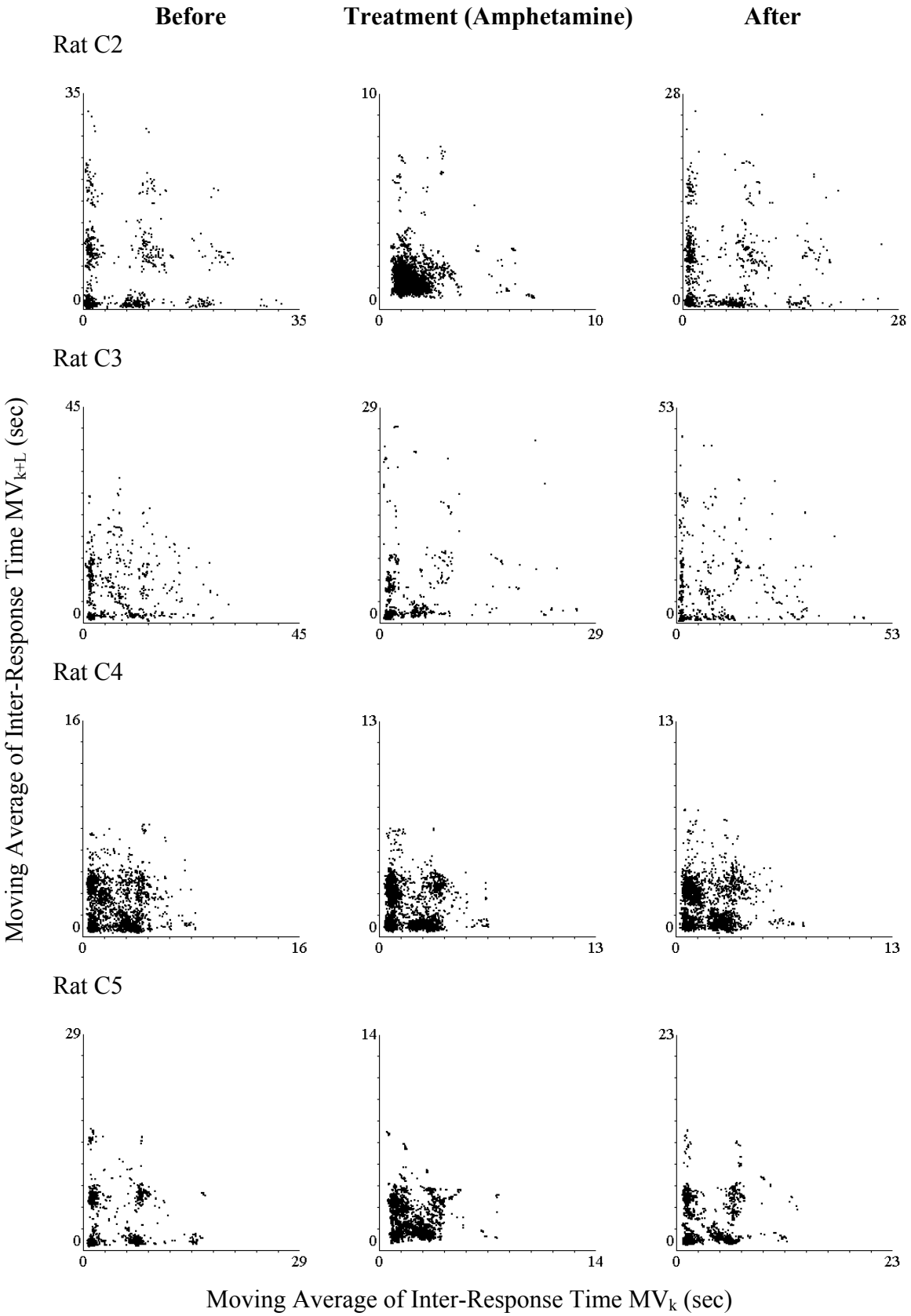

Figure 38: (continued from the previous page) Effects of amphetamine injection on the patterns of the ERMs. The treatments was given 15 minutes before the trial. The ERMs on the day before and after the treatment are shown in the left and right columns. The reactions to amphetamine treatment were not the same for each animal. However, all the ERMs on the day after treatment were recovered to the original patterns on the day before treatment. (continued in the next page)

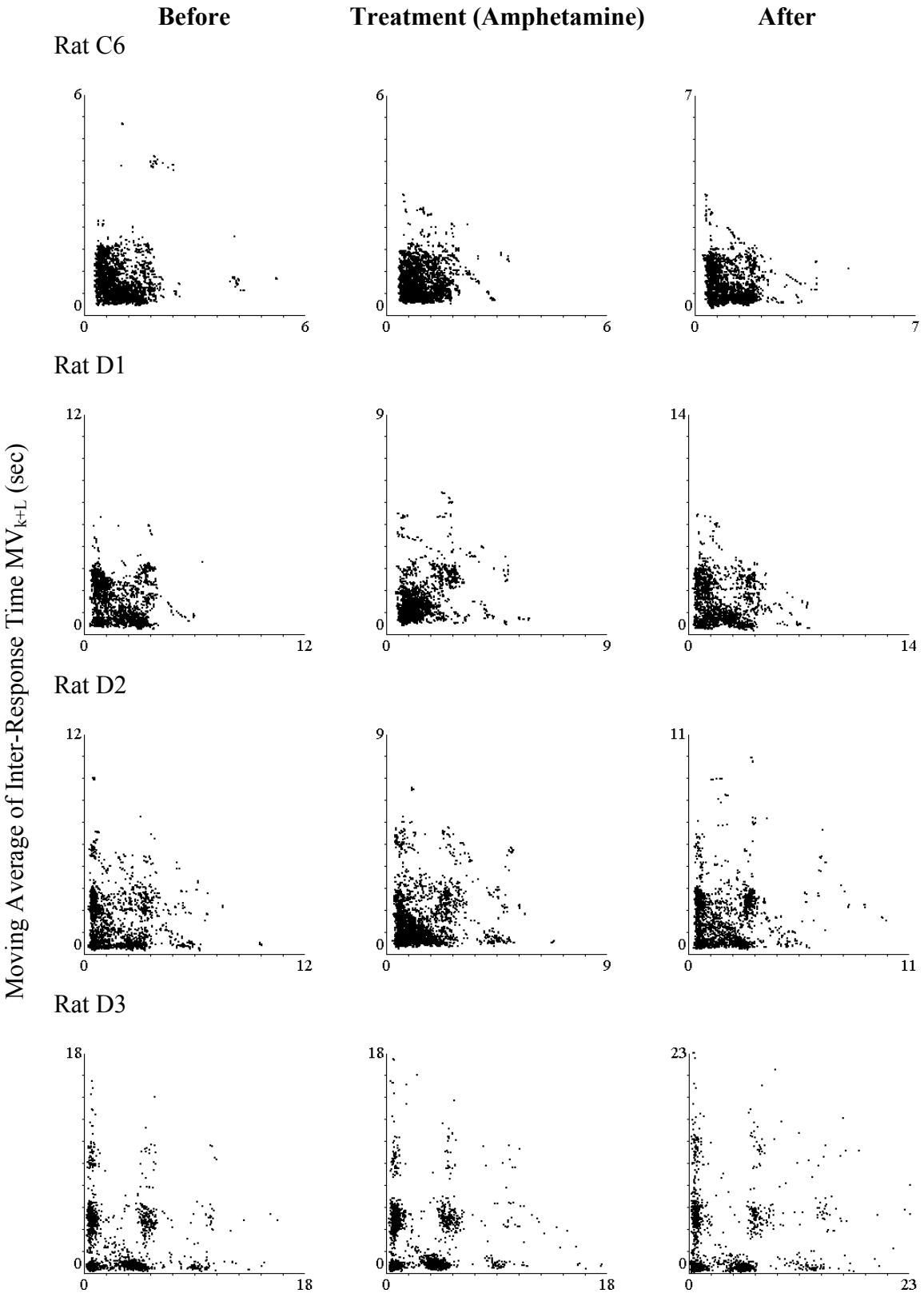

Figure 38: (continued from the previous page) Effects of amphetamine injection on the patterns of the ERMs. The treatments was given 15 minutes before the trial. The ERMs on the day before and after the treatment are shown in the left and right columns. The reactions to amphetamine treatment were not the same for each animal. However, all the ERMs on the day after treatment were recovered to the original patterns on the day before treatment. (continued in the next page)

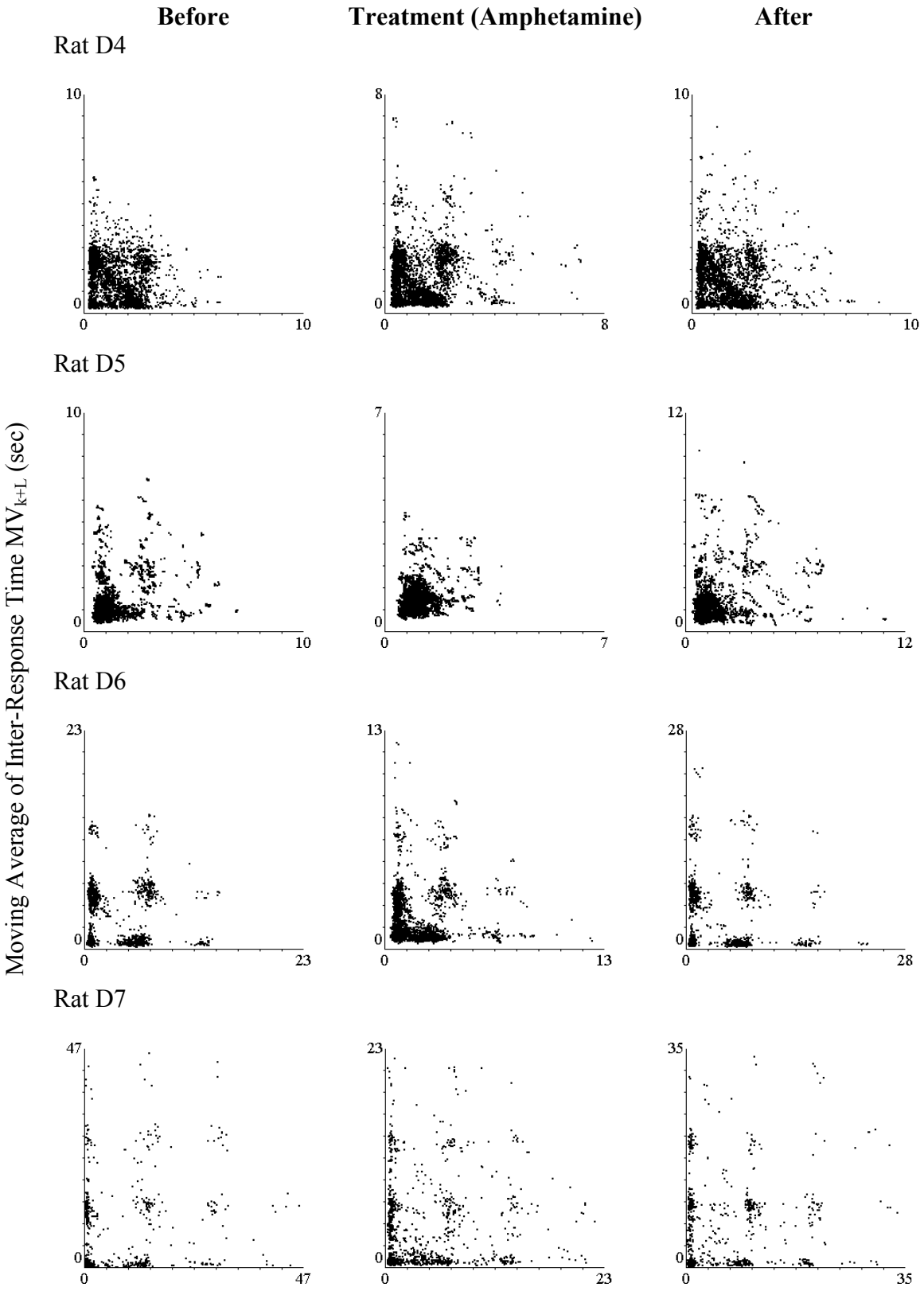

Figure 38: (continued from the previous page) Effects of amphetamine injection on the patterns of the ERMs. The treatments was given 15 minutes before the trial. The ERMs on the day before and after the treatment are shown in the left and right columns. The reactions to amphetamine treatment were not the same for each animal. However, all the ERMs on the day after treatment were recovered to the original patterns on the day before treatment. (continued in the next page)

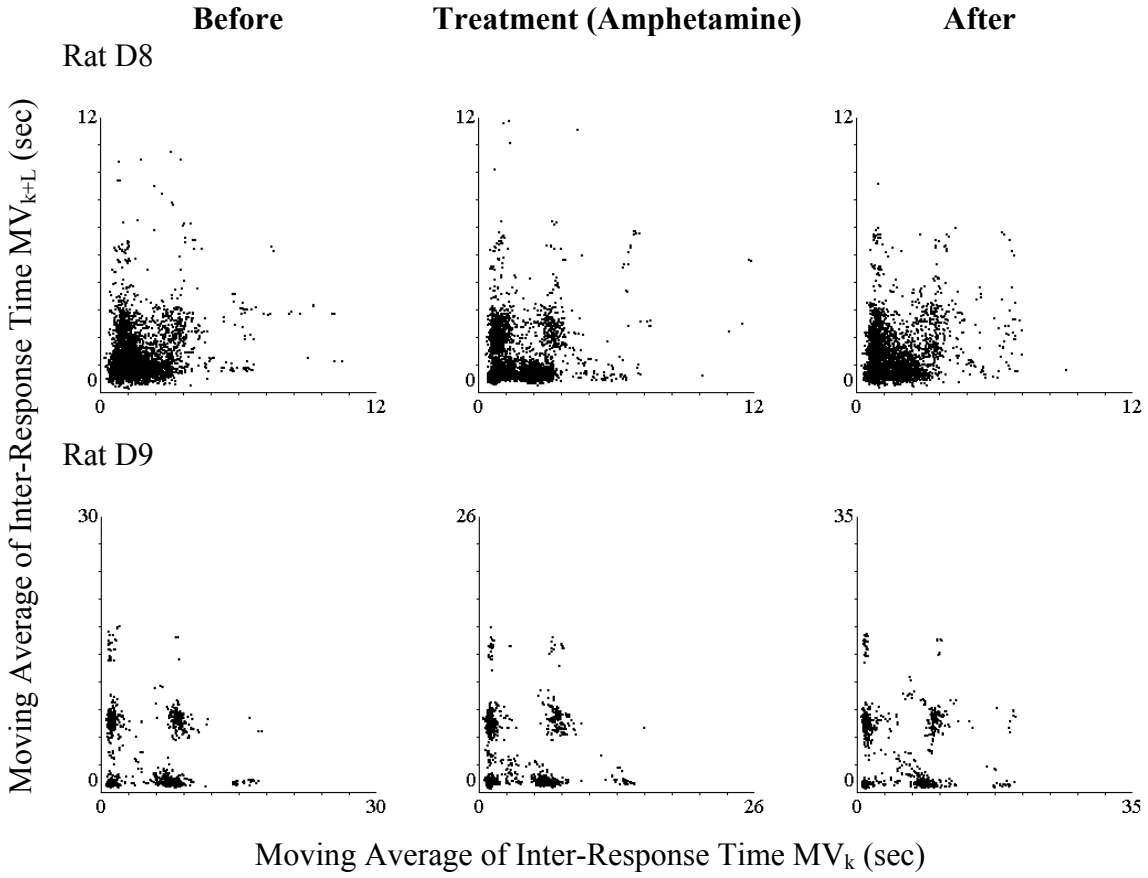

Figure 38: (continued from the previous page) Effects of amphetamine injection on the patterns of the ERMs. The treatments was given 15 minutes before the trial. The ERMs on the day before and after the treatment are shown in the left and right columns. The reactions to amphetamine treatment were not the same for each animal. However, all the ERMs on the day after treatment were recovered to the original patterns on the day before treatment.

L-type structure can be identified in addition to the lattice. The changes of the ERM-patterns of rats C1, C4 and D8 are also interesting. Under the drug-free conditions their ERM-patterns revealed triangle structures. After receiving amphetamine injection, the ERM-patterns were changed to L-types.

The total number of responses in the 90-minute sessions during the whole treatment phase are outlined in table 6. In addition to the absolute number of responses, the percentage changes in the number of responses on the treatment days in comparison with the days before them are shown in the parenthesis. First we can see that, although no major changes in the ERM-patterns are observed on the day of saline-treatment, there are still several animals that

revealed a quite different amount of operant activity on that day. For example, rats B6, D5, D6 and D8 had 20% ~ 38% increases or decreases in the total number of responses. Under the influence of amphetamine some animals showed comparable, or even smaller changes in the number of responses. However, their ERM-patterns revealed qualitative changes. For example, rats C4 and D8 showed clear qualitative changes of ERM-patterns from triangle to L-type structures, and the changes in their number of responses were 34% and 0.3% respectively. The latter implies practically no changes in the amount of operant activity. However, the quality of the operant behavior was different, since the ERM-patterns had changed. On the other hand, rats B4, C6 and D9 showed very little changes in the structures of ERM-patterns, and their changes in the number of responses were 23%, 2%, and 19% respectively. It seems that qualitative changes of ERM-patterns, which imply changes of behavioral dynamics, are not necessarily correlated with changes in the amount of responses.

Furthermore, it is interesting to note that rats B3, C2 and C5 showed more than 100% increase in the number of responses, and they also had similar qualitative changes in the structures of ERM-patterns, namely, from lattice structures to a very dense triangle cluster near the left bottom corner. Finally, one animal, rat D3, lowered its number of operant responses for about 12% under the influence of 1mg/kg amphetamine, and this animal also showed very little changes in ERM-patterns. Since it is the only animal that decreases its operant activity on the day of amphetamine treatment, it is not possible to tell how this decrease is correlated with changes (or no change) in the ERM-patterns. It might be interesting to compare this case with rats C6 and D8. Both animals showed hardly any changes in the number of responses (2% and 0.3% respectively) under the influence of amphetamine. While rat C6 had very little changes in the ERM-patterns, that of rat D8 changed from triangle to L-type on the day of amphetamine treatment.

Table 6 Number of responses per session in the treatment phase

	Schedule	Before	Saline	Between	Amphetamine	After
B1	FI90s	1521	---	---	2059 (35%)	1106
B2	FI60s	3136	3012 (- 4%)	---	---	2832
B3	FI40s	838	---	---	4538 (442%)	974
B4	FI60s	4222	---	---	5198 (23%)	3803
B5	FI40s	3413	3427 (0.4%)	---	---	3274
B6	FI90s	636	495 (- 22%)	---	---	476
C1	FI60s	2585	---	---	3920 (52%)	2645
C2	FI40s	1039	---	---	3610 (247%)	1230
C3	FI90s	788	---	---	1113 (41%)	672
C4	FI40s	2252	---	---	3014 (34%)	2781
C5	FI90s	1224	---	---	2607 (113%)	1663
C6	FI60s	5904	---	---	6025 (2%)	5052
D1	FI60s	3201	3163 (-1%)	2978	4190 (41%)	2669
D2	FI40s	3141	3638 (16%)	3267	4094 (25%)	3505
D3	FI20s	2345	2047 (-13%)	2179	1927 (-12%)	1562
D4	FI20s	3984	3618 (-9%)	3576	4493 (26%)	3491
D5	FI60s	3761	4511 (20%)	3971	5266 (33%)	3049
D6	FI40s	1796	1358 (-25%)	1679	2976 (77%)	1404
D7	FI40s	1097	682 (-38%)	886	1605 (81%)	950
D8	FI20s	2990	3161 (6%)	3086	3096 (0.3%)	3185
D9	FI60s	996	896 (-10%)	1144	1360 (19%)	968

Finally it should be noted that the comparisons between changes in the number of responses and in the ERM-patterns discussed above are only partially quantitative, since there is not yet a definition to quantify the changes of ERM-patterns from session to session. This might be a necessary step in the further development of the ERM as an analyzing tool in the future.

4.3 Computer simulation VII

The data of three rats C1, D6 and D8 were used as targets in the simulation VII to study the effects of amphetamine treatments. Their IRT data sets were already the targets in

simulation II. Rat B5 also took part in simulation II. However, it was not treated with amphetamine. The parameters used in simulation VII are outlined in table 7. They were acquired using similar procedures discussed in section 3.3.2. The averaged scallop curve, the IRT-distribution and the ERMs are shown in figures 39. Roughly speaking, the results of simulations VIIa and VIIc can match their experimental targets quite well. The averaged scallop curve and the IRT distribution of simulation VIIb show relatively larger deviations from their experimental targets. Nevertheless, the main features of the experimental ERM-patterns, in this case the L-type structures, are still clearly identifiable in the simulated ERM.

Table 7 Parameters for simulation VII

	VIIa	**VIIb**	**VIIc**
Target	D6	D8	C1
$\mathbf{k_P}$	0.0151	0.00574	0,00701
$\mathbf{M_P}$	0.0103	0.1796	0,0101
$\mathbf{M_R}$	0.8118	0.7575	0,7979
$\mathbf{A_W}$	0.1311	0.8907	0,1151
$\mathbf{O_W}$	0.00202	0.0154	0,0161
$\mathbf{M_1}$	0.0411	0.1669	0,0550
$\mathbf{A_1}$	0.5112	0.0574	0,1491
$\mathbf{O_1}$	0.00303	0.0287	0,0497
$\mathbf{M_2}$	0.0300	0.1276	0,0399
$\mathbf{A_2}$	0.3147	0.0792	0,3046
$\mathbf{O_2}$	0.00201	0.0111	0,00101
SLQ	0.0119	0.0423	0,0032

The target data sets in simulation VII are from sessions in which animals ran the trial under the influence of amphetamine, while those in simulation II are the products of behavior of the same animals prior to the treatment. Thus, comparison between the parameter settings of those pairs of simulations, whose target data sets are produced by the same animals, might give hints to the understanding of the effects of amphetamine on the dynamics of FI-responding. Several findings are interesting, and will be discussed below:

Firstly, the values of $\mathbf{M_P}$ in simulations VIIa, VIIb and VIIc are much smaller than those in simulations IIa, IIe and IIc. At the same time, the values of parameter $\mathbf{M_R}$ are approximately the same in both simulations II and VII. The parameter $\mathbf{M_P}$ decides the

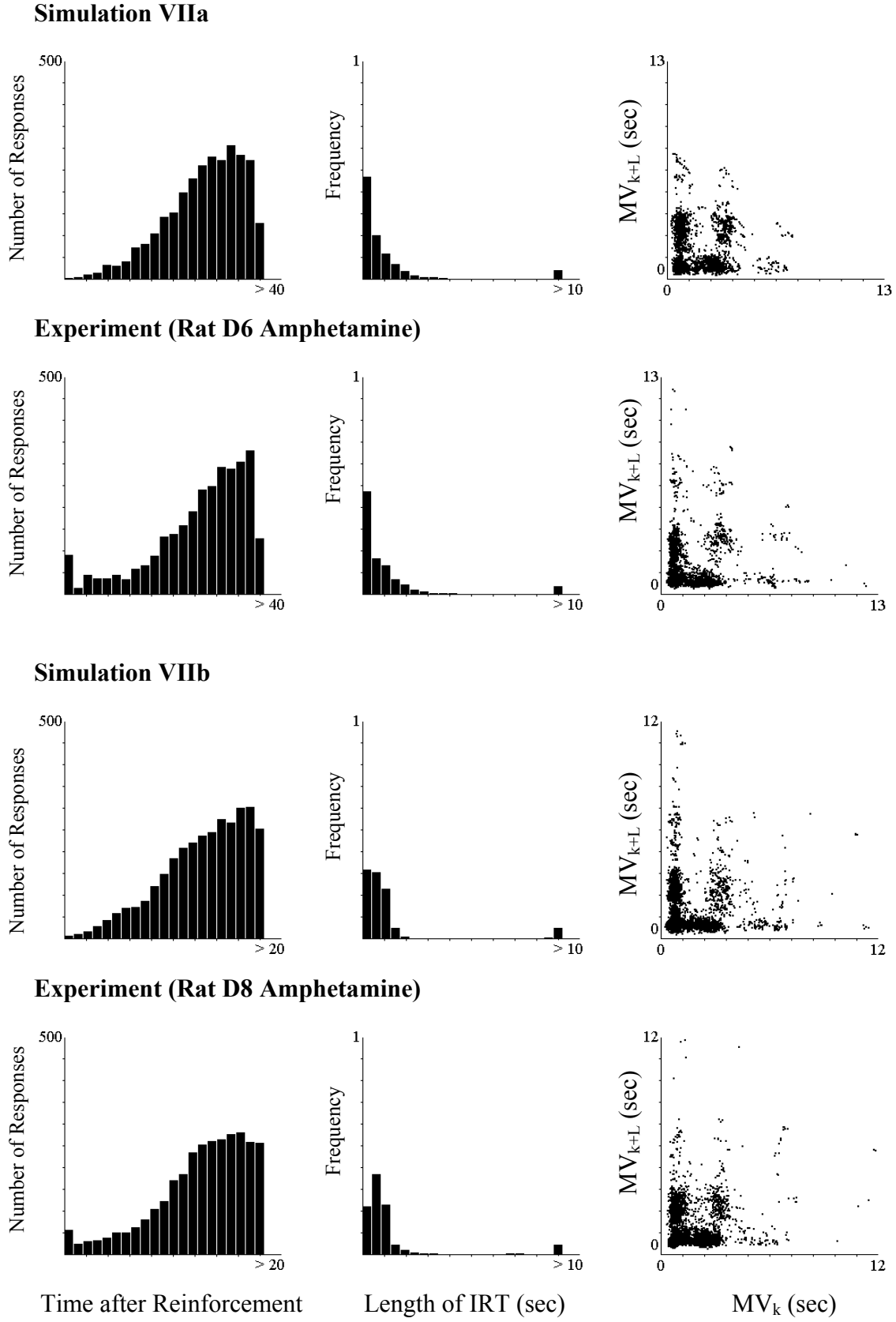

Figure 39: Simulation studies on the effects of amphetamine. Results of simulation VIIa can be fitted to its experimental target quite well. Results of simulation VIIb have small but identifiable deviations from its targets in the IRT distribution. However, the main characters of the experimental ERM-patterns are still quite well simulated. (continued in the next page)

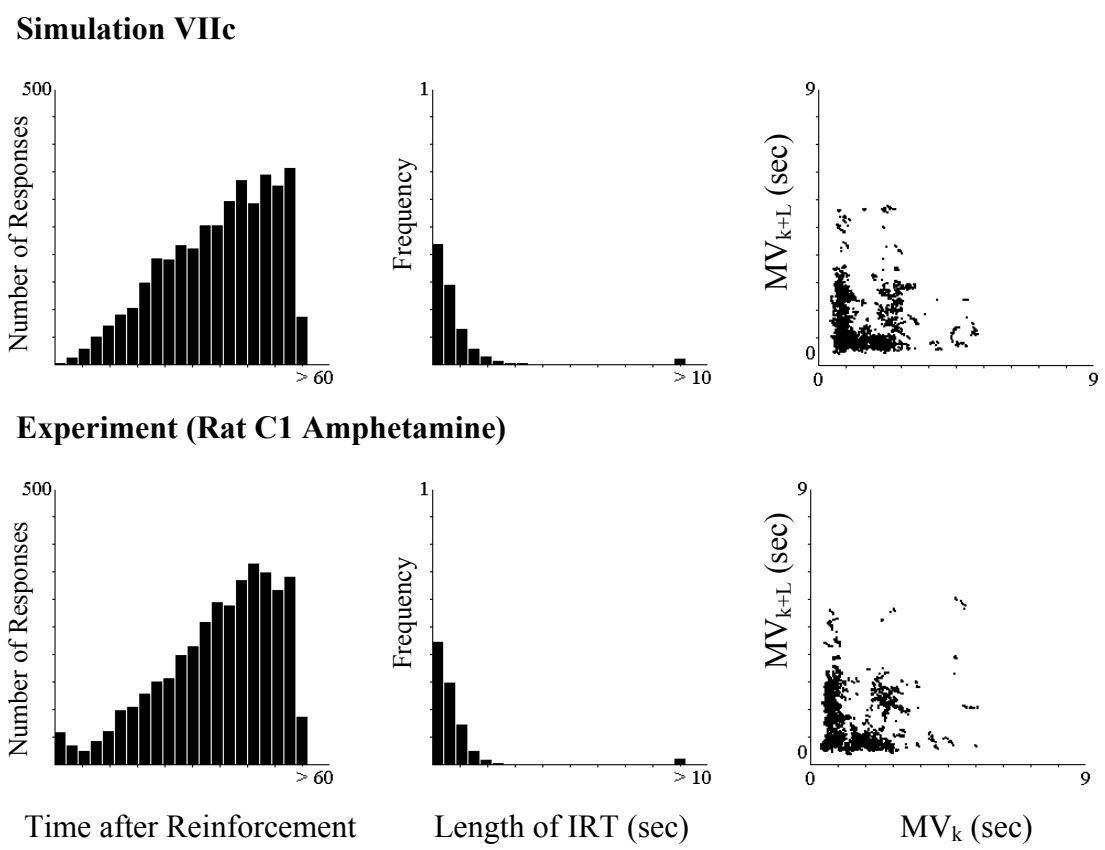

Figure 39: (continued from the previous page) Simulation studies on the effects of amphetamine. Results of simulation VIIc can be fitted to its experimental target quite well.

probability of switching of behavioral states from "responding" to "pause". The smaller values can be interpreted as decreasing the tendency of animals' returning back to the "pause" state when they are under the influence of amphetamine.

Secondly, the values of parameter $\mathbf{k_P}$ in simulation VII are approximately the same as in simulation II, when compared between simulations using the same target animal. At the same time, the parameters $\mathbf{A_W}$ and $\mathbf{O_W}$ change. The parameter $\mathbf{k_P}$ controls the speed of the internal clock of the model, and the parameters $\mathbf{A_W}$ and $\mathbf{O_W}$ adjust the form of the weights array (figure 27). Since their effects on the averaged scallop curve compensate each other, it is still possible, that similar effects can be achieved by simultaneously changing $\mathbf{k_P}$, and

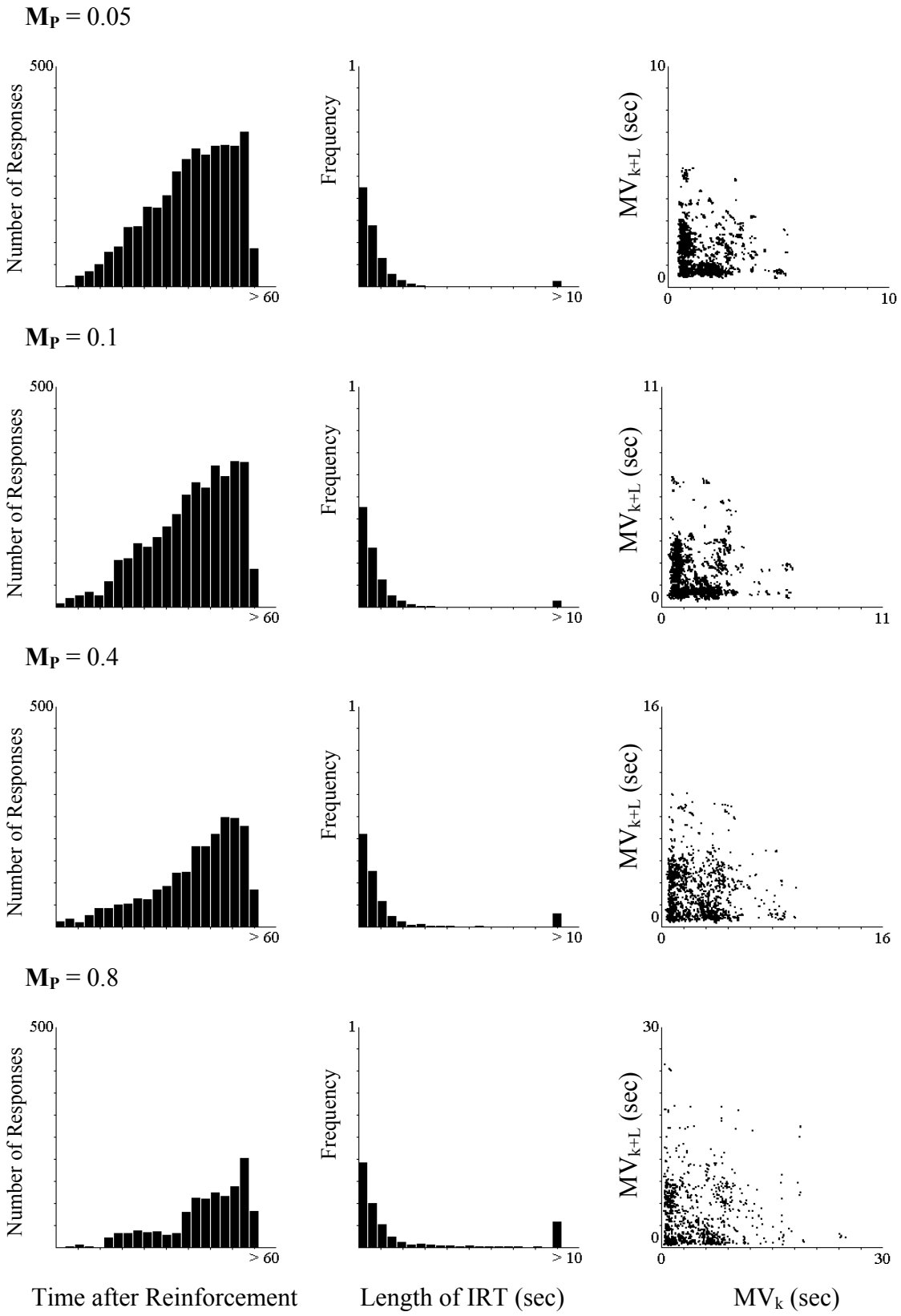

Figure 40: Effects of using different values of $\mathbf{M_P}$. The averaged scallop curve shifts towards the right with increasing $\mathbf{M_P}$, and at the same time the distribution of data points in the ERMs becomes more diffuse. However, the main characters of the ERM-patterns are conserved. The IRT distributions are hardly affected.

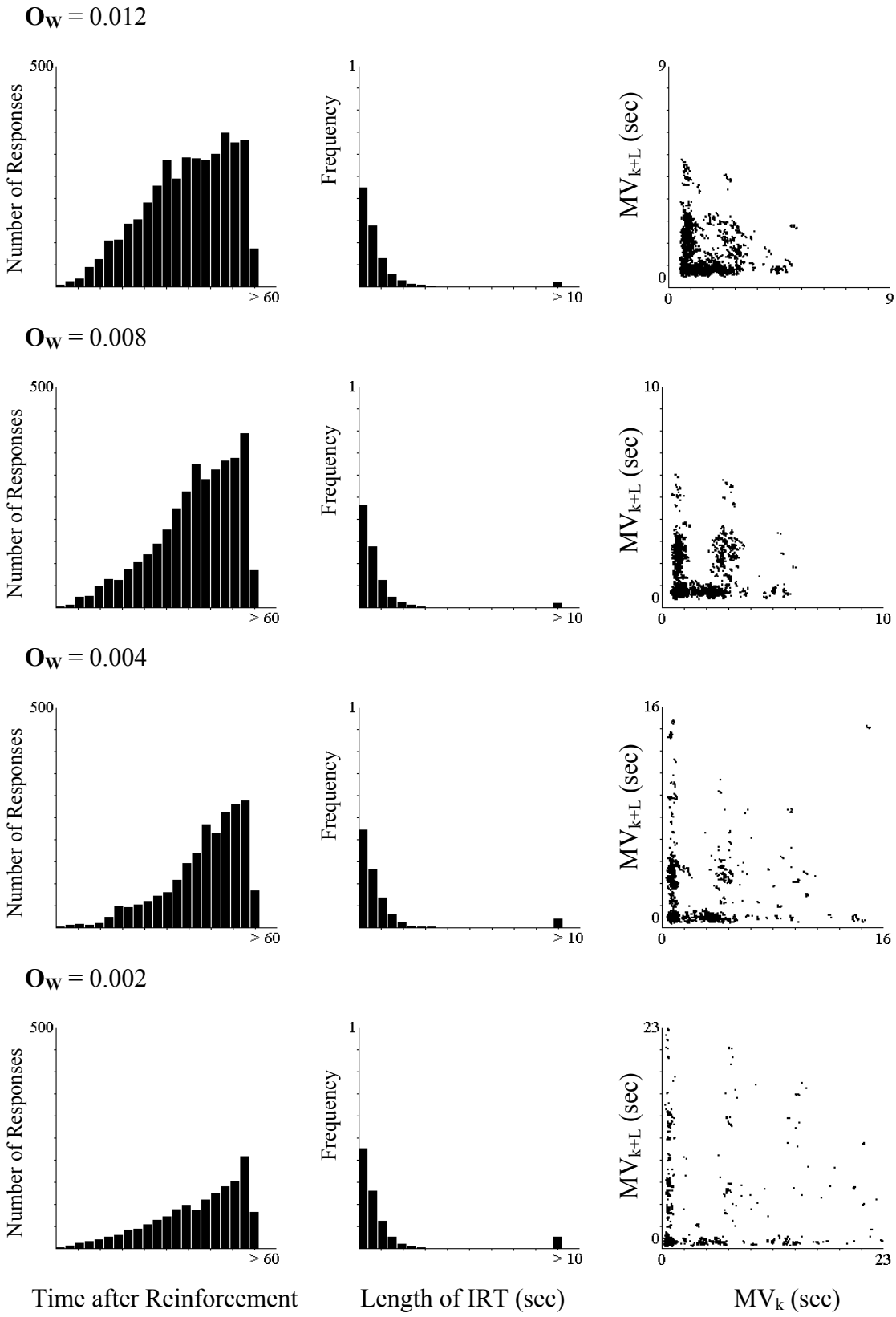

Figure 41: Effects of using different values of O_W. The averaged scallop curve shifts towards the right with decreasing O_W. At the same time, both the distribution of data points and the main characters of patterns are changed in the ERMs. As in figure 51, the IRT distributions are hardly affected.

adjusting $\mathbf{A_W}$ and $\mathbf{O_W}$ accordingly. However, as discussed previously in section 3.7.7, the dispersion of data points in ERMs will differ slightly, if the parameter $\mathbf{k_P}$ changes (figure 33).

The effects of varying $\mathbf{M_P}$ are demonstrated again in figure 40, in which the same parameter settings as in simulation VIIc, except for $\mathbf{M_P}$, were in use. We can clearly see that the L-type structure with clear-cut boundary changes to a diffuse triangle when $\mathbf{M_P}$ increases. Furthermore, the form of the averaged scallop curve also changes. The same changes of the averaged scallop curve can be achieved by decreasing the values of $\mathbf{O_W}$, as demonstrated by the examples shown in figure 41. At the same time, the distribution of IRT remains relatively unchanged in all parameter settings. However, figures 40 and 41 show completely different changes of ERM-patterns. This is another example to demonstrate that the averaged scallop curve and the IRT-distribution are not sufficient to describe the dynamics of FI-responding.

5 General Discussions

5.1 Conclusions of the present study

5.1.1 ERM: A new method for the non-linear dynamical analysis of operant behavior

One achievement of the present work is the improved analyzing ability of the "extended return map (ERM)" over the original "return map (RM)". Comparison between the two analyzing tools shown in figures 5-8 reveals that the well organized lattice, triangle and L-type structures in the ERMs of rats under the control of fixed-interval (FI) schedules are not visible in RMs. The patterns seen in the ERMs are comparable to the trajectory in the phase space and reflect dynamic properties of the system under study (Kantz & Schreiber 1997; Liebovitch 1998). Thus, we can state that the ERM-patterns are traces of the behavioral state of the animals during the experiment. The regular structures in the ERMs of FI-schedule controlled behaviors suggest a kind of periodicity.

However, since time series data from an experimental study contain only a limited number of elements and are often contaminated with noise, the absolute value of a nonlinear dynamic analysis could be erroneous and might indicate false deterministic relationships of the system's dynamics. To exclude this possibility, it is necessary to look at the surrogate data sets, which share the same first order correlation with the experimental data, but have the higher order correlation destroyed (Theiler et al. 1992; Liebovitch 1998). In the present work, we produced surrogate data sets using exactly the same data as the experiments. We simply randomized their sequential order. The direct comparison between the surrogate and the experimental ERMs suggests: 1) the separation of clusters, 2) the form and density of the "center-cluster", and 3) the data points distributed along the diagonal direction are important elements that reflect the dynamic properties of FI-responding. The meaning of the large cluster near the left-bottom corner, both L- and triangle form, on the other hand, might be relatively unclear. Furthermore, the calculation of the surrogate distribution of correlation

dimension, and the comparison of the experimental value with this distribution, show that the probability to obtain the experimental sequence of IRT data is very low for almost all of the animals. Only one rat showed about 12% of this "by-chance-probability". Another rat showed about 6% by-chance-probability.

There are several explanations for the varieties of ERM-patterns found. For one, different ERM-patterns might reflect subgroups within the animals. Since the Wistar rats used are genetically heterogeneous, and it is possible to breed special subtypes out of genetically heterogeneous strains of rats (for example: Okamoto & Aoki 1963), it would not be surprising that different subtypes of behaviors can be found under similar experimental conditions. On the other hand, different ERM-patterns could be co-existent stable states of behavior under the same experimental conditions. This phenomenon is well known in the study of nonlinear dynamics. For example, when a chemical system is pulled away from its equilibrium point to a far-from-equilibrium state, it might undergo several so-called bifurcations (Prigogine & Lefever, 1968; Nicolis & Prigogine, 1977; Prigogine, 1980). In a bifurcation point, systems can evolve into one of several stable states. The phenomenon of bifurcation was also studied mathematically, for example, in catastrophe theory (Thom 1975; Castrigiano & Hayes 1993).

The acquisition process underlying schedule control over operant behavior could be regarded as such a process of evolution. Upon the abrupt change of reinforcement schedules, the animals must adapt their behavior accordingly. This process is analog to the pulling of chemical systems from their equilibrium state. Even under the control of the same reinforcement schedule, and under the presumption that the individual differences are small, animals could be expected to develop different types of stable behaviors according to a mechanism analog to the bifurcation discussed above. The ERM could serve as a tool to assess such processes, as revealed by figures 12-20.

Although we can see how the specific patterns of behavioral dynamics of the animals developed over time under the control of given reinforcement schedules, the patterns in the ERMs do not give quantitative measures of the "progress" of the animal's behavior. Nor can we quantitatively describe whether or not the animal's behavior has arrived at a steady state. For example, it would be very helpful if we could have a measure to quantify the "difference" of ERM-patterns from session 15 and session 26 shown in figure 11. This will be our next step in the further development of the ERM as an analyzing tool.

5.1.2 Dynamics of FI-responding

The dynamics of FI-responding reflected in the different ERM-patterns can be better understood using theoretical models and simulation studies. The first simulation in the present work supports the so-called "two-state" conception suggested by other authors (Schneider 1969; Dews 1978; Shull 1991). However, it might be wrong to declare that the "two-state" conception is sufficient to describe FI-responding. Further analytical considerations and simulation studies suggest that at least the acceleration of the rate of responses, and multiple switches of behavioral states during the inter-reinforcement periods are necessary elements of FI-responding. Furthermore, the traditional analyzing tools, namely the averaged scallop curve and the IRT distribution, are not sufficient to assess these additional elements. The ERM can serve as a useful supplement to the analysis of operant behavior.

We also proposed a comprehensive dynamical model to simulate different types of experimental ERM-patterns. The model is not purely deterministic, as in most of the theoretical studies on chaotic systems. However, the model consists of a set of complicated functions which possess a "long term" dynamical relationship. It can generate IRT data that can simulate the main features, namely the lattice, L-type and triangle structures of the experimental ERM-patterns. The simulation studies suggest that the mechanism responsible

for the long term dynamics of FI-responding, and that for the generation of operant events under a given "rate" of responses might work relatively independently. While the speed of a hypothetical internal clock and the switches between behavioral states affect the main structures of ERM-patterns considerably, the same type of ERM-patterns can be generated by two different parameter settings of the events-generating mechanism that produce very different forms of IRT-distributions.

5.1.3 Application in behavioral pharmacological studies

We also tested the possibility of using the ERMs in behavioral pharmacological applications. We applied the ERM to analyze FI-responding of rats that were injected intra-peritoneally with 1mg/kg amphetamine 15 minutes before they started a 90-minute session in Skinner boxes. Since amphetamine with this dosage has been reliably shown to have effects on FI-responding of rats, it is quite certain that the behavior of animals would change. The only question is, whether or not there are changes in the dynamics of FI-responding, and whether or not the ERM is able to assess these changes.

The results clearly indicate that considerable changes of ERM-patterns could be observed after animals received 1 mg/kg amphetamine injection. Only very few and non-qualitative changes were observed when the animals were treated with saline, although some animals decreased or increased the total number of responses in the 90-minute session up to 38%. On the other hand, some animals increased the total number of responses in the 90-minute session after amphetamine treatment only about 40% or even less, but the changes in their ERMs were large. In other words, changes in the total number of responses might not automatically imply changes in ERM-patterns, and vice versa. While the former is equivalent to changes in the averaged rate of responses, the latter can be regarded as a change in behavioral modus. Besides, the results of the ERM-analysis suggest at least qualitatively that different types of reactions upon the treatment with amphetamine under this dosage can be

observed among a group of animals, and the reacting types might not be correctly represented by a single value, namely, the rate of response. All these finding arouse the concern of using rate of responses as a measure of the effect of pharmacological treatments, such as amphetamine.

The simulation studies on the effect of amphetamine treatment were performed only on three animals that had already been used in the previous simulation studies. Qualitatively the simulated and experimental results matched well. Again, the lack of a quantitative measure of the differences between ERM-patterns is a problem that requires solving; this shall be the goal in future studies. In addition to the shape of the averaged scallop curve, comparisons between parameter settings of simulations using the same animal's "drug-free" and "amphetamine" data sets as targets indicates the importance of parameter $\mathbf{M_P}$, which decides the rate of switching from the "response" back to the "pause" behavioral states. While the traditional analysis has already suggested that 1 mg/kg amphetamine intra-peritoneal injection can on the average increase the rate of responding, and flatten the scallop curve of FI-responding, the analysis using the ERM, in combination with simulation studies using our dynamical model, can additionally indicate the change of the probability that a animal will switch between behavioral states.

It is true that the analysis using rate of responses or the averaged scallop curve is more useful than the ERM-analysis for providing an averaged measurement of the behavior of a "group" of animals under the same conditions. On the other hand, whether or not this "group" of animals shall be regarded as a "group", given that they react not only quantitatively, but also qualitatively heterogeneous, is also a fundamental question, that can be addressed via an ERM-analysis.

5.2 Perspectives

The application of the new analyzing tool, the extended return map (ERM), to operant

behavior under the control of fixed-interval (FI-) schedules has successfully been shown to be superior to the original return map (recurrent plot). Furthermore, analytical considerations as well as simulation studies showed that the ERM can deliver new information about the dynamics of FI-responding which traditional analyses, such as the averaged scallop curve and IRT distribution, fail to do. This tool provides a new possibility to study behavior from the aspect of dynamics. In the present work only FI-schedules were investigated. Many other schedules, for example the variable-interval schedules, could also be analyzed in terms of behavioral dynamics. Furthermore, it could be interesting to look at switching behavior of animals between two levers in a Skinner box, since animals tend to switch between two levers. Many efforts have been made to study the relationship between the rate of responses on two levers and the different schedules associated with the levers, for example Herrnstein's equation (1970). It would, therefore, also be interesting to look at the dynamics of switching between two such levers.

The dynamical analysis of amphetamine effects on behavior also produced fruitful results. However, it probably raised a number of unanswered questions. Firstly, the weights array of the dynamical model was assumed to be defined by a sigmoid function, for simplicity. It would be important to find a learning rule that can adapt the weights automatically, so that the model can "learn" to respond to new reinforcement schedules, for example from a continuous reinforcement to a FI-schedule. Secondly, it might be interesting to compare the model of the present work with existing theories proposed by other authors, for example Killeen and Fetterman's model or Hoyert's model (Killeen & Fetterman 1988; Hoyert 1992). The model proposed by Hoyert is a deterministic model, under the constraint that it deals with rate of responses. In order to proceed with such a comparison, there must be a way to quantify the goodness of fit of simulated and experimental data. In other words, we need a definition to quantify the differences between two ERMs. The lack of such a method

is a major problem, since it might also be important to quantify the difference between ERM-patterns in pharmacological studies, or from ERMs acquired in different sessions during the process of learning of the specific behavioral dynamics under a certain experimental condition.

Finally, the progress in the present work provides a possibility to look at many physiological as well as pharmacological studies on operant behavior from a different point of view. Previous studies usually implemented the rate of responding, or sometimes the changes in the averaged scallop curve as dependent variables. Our studies on the effects of amphetamine, however, raise questions about this approach. Firstly, there might be changes in behavior that can be seen in the ERM-patterns, but are not manifested in rate of responses. Secondly, some changes of behavior induced by amphetamine have both quantitative as well as qualitative characters. In any case, we have demonstrated that by using ERMs as an analyzing tool, it is possible to gain information from pharmacological and behavioral studies, which is not provided by the conventional analytical techniques. An ideal tactic might be to apply both conventional and non-linear dynamic tools in parallel in order to maximize information in cases where the latter techniques are applicable.

6 References

Achermann, P., Hartmann, R., Gunzinger, A., Guggenbuhl, W. and Borbely, A.A. (1994). All-night sleep EEG and artificial stochastic control signals have similar correlation dimensions. *Electroencephalography and Clinical Neurophysiology*, **90**, 384-387.

Babloyantz, A. (1985). Evidence of chaotic dynamics of brain activity during the sleep cycle. *Physics Letters A*, **111**, 152-156.

Branch, M.N. and Gollub, L.R. (1974). A detailed analysis of the effects of d-amphetamine on behavior under fixed-interval schedules. *Journal of the Experimental Analysis of Behavior*, **21**, 519-539.

Braun, T. and Lisbôa, J.A. (1994). Characterization of homoclinic chaos in a glow discharge through return maps. *International Journal of Bifurcation and Chaos*, **4**, 1483-1493.

Casdagli, M.C., Iasemidis, L.D., Savit, R.S., Gilmore, R.L., Roper, S.N. and Sackellares, J.C. (1997). Non-linearity in invasive EEG recording from patients with temporal lobe epilepsy. *Electroencephalography and Clinical Neurophysiology*, **102**, 95-108.

Castrigiano, D.P.L. and Hayes, S.A. (1993). *Catastrophe Theory*. Reading, Mass.: Addison-Wesley.

Church, R.M. (1984). Properties of the internal clock. In J. Gibbon and L. Allan (Eds.), *Annals of the New York Academy of Sciences, Vol. 423, Timing and Time Perception* (pp. 566-582). New York: New York Academy of Sciences.

Church, R.M., Meck, W.H. and Gibbon, J. (1994). Application of scalar timing theory to individual trials. *Journal of Experimental Psychology: Animal Behavior Processes*, **20**, 135-155.

Dews, P.B. (1958). Studies of behavior IV: Stimulant actions of methamphetamine. *The Journal of Pharmacology and Experimental Therapeutics*, **122**, 137-147.

Dews. P.B. (1978). Studies on responding under fixed-interval schedules of reinforcement: II The scalloped pattern of the cumulative record. *Journal of the Experimental Analysis of Behavior*, **29**, 67-75.

Faure, P. and Korn, H. (1997). A nonrandom dynamic component in the synaptic noise of a central neuron. *Proceedings of the National Academy of Sciences of the United States of America*, **94**, 6506-6511.

Ferster, C.B., and Skinner, B.F. (1957). *Schedules of Reinforcement*. New York: Appleton-Century-Crofts.

Gibbon, J. (1977). Scalar expectancy theory and Weber's law in animal timing. *Psychological Review*, **84**, 279-325.

Gleick, J. (1987). *Chaos - Making a New Science*. New York: Penguin Books.

Grassberger P. (1983). Generalized dimensions of strange attractors. *Physics Letters*, **97A**, 227-230.

Greenshaw, A.J., Sanger, D.J. and Blackman, D.E. (1985). Effects of d-amphetamine and of β-phenylethylamine on fixed interval responding maintained by self-regulated lateral hypothalamic stimulation in rats. *Pharmacology Biochemistry and Behavior*, **23**, 519-523.

Gregson, R.A.M. (1995) *Cascades and Fields in Nonlinear Psychophysics*. Singapore: World Scientific.

Gregson, R.A.M. (1998) Effects of random noise and internal delay in nonlinear psychophysics. *Nonlinear Dynamics, Psychology, and Life Science*, **2**, 73-94.

Gregson, R.A.M. (1999) Confident judgments for discrimination in nonlinear psychophysics. *Nonlinear Dynamics, Psychology, and Life Science*, **3**, 31-48.

Guastello, S.J. (1995). *Chaos Catastrophe and Human Affairs*. Mathwah, NJ: Erlbaum.

Guastello, S.J. (1998). Creative problem solving groups at the edge of chaos. *Journal of Creative Behavior*, **32**, 38-57.

Guzzetti S., Signorini M.G., Cogliati C., Mezzetti S., Porta A., Cerutti S. and Malliani A. (1996). Non-linear dynamics and chaotic indices in heart rate variability of normal subjects and the heart-transplanted patients. *Cardiovascular Research*, **31**, 441-446.

Hayashi, H., Ishizuka, S., Ohta, M. and Hirakawa, K. (1982). Chaotic behavior in the Onchidium giant neuron under sinusoidal stimulation. *Physics Letters A*, **88**, 435-438.

Hayashi, H., Ishizuka, S. and Hirakawa, K. (1983). Transition to chaos via intermittency in the Onchidium pacemaker neuron. *Physics Letters A*, **98**, 474-476.

Hayashi, H. and Ishizuka, S. (1992). Chaotic nature of bursting discharges in the Onchidium pacemaker neuron. *Journal of Theoretical Biology*, **156**, 269-291.

Hayashi, H. and Ishizuka, S. (1995). Chaotic responses of the hippocampal CA3 region to a mossy fiber stimulation in vitro. *Brain Research*, **686**, 194-206.

Heath, R. A. (2000). The Ornstein-Uhlenbeck model for decision time in cognitive tasks: An example of control of nonlinear network dynamics. *Psychological Research*, **63**, 183-191.

Heath, R.A., Kelly, A. and Longstaff, M. (2000). Detecting non-linearity in psychological data: techniques and applications. *Behavior Research Methods, Instruments & Computers*, **32**, 280-289.

Hentschel, H.G.E. and Procaccia, I. (1983). The infinite number of generalized dimensions of fractals and strange attractors. *Physica*, **8D**, 435-444.

Herrnstein R.J. (1970). On the law of effect. *Journal of the Experimental Analysis of Behavior*, **13**, 243-266.

Herrnstein R.J. (1974). Formal properties of the matching law. *Journal of the Experimental Analysis of Behavior,* **21**, 159-164.

Herrnstein R.J. and Morse W.H. (1958). A conjunctive schedule of reinforcement. *Journal of the Experimental Analysis of Behavior*, **1**, 15-24.

Hoyert, M.S. (1992). Order and chaos in fixed–interval schedules of reinforcement. *Journal of the Experimental Analysis of Behavior*, **57**, 339 – 336.

Hunt, G.E. and Dale, M.A. (1992). Reward summation and the effects of pimozide, clonidine, and amphetamine on fixed-interval responding for brain stimulation. *Pharmacology Biochemistry and Behavior*, **42**, 563-577.

Ishizuka, S. and Hayashi, H. (1996). Chaotic and phase-locked responses of somatosensory cortex to a periodic medial lemniscus stimulation in the anesthetized rat. *Brain Research*, **686**, 194-206.

Ishizuka, S. and Hayashi, H. (1998). Spontaneous epileptiform bursts and long-term potentiation in rat CA3 hippocampal slices induced by chaotic stimulation of mossy fibers. *Brain Research*, **790**, 108-14.

Ivanov, P.C., Rosenblum, M.G., Peng, C.K., Mietus, J., Havlin, S., Stanley, H.E. and Goldberger, A.L. (1996). Scaling behaviour of heartbeat intervals obtained by wavelet-based time-series analysis. *Nature*, **383**, 323-327.

Jing, H. and Takigawa, M. (2000). Topographic analysis of dimension estimates of EEG and filtered rhythms in epileptic patients with complex partial seizures. *Biological Cybernetics*, **83**, 391-397.

Kantz H. and Schreiber T. (1997). *Nonlinear Time Series Analysis*. New York: Cambridge University Press.

Kelly, A., Heathcote, A., Heath, R. and Longstaff M. (2001). Response-time dynamics: Evidence for linear and low-dimensional nonlinear structure in human choice sequences. *The Quarterly Journal of Experimental Psychology*, **54A**, 805-840.

Killeen, P. and Fetterman, G (1988). A behavioral theory of timing. *Psychological Review*, **95**, 274-295.

Killeen, P. (1994). Mathematical principles of reinforcement. *Behavioral and Brain Sciences*, **17**, 105-172.

Lefebvre, J.H., Goodings, D.A., Kamath, M.V. and Fallen, E.L. (1993). Predictability of normal heart rate rhythms and deterministic chaos. *Chaos*, **3**, 267-276.

Lehnertz, K. and Elger, C.E. (1995) Spatio-temporal dynamics of the primary epileptogenic area in temporal lobe epilepsy characterized by neuronal complexity loss. *Electroencephalography and Clinical Neurophysiology*, **108**, 108-117.

Li, J.S. and Huston, J.P. (2002). Nonlinear dynamics of operant behavior: A new approach via the extended return map. *Reviews in the Neurosciences*, **13**, 31-57.

Li, T.Y. and Yorke J.A. (1975). Period three implies chaos. *The American Mathematical Monthly*, **82**, 985-992.

Libchaber, A. and Maurer, J. (1982). A Rayleigh-Bénard experiment: helium in a small box. In: Riste, T. (Ed.), *Nonlinear Phenomena at Phase Transitions and Instabilities*. New York: Plenum press, in cooperation with NATO Scientific Affairs Division, pp. 259-286.

Liebovitch, L.S. (1998). *Fractals and Chaos: Simplified for the Life Sciences*. New York: Oxford University Press.

Lorenz, E.N. (1962). Simplified dynamic equations applied to the rotating basin experiments. *Journal of Atmospheric Science*, **19**, 39-51.

Lorenz, E.N. (1963). Deterministic nonperiodic flow. *Journal of Atmospheric Science*, **20**, 130-141.

Machado, A. (1997). Learning the temporal dynamics of behavior. *Psychological Review*, **104**, 241-265.

Machado, A. and Cevik, M. (1998). Acquisition and extinction under periodic reinforcement. *Behavioural Processes*, **44**, 237-262.

Marion, J.B. and Thornton, S.T. (1995). *Classical Dynamics of Particles and Systems*, 4th. Edition. San Diego: Saunders College Publication.

Marquardt, D.H. (1963). An algorithm for least-squares estimation of non-linear parameters. *Journal of the Society for Industrial Applied Mathematics*, **2**, 431-441.

Matsumoto, M. and Nishimura, T. (1998). Mersenne Twister: A 623-dimensionally equidistributed uniform pseudorandom number generator. *ACM Transactions on Modeling and Computer Simulation: Special Issue on Uniform Random Number Generation*, **8**, 3-30.

Meyer, M., Stiedl, O. and Kerman, B. (2003). Discrimination by multifractal spectrum estimation of human heartbeat interval dynamics. *Fractals*, in press.

Nicolis, G. and Prigogine, I. (1977). *Self-organization in non-equilibrium systems*. New York: John Wiley & Sons, Inc., pp. 70-159.

Okamoto, K and Aoki, K. (1963). Development of a strain of spontaneously hypertensive rats. *Japanese Circulation Jounal*, **27**:282-93.

Osborne, A.R. and Provenzale, A. (1989). Finite correlation dimension for stochastic systems with power-law spectrum. *Physica D*, **35**, 357-381.

Ott, E., Sauer, T. and Yorke, J. A. (1994). *Coping with Chaos: Analysis of Chaotic Data and the Exploitation of Chaotic Systems*. New York: John Wiley & Sons, Inc.

Packard, N.H., Crutchfield, J.P., Farmer, J.D. and Shaw, R.S. (1980). Geometry from a time series. *Physical Review Letters*, **45**, 712-716

Palya, W.L. (1992). Dynamics in the fine structure of schedule-controlled behavior. *Journal of the Experimental Analysis of Behavior*, **57**, 267 – 287.

Poon C.S. and Merrill, C.K. (1997). Decrease of cardiac chaos in congestive heart failure. *Nature*, **389**, 492-495.

Press, W.H., Teukolsky, S.A., Vetterling, W.T. and Flannery, B.P. (1992). *Numerical Recipes in C*. New York: Cambridge University Press.

Prigogine, I. and Lefever, R. (1968). Symmetry breaking instabilities in dissipative systems, II. *The Journal of Chemical Physics*, **48**, 1695-1700.

Prigogine, I. (1980). *From Being to Becoming: Time and Complexity in the Physical Sciences* San Francisco: W. H. Freeman & Co..

Prigogine, I. and Stengers, I. (1984). *Order out of Chaos*. London: Heinemann.

Prigogine, I. and Stengers, I. (1997). *The End of Certainty, Time, Chaos and the New Laws of Nature.* New York: The Free Press.

Rayleigh, L. (1916). On the convective currents in a horizontal layer of fluid when the higher temperature is on the under side. *Philosophical Magazine*, **32**, 529-546.

Roper, T.J. (1978). Diversity and substitutability of adjunctive activities under fixed-interval schedules of food reinforcement. *Journal of the Experimental Analysis of Behavior*, **30**, 83-96.

Röschke, J., Fell, J. and Beckmann, P. (1993). The calculation of the first positive Lyapunov exponent in sleep EEG data. *Electroencephalography and Clinical Neurophysiology*, **86**, 348-352.

Röschke, J, Fell, J. and Mann, K. (1997). Non-linear dynamics of alpha and theta rhythm: correlation dimension and Lyapunov exponents from healthy subject's spontaneous EEG. *International Journal of Psychophysiology*, **26**, 251-261.

Sagvolden, T., Aase, H. and Berger D.F. (1998). Altered reinforcement mechanisms in attention-deficit/hyperactivity disorder. *Behavioural Brain Research*, **94**, 61-71.

Sauer, T. (1994). Reconstruction of dynamical systems from interspike intervals. *Physical Review Letters*, **72**, 3811-3814.

Sauer, T., Yorke, M. and Casdagli, M. (1991). Embedology. *Journal of Statistical Physics*, **65**, 579-616

Schneider, A.B. (1969). A two-state analysis of fixed-interval responding in the pigeon. *Journal of the Experimental Analysis of Behavior*, **12**, 677-687.

Segal, S.A., Moerschbaecher, J.M. and Thompson, D.M. (1981). Effects of phencyclidine, d-amphetamine and pentobarbital on schedule-controlled behavior in rats. *Pharmacology Biochemistry and Behavior*, **15**, 807-812.

Shadlen, M.N. and Newsome, W.T. (1994). Noise, neural codes and cortical organization. *Current Opinion in Neurobiology*, **4**, 569-579.

Shaw, R.S. (1984). *The Dripping Faucet as a Model Chaotic System*. Santa Cruz, CA: Aerial Press.

Shull, R.L. (1991). Mathematical description of operant behavior: An introduction. In I. H. Iversen & K. A. Lattal (Eds.), *Techniques in the behavioral and neural sciences: Vol. 6. Experimental Analysis of Behavior* (Part 2, pp. 243-282). Amsterdam: Elsevier.

Sidman, M. (1960) *Tactics of scientific research*. New York: Basic Books.

Skinner, B.F. (1935). Two types of conditioned reflex and a pseudo type. *Journal of General Psychology*, **12**, 66-77.

Skinner, B.F. (1937). Two types of conditioned reflex: A reply to Konorski and Miller. *Journal of General Psychology*, **16**, 272-279.

Skinner, B.F. (1938). *The Behavior of Organisms*. New York: Appleton-Century-Crofts.

Softky, W.R. and Koch, C. (1993). The highly irregular firing of cortical cells is inconsistent with temporal integration of random EPSPs. *Journal of Neuroscience*, **13**, 334-350.

Stewart, J.N. and Peregoy, P.L. (1983). Catastrophe theory modeling in psychology. *Psychological Bulletin*, **94**, 336-362.

Suzuki H, Aihara K., Murakami J. and Shimozawa T. (2000). Analysis of neural spike with interspike interval reconstruction. *Biological Cybernetics*, **82**, 305-311

Ta'eed, L.K., Ta'eed, O. and Wright, J.E. (1988). Determinants involved in the perception of the Necker cubes: An application of the catastrophe theory. *Behavioral Science*, **33**, 97-115.

Takens, F. (1981). Detecting strange attractors in turbulence. In D. A. Rand & L. S. Young (Eds.), *Lecture notes in mathematics* (pp. 336 – 381). New York: Springer–Verlag.

Takigawa, M., Fukuzako, H., Ueyama, K., Takeuchi, K., Fukuzako, T., Hokazono, Y. and Hirakawa, K. (1994). Chaos in brain function. *Neurosciences*, **20**, 67-73.

Tewes, P.A. and Fischman, M.W. (1982). Effects of d-amphetamine and diazepam on fixed-interval, fixed-ratio responding in humans. *Journal of Pharmacology and Experimental Therapeutics*, **211**, 373-383.

Theiler, J., Eubank, S., Longtin, A., Garldrikian, B and Farmer, J.D. (1992). Testing for nonlinearity in time series: The method of surrogate data. *Physica D,* **58**, 77-94.

Thom, R. (1975). *Structural Stability and Morphegenesis*. New York: Benjamin-Addison-Wesley.

Thorndike, E.L. (1911) *Animal Intelligence*. New York: The Macmillan Company. Transaction Ed. (2000): *Animal Intelligence: Experimental Studies*, New Brunswick, New Jersey: Transaction Publishers.

Weiss, B. (1970). The fine structure of operant behavior during transition states. In W. N. Schoenfeld (Ed.), *The Theory of Reinforcement Schedules*. New York: Appleton-Century-Crofts, Educational Division, Meredith Corporation.

Wenger, G.R. and Dews, P.B. (1976). The effects of phencyclidine, ketamine, d-amphetamine, and pentobarbital on schedule-controlled behavior in the mouse. *The Journal of Pharmacology and Experimental Therapeutics*, **196**, 616-624.

Yamamoto, Y., Hughson, R.L., Sutton, J.R., Cymerman, A., Fallen, E.L. and Kamath, M.V. (1993). Operation Everest II: An indication of deterministic chaos in human heart rate variability at simulated extreme altitude. *Biological Cybernetics*, **69**, 205-212.